

**Multi-scale hydrogeomorphic influences on bull trout spawning habitat
in snowmelt-dominated headwater streams**

by

Jared Robinson Bean

Bachelor of Arts, Middlebury College, Middlebury, VT 2010

Thesis

Presented in partial fulfillment of requirements of the degree of

Master of Science
in Geosciences

The University of Montana
Missoula, MT

Fall 2012

Approved by:

Sandy Ross, Dean of the Graduate School
Graduate School

Dr. William W. Woessner, Co-Chair
Department of Geosciences

Dr. Andrew C. Wilcox, Co-Chair
Department of Geosciences

Dr. Clint C. Muhlfeld
USGS Northern Rocky Mountain Science Center &
Flathead Lake Biological Station

1 Acknowledgements

2
3
4
5
6
7
8
9
10
11
12
13
14
15
16
17
18
19
20
21
22
23
24

I would like to thank the individuals and organizations that helped make this study possible. I thank my co-advisors, William Woessner and Andrew Wilcox, for the opportunity to work on this project and for their guidance and encouragement. Thank you also to Clint Muhlfeld for helping land the project and guide me through the process. Thank you to my lab group colleagues for your comments and suggestions at various points during this study. Thank you to Johnnie Moore for useful insights on my research proposal. Thank you to everyone who assisted me in the field: Ali White, Franklin Dekker, Sharon Bywater-Reyes, Nicholas Banish, Allie Tincher, Ben Gardner, Thomas Pallin, Zack Rambo, Rob Livesay, Thomas Bean, Lisa Bean, Andy Bean, and Phil Ehrlich. Thank you to Vin D’Angelo for helping with logistics. Thank you to Carter Fredenberg, Brady Miller, Ben Galloway, Tommy Peterson, and Joe Giersch for helping to show me the ropes in the Park. Thank you to Chris Downs, John Fraley, and Mark Deleray for letting me tag-along on redd counts. Thank you to Tom Weaver and John Fraley for advising me on study reach location selection and providing other background information. Thank you to Dan Kotter for helping me get started. Thank you to the Glacier National Park staff, especially Chris Downs, Tara Carolin, and Scott Emmerich, for allowing me to work in such an incredible field area. Thank you to the UM Geosciences Department faculty and staff, especially Aaron Deskins, Christine Foster, Loreene Skeel, and Wendy Wollett for all that you do. Thank you to Marco Maneta and Heiko Langner for helping with data analyses. This work was financially supported by grants from the USGS, the Cooperative Ecosystems Studies Unit (CESU), the National Park Service, the Montana Institute on Ecosystems (NSF EPSCoR program grant EPS-1101342), and the Montana Water Center. Any opinions, findings and conclusions or recommendations expressed in this material are those of the author(s) and do not necessarily reflect the views of the funding agencies.

26

27 Multi-scale hydrogeomorphic influences on bull trout spawning habitat in snowmelt-dominated
28 headwater streams

29

30 Committee Chairpersons: William Woessner and Andrew Wilcox

31 External Committee Member: Clint Muhlfeld

32

33 Abstract

34

35 I investigated relationships between geomorphology, hydrogeology, and bull trout (*Salvelinus*
36 *confluentus*) redd occurrence and density at multiple spatial scales in gravel-bed, pool-riffle, snowmelt
37 dominated headwater streams of northwestern Montana. Subreach redd occurrence tended to be
38 associated with the finest available textural facies. In subreach streambed sections hosting bull trout
39 redds, redd density was significantly (at $\alpha=0.05$) positively related to bankfull Shields stress (τ_{bf}^* , $p=0.04$)
40 and bankfull Shields stress adjusted for grain stress only (τ_{bf}^{**} , $p=0.02$). In stream reaches hosting bull
41 trout redds, reach-average redd density was significantly positively related to reach-average τ_{bf}^{**}
42 ($p=0.02$) and reach-average streambed grain size (D_{16} , $p=0.01$; D_{50} , $p=0.02$, D_{84} , $p=0.02$). Spawning
43 reaches exhibited high streambed horizontal and vertical hydraulic conductivities, and streambed
44 temperatures were dominated by stream water diurnal cycles to a depth of at least 25 cm. Groundwater
45 provided substantial thermal moderation of stream water for multiple high density spawning reaches. At
46 the valley-scale, redd occurrence tended to be associated with unconfined alluvial valleys. Many
47 previous studies highlight the thermal sensitivity of bull trout. My spawning gravel competence results
48 indicate that a shift in the timing of high flows could increase the likelihood of redd scour during the bull
49 trout egg incubation period.

50

51

52

53

Table of Contents

54

55 Acknowledgements.....ii

56 Abstract.....iii

57 List of Figuresv

58 List of Tablesvii

59 **INTRODUCTION** **1**

60 Background 1

61 Hypotheses justification 5

62 **METHODS**.....**6**

63 Study area 6

64 1A&B) Reach-scale physical characterization 9

65 2A&B) Valley-scale physical characterization 14

66 Statistical analyses 15

67 **RESULTS** **16**

68 1A) Reach-scale fluvial geomorphology..... 18

69 1B) Reach-scale hydrogeology 24

70 2A) Valley-scale geomorphology 29

71 2B) Valley-scale hydrogeology 33

72 **DISCUSSION**.....**39**

73 1A) Reach-scale fluvial geomorphology..... 40

74 1B) Reach-scale hydrogeology 41

75 2A) Valley-scale geomorphology 43

76 2B) Valley-scale hydrogeology 44

77 The Big Picture 46

78 **CONCLUSIONS** **48**

79 List of abbreviations and symbols..... 48

80 **REFERENCES**..... 49

81

82 Appendix 1A: Reach-scale geomorphology 59

83 Appendix 1B: Reach-scale hydrogeology 88

84 Appendix 2A: Valley-scale geomorphology 96

85 Appendix 2B: Valley-scale hydrogeology 98

86

List of Figures

87

88 Figure 1. Illustration of multi-scale approach. 4

89 Figure 2. Study area. 7

90 Figure 3. Aerial photographs of the 6 study reaches and 2011 redds..... 8

91 Figure 4. iButton vertical array design..... 13

92 Figure 5. North and Middle Fork River discharge from February 2011 to July 2012..... 17

93 Figure 6. Redd locations in relation to study reach channel long profile, mean surface grain size, bankfull
94 Shields stress, and bankfull adjusted Shields stress 19

95 Figure 7. Examples of redds in concave-up bedforms 20

96 Figure 8. Median surface grain size (D_{50}) of the primary textural facies of each study reach and summary
97 of textural facies used by spawning bull trout..... 20

98 Figure 9. Subreach-scale a) bankfull and b) bankfull adjusted Shields stress (τ^*_{bf} , τ^{**}_{bf}) versus subreach
99 redd density 21

100 Figure 10. Reach-average grain size metrics (D_{16} , D_{50} , D_{84}) versus reach-averaged redd density
101 21

102 Figure 11. Reach-averaged a) bankfull and b) bankfull adjusted Shields stress (τ^*_{bf} , τ^{**}_{bf}) versus reach-
103 averaged redd density 22

104 Figure 12. Reach-average streambed slope versus reach-average median surface grain size (D_{50})
105 22

106 Figure 13. Distribution of subreach-scale bankfull adjusted Shields stress in each study reach
107 23

108 Figure 14. Vertical hydraulic gradient (VHG) range for September and October in each study reach
109 26

110 Figure 15. Summary plots of hydrogeologic variables measured in the study reaches 27

111 Figure 16. Reach-average hydrogeologic variables versus reach-average redd density (redds/m²)
112 28

113 Figure 17. Reach-average median surface grain size (D_{50}) versus reach-average a) horizontal hydraulic
114 conductivity (K_h) and b) vertical hydraulic conductivity (K_v)..... 28

115 Figure 18. Reach-average bankfull adjusted Shields stress (τ^{**}_{bf}) versus reach-average a) horizontal
116 hydraulic conductivity (K_h) and b) vertical hydraulic conductivity (K_v)..... 29

117 Figure 19. Valley confinement and 2011 bull trout redd occurrence in each study streams..
118 31

119 Figure 20. Reach-average valley confinement ratio (VCR) versus reach-average geomorphic variables
120 32

121 Figure 21. Reach-average valley confinement ratio (VCR) versus reach-average hydrogeologic variables
122 33

123 Figure 22. Ole Creek water table contour map encompassing OLE_{mc} and OLE_{sc} on 9/11/11..
124 35

125 Figure 23. Location of catchment-scale water temperature dataloggers and 2011 bull trout redds
126 36

127 Figure 24. Comparison of the average, standard deviation, and rate of change in stream temperature in
128 September for various longitudinal locations in each study stream 37

129 Figure 25. Coefficient of variation (C_v) in water temperature of the catchment-wide temperature sensors
130 38

131 Figure 26. Spatial comparison of diurnal water temperature oscillations in the Ole Creek catchment
132 39

133 Figure 27. Air temperature in each of the study reaches ~1-2 m about the ground or water surface
134 39

135	Figure 28. Illustration of potentially inaccurate heat and fluid flow analytical model calculation of specific	
136	discharge magnitude and direction	42
137	Figure 29. Conceptual models illustrating the interaction of hyporheic and groundwater flow paths in	
138	relation to bedforms.....	42
139		

140 **List of Tables**

141 Table 1. Physical factors that influence bull trout and other salmonid spawning site selection

142 5

143 Table 2. Summary of study reach geomorphic field measurements 10

144 Table 3. Study reach bankfull discharge estimation criteria 10

145 Table 4. Number of in-stream piezometers per study reach 12

146 Table 5. Historical redd count numbers for study streams 17

147 Table 6. Study reach geomorphic characteristics and 2011 redd numbers per study reach ..

148 18

149 Table 7. Reach-average correlations between measured physical variables and redd density

150 24

151 Table 8. Average channel and streambed water temperature from 9/19/11-9/30/11 – during the

152 spawning period 25

153 Table 9. Dependency of reach-average hydrogeologic variables on reach-average geomorphic variables

154 29

155 Table 10. Bull trout 2011 redd distribution per valley type in study streams 32

156 Table 11. Valley confinement ratios per study reach 32

157

158

159 **INTRODUCTION**

160 Research at the intersection of fluvial geomorphology, hydrology, and ecology has expanded in
161 recent years (e.g. Poole, 2010), but an improved understanding of physical and associated ecological
162 processes is needed to develop effective conservation and management practices for aquatic
163 ecosystems. Preserving and improving spawning habitat requires defining key physical and ecological
164 processes controlling spawning site selection and successful fry emergence (e.g. Kondolf 2000;
165 Montgomery et al., 1996; Moir et al., 2002; Kondolf et al., 2008; Tonina and Buffington, 2009b). Species-
166 specific spawning habitat suitability questions remain, especially for bull trout (*Salvelinus confluentus*)
167 whose native range includes the northern Rocky Mountains and Pacific Northwest.

168 The purpose of this study was to determine primary micro-, subreach-, reach-, and valley-scale
169 physical factors influencing bull trout spawning occurrence in snowmelt-dominated systems. I
170 hypothesized:

- 171 1. At the subreach- and reach-scales, spawning locations are associated with channel sections of
172 A) low spawning sediment mobility at bankfull flows; and
173 B) extensive local streambed hyporheic exchange.
- 174 2. At the valley-scale, spawning locations are associated with alluvial valley segments where
175 A) the stream valley narrows; and
176 B) hyporheic water and groundwater discharges to the stream.

177 I review what is known about these topics below, explain the basis of these hypotheses, and, in the
178 subsequent analysis and discussion of my data, reinterpret and broaden current understanding of
179 physical process controls on bull trout spawning habitat.

180
181 Background

182 Large-scale connectivity of cold, clean, complex habitats is directly associated with robust bull
183 trout populations (e.g. Rieman and McIntyre, 1993; Muhlfeld et al., 2003; Muhlfeld and Marotz, 2005;
184 Dunham et al., 2008; Al-Chokhachy et al., 2010). Bull trout spawn in cold-water, gravel-bedded,
185 headwater streams (e.g. Fraley and Shepard, 1989). Habitat destruction, fragmentation, invasive
186 species, overharvest, and climate warming have led to a decline in bull trout populations throughout
187 much of their native range (Rieman et al., 1997). Bull trout have been listed as a threatened species
188 since 1998 (U.S. Office of the Federal Register, 1998). Critical habitat designations for bull trout in the
189 United States include areas in Montana, Idaho, Washington, Oregon, and Nevada (US Office of the
190 Federal Register, 2010); bull trout also inhabit parts of Western Canada (e.g. Rieman and McIntyre,
191 1993).

192 Bull trout exhibit two distinct life history forms, migratory and resident. Migratory forms often
193 exceed 60 cm in length; they spend much of their adult life in large lake and river systems and migrate
194 to small headwater streams to spawn (e.g. Goetz, 1989; Fraley and Shepard, 1989; Rieman and
195 McIntyre, 1993). In contrast, resident bull trout range in length from 15 to 30 cm and spend their entire
196 life in headwater streams (e.g. Goetz, 1989; Rieman and McIntyre, 1993). Adult bull trout typically
197 spawn annually or biennially from late August to October (Fraley and Shepard, 1989; McPhail and
198 Murray, 1979; Baxter and Hauer, 2000; Dunham et al., 2001) and fry emerge from the streambed
199 gravels in February through April (Baxter and Hauer, 2000).

200 The bull trout is a member of the Salmonidae family and the Salmoninae subfamily. Whereas all
201 fish species of the Salmonidae family are commonly referred to as “salmonids”, the use of the term
202 “salmonid” in this paper refers only to salmonids in the Salmoninae subfamily (e.g. trout, salmon, and
203 char). The literature describing bull trout spawning habitat characteristics (e.g. Fraley and Shepard,
204 1989; Rieman and McIntyre, 1993; Baxter and Hauer, 2000) is small in comparison to the collective body
205 of literature on related salmonid species (e.g. Kondolf, 2000; Buffington et al., 2004; Moir et al., 2009;
206 Montgomery et al., 1996; Montgomery et al., 1999; Tonina and Buffington, 2009b). I therefore draw on

207 the findings of studies on related salmonids to build a conceptual model of the physical conditions and
208 processes that may influence bull trout spawning habitat suitability.

209 At various spatial scales, geomorphic and hydrogeologic conditions are commonly cited as
210 important factors in salmonid spawning site selection and successful fry emergence (Figure 1, Table 1).
211 At the micro- or patch-scale, streambed grain size constrains the abundance of potential salmonid
212 spawning habitat (e.g. Kondolf and Wolman, 1993; Buffington et al., 2004) (Figure 1a, Table 1a). Optimal
213 spawning substrate for bull trout is unembedded, well-sorted gravel-cobble deposits (Fraley and
214 Shepard, 1989; Baxter and Hauer, 2000; Al-Chokhachy et al., 2010). Suitable median surface grain sizes
215 (D_{50}) for bull trout spawning range from 8 mm to 64 mm (Baxter and McPhail, 1996; Dunham et al.,
216 2001). Bull trout redd tailspill thicknesses have been observed in the range of about 15-25 cm (e.g.
217 Weaver and Fraley, 1991). Migratory bull trout in western Washington reportedly bury their eggs at an
218 average depth of 10-15 cm (DeVries, 1997; Shellberg, 2002).

219 The pit and tailspill of a salmonid redd functions to create a micro-scale concave-up streambed
220 curvature within a given bedform and theoretically induces stream water flow through the tailspill
221 hosting the eggs (e.g. Tonina and Buffington, 2009b). This modification of the streambed increases the
222 hydraulic conductivity of the tailspill hosting the eggs by winnowing fines from the substrate matrix and
223 therefore increasing intragravel flow velocities and dissolved oxygen concentrations within the redd
224 (e.g. Tonina and Buffington, 2009b). High hydraulic conductivity and intragravel flow rates in redds are
225 necessary for supplying oxygenated water to incubating eggs and removing metabolic waste (Cordone
226 and Kelley, 1961; Chevalier et al., 1984; Bjornn and Reiser, 1991). Embryo survival and fry emergence
227 success is vulnerable to deposition of fine sediments within redd gravels, a process that reduces the
228 rates of water exchange and waste removal (e.g. Fraley and Shepard, 1989; Kondolf, 2000). The survival
229 of bull trout embryos is optimized at water temperatures ranging from 2-4°C (McPhail and Murray,
230 1979).

231 Scaling up from the patch-scale, relationships between spawning locations and physical
232 conditions at the subreach-scale are also important (e.g. Moir et al., 2009; Figure 1b, Table 1b).
233 Geomorphically, at the subreach-scale, salmonid spawning frequency has been linked to streambed
234 sections of low spawning sediment mobility at bankfull flows (e.g. Moir et al., 2009). Additionally,
235 salmonids have evolved life history strategies including fall spawning and late-winter fry emergence that
236 are adapted to avoid peak spring flows associated with snowmelt-dominated hydrographs (e.g. Tonina
237 and McKean, 2010). Furthermore, large salmonids in gravel-bed, pool-riffle streams tend to bury their
238 eggs below bankfull discharge scour depths to avoid scour of incubating eggs (Montgomery et al., 1996).
239 In alluvial rivers, bankfull discharges are considered to be geomorphically significant in that they control
240 channel morphology and streambed mobilization (e.g. Wolman and Miller, 1960; Moir et al., 2009);
241 these flows tend to occur about every 1.5 to 2 years (e.g. Williams, 1978). In gravel-bed streams,
242 streambed disturbance depths during bedload transport are typically less than 2 times surface D_{90}
243 (DeVries, 2002). Large woody debris and side channels increase hydraulic roughness and spawning
244 habitat complexity and help protect incubating salmonid eggs from scour (e.g. Shellberg et al., 2010;
245 Buffington and Montgomery, 1999b).

246 At the subreach-scale, salmonids tend to spawn in concave-up bedforms (e.g. pool tail-outs)
247 where streambed pressure gradients induce stream water flow through the bedform and back into the
248 stream (e.g. Keller et al., 1990; Kondolf, 2000; Baxter and Hauer, 2000). This mixing zone of surface and
249 shallow subsurface water beneath and adjacent to the stream channel is known as the hyporheic zone
250 (e.g. White, 1993; Woessner, 2000; Tonina and Buffington, 2009a). Whereas groundwater can be
251 thought of as subsurface water of considerable residence time, hyporheic water can be classified as the
252 water that originates in the stream channel, travels through the subsurface, and returns to the stream
253 channel within a timeframe that preserves surface water characteristics (e.g. temperature, dissolved
254 oxygen, etc.) (e.g. Kazezyilmaz-Alhan and Medina, 2006; Tonina and Buffington, 2009a). Hyporheic flow

255 is driven by spatial changes in 1) total streambed pressure gradients (energy head gradients), 2) cross-
256 sectional alluvial area, and/or 3) streambed hydraulic conductivity (Tonina and Buffington, 2009a).
257 Hyporheic mixing underpins stream ecosystems (e.g. Stanford and Ward, 1993; Tonina and Buffington,
258 2011), and salmonid spawning habitat specifically (e.g. Baxter and Hauer, 2000, Tonina and Buffington,
259 2009b) because it impacts stream temperature and enhances the exchange of water and solutes
260 between the stream, streambed, and banks (e.g. Arrigoni et al., 2008; Tonina and Buffington, 2011).

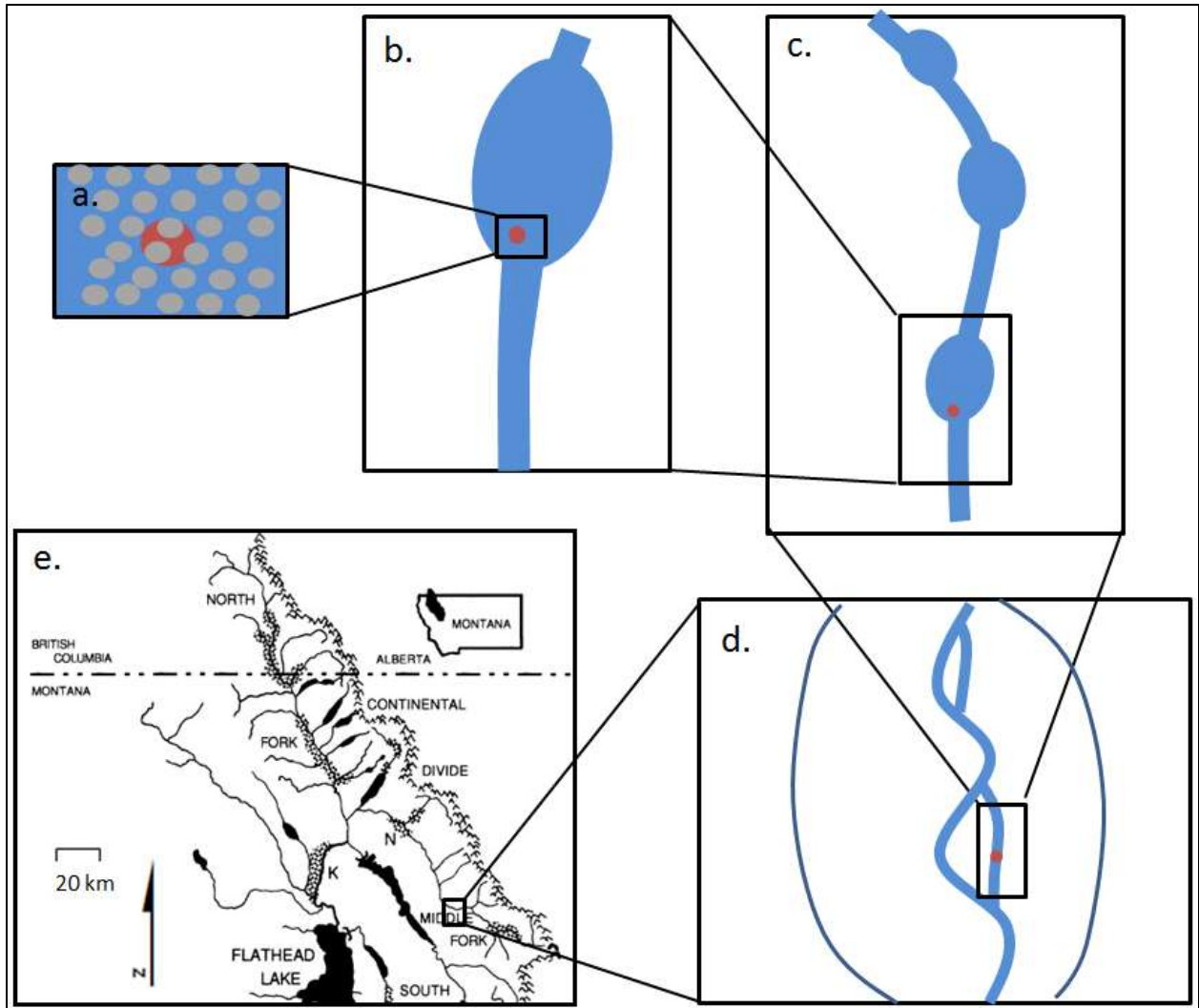
261 Streambed flux direction also influences spawning site selection for many salmonid species (e.g.
262 Kondolf, 2000); and the preferred direction and magnitude can vary among different species. For
263 example, bull trout and Chinook salmon (*Oncorhynchus tshawytscha*) have been observed to
264 preferentially spawn in streambed gravel where stream water infiltrates (influent or losing stream
265 sections, areas of downwelling stream water) (e.g. respectively Baxter and Hauer, 2000; Vronskiy,
266 1972). In contrast, chum salmon (*O. keta*) and brook trout (*S. fontinalis*) have been observed selecting
267 upwelling streambed sections (effluent or gaining stream sections, areas of upwelling hyporheic and/or
268 groundwater) (e.g. respectively Tautz and Groot, 1975; Van Grinsven et al., 2012).

269 Many researchers have observed that some salmonid species – including bull trout – typically do
270 not spawn in streambed patches with seemingly acceptable substrate and bedform conditions (e.g.
271 Burner, 1951; Baxter and Hauer, 2000). Several researchers propose that the lack of a preferred
272 streambed flux magnitude and direction may explain this phenomenon (e.g. Healey, 1991; Baxter and
273 Hauer, 2000; Hansen, 1975; Van Grinsven et al., 2012). Stream temperature also influences bull trout
274 spawning behavior; bull trout tend to spawn in the fall as daily average water temperatures decline
275 below 9°C (Fraley and Shepard, 1989; Muhlfeld et al., 2006).

276 At the reach- and valley-scale, in headwater catchments, bull trout tend to spawn in pool-riffle
277 channels (<1.5% slope: Fraley and Shepard, 1989; Montgomery et al, 1999), usually within alluvial valley
278 sections (e.g. Baxter and Hauer, 2000; Figure 1c,d; Table 1c,d). Hydraulic roughness (e.g. wood, bank,
279 and bar roughness; flow diversions or side channels) influences the distribution of streambed gravel
280 textural facies and therefore, the location and abundance of potentially suitable spawning gravels (e.g.
281 Buffington and Montgomery, 1999b; Buffington et al., 2004).

282 Also at the reach- and valley-scale, stream channel sections that receive groundwater discharge
283 are often linked to bull trout spawning habitat (e.g. Weaver and White, 1985; Fraley and Shepard, 1989;
284 Baxter and Hauer, 2000) and other salmonid spawning habitat (e.g. Benson, 1953; Latta, 1964; Hansen,
285 1975, Curry and Noakes, 1995; Van Grinsven et al., 2012). Changes in alluvial depth and valley width
286 influence surface water – groundwater exchange. An increase in alluvial depth and width (e.g. transition
287 from confined to unconfined valley) causes movement of water from the channel to the alluvium (e.g.
288 hyporheic flow and groundwater recharge) whereas a decrease in depth and width (e.g. transition from
289 unconfined to confined valley) causes movement of water from the alluvium to the channel (e.g.
290 hyporheic and groundwater discharge) (e.g. Stanford and Ward, 1993; Baxter and Hauer, 2000;
291 Malcolm et al., 2005). Upwelling groundwater is often nutrient-rich and can promote patches of
292 increased primary productivity within stream reaches (e.g. Boulton et al., 2010). Groundwater
293 temperature is relatively constant at depths of 10-25 m and can be estimated as 1-2°C warmer than
294 mean annual air temperature (e.g. Kasenow, 2001). Stream sections receiving groundwater discharge
295 are often considered thermal refugia for fish (e.g. McCullough et al., 2009). In summer, groundwater
296 discharge can provide cold water refugia; in winter, it can provide warm water refugia (Gibson, 1966;
297 Cunjak and Power, 1986; Nielsen et al., 1994). Upwelling groundwater can also prevent anchor ice
298 formation in winter, a condition viewed as potentially adverse to embryo and fry survival (e.g. Benson,
299 1955; Baxter and Hauer, 2000). In addition, redd temperature regimes impact salmonid egg incubation
300 time (e.g. Hansen, 1975; Weaver and White, 1985). Variations in streambed temperature can provide
301 population resilience through variable emergence timing (Hansen, 1975).

302



303
 304 Figure 1. Spatial scales referenced in my conceptual model: (a) micro- or patch-scale; (b) subreach
 305 scale; (c) reach-scale; (d) valley-scale; (e) basin-scale (the inset basin-scale image is modified from Stanford and Ward, 1993).
 306

307 Table 1. Multi-scale physical factors that influence bull trout and other salmonid species' spawning site selection.
 308 Literature examples are listed as pertaining specifically to bull trout, or another salmonid species, or to salmonids
 309 in general. See Figure 1 for illustrations of the spatial scales.

SPATIAL SCALE	CONCEPTUAL MODEL FACTORS
a. Micro- or patch-scale (centimeters to meters)	<ul style="list-style-type: none"> mobile, well-sorted gravels to cobbles (e.g. <u>bull trout</u>: e.g. Fraley and Shepard, 1989; Baxter and Hauer, 2000; Al-Chokhachy et al., 2010; <u>salmonids</u>: e.g. Kondolf and Wolman, 1993) redd construction that winnows fines, increases hydraulic conductivity, induces or increases downward hyporheic flow through the redd's tailspill, and increases dissolved oxygen supply around the redd (<u>salmonids</u>: e.g. Tonina and Buffington, 2009b)
b. Subreach-scale (tens of meters)	<ul style="list-style-type: none"> concave-up bedforms (e.g. pool tail-outs) that induce downward hyporheic flow (<u>bull trout</u>: e.g. Baxter and Hauer, 2000; <u>salmonids</u>: e.g. Keller and Kondolf, 1990; Tonina and Buffington, 2009b) streambed sections with a specific (preferred) streambed flux direction and magnitude (e.g. <u>bull trout</u>: e.g. Baxter and Hauer, 2000; <u>salmonids</u>: e.g. Healey, 1991) low mobility of spawning sediment at bankfull flows (<u>salmonids</u>: e.g. Moir et al., 2009)
c. Reach-scale (tens to hundreds of meters)	<ul style="list-style-type: none"> channel slopes < 1.5% (<u>bull trout</u>: e.g. Fraley and Shepard, 1989) pool-riffle channels (<u>bull trout</u>: e.g. Baxter and Hauer, 2000; <u>salmonids</u>: e.g. Montgomery et al., 1999). reaches with stream temperatures moderated by groundwater input (<u>bull trout</u>: e.g. Baxter and McPhail, 1999; Baxter and Hauer, 2000; <u>brown trout</u>: e.g. Hansen et al., 1975; <u>coaster brook trout</u>: e.g. Van Grinsven et al., 2012) avoidance of streambed patches of direct groundwater upwelling (<u>brown trout</u>: e.g. Hansen et al., 1975; <u>Atlantic salmon</u>: e.g. Malcolm et al., 2005)
d. Valley-scale (hundreds of meters to kilometers)	<ul style="list-style-type: none"> alluvial valley segments in sections of alluvial valley narrowing (<u>bull trout</u>: e.g. Baxter and Hauer, 2000; <u>Atlantic salmon</u>: e.g. Malcolm et al., 2005) the distribution of spawning appropriate gravels (<u>salmonids</u>: e.g. Buffington et al., 2004; Buffington and Montgomery, 1999b)
e. Basin-scale (kilometers to hundreds of kilometers)	<ul style="list-style-type: none"> large-scale connectivity (e.g. minimal anthropogenic migration barriers and streamflow regime alteration: Muhlfeld et al., 2011; low road density: Baxter et al., 1999) of complex local habitat (<u>bull trout</u>: e.g. Muhlfeld et al., 2003; Muhlfeld and Marotz, 2005; Dunham et al., 2008; Al-Chokhachy, et al., 2010)

310
 311 Hypotheses justification
 312 Hypothesis 1A is based on the premise that redds are created where spawning-appropriate
 313 gravels have a low potential for scour in high flow events (e.g. Moir et al., 2009). Hypothesis 1B is based
 314 on the premise that stream water cycling through the stream, banks, floodplain, and regional
 315 groundwater system influences bull trout spawning site selection because it enhances the delivery of
 316 dissolved oxygen and other nutrients to and removes waste products from eggs incubating in streambed
 317 gravels (e.g. Baxter and Hauer, 2000; Tonina and Buffington, 2011). Hypotheses 2A and 2B are based on
 318 the premise that bull trout redd occurrence is commonly associated with unconfined alluvial valleys and
 319 groundwater discharge to the stream channel (e.g. Baxter and Hauer, 2000). Valley narrowing is
 320 incorporated in hypothesis 2A because a decrease in valley width can decrease cross-sectional alluvial

321 area and can result in hyporheic and groundwater discharge to the stream channel (e.g. Stanford and
322 Ward, 1993; Baxter and Hauer, 2000; Tonina and Buffington, 2009a).

323 I address the subreach-scale hypotheses through field measurements of physical variables in
324 historical high-density spawning reaches of gravel-bed, pool-riffle, mountain headwater streams. I
325 address the valley-scale hypotheses by using remotely sensed delineations of unconfined valleys as well
326 as catchment-scale stream, streambed, and floodplain water temperature measurements. My findings
327 are applicable to salmonid spawning habitat conservation, fisheries management, and stream
328 restoration.

329

330 **METHODS**

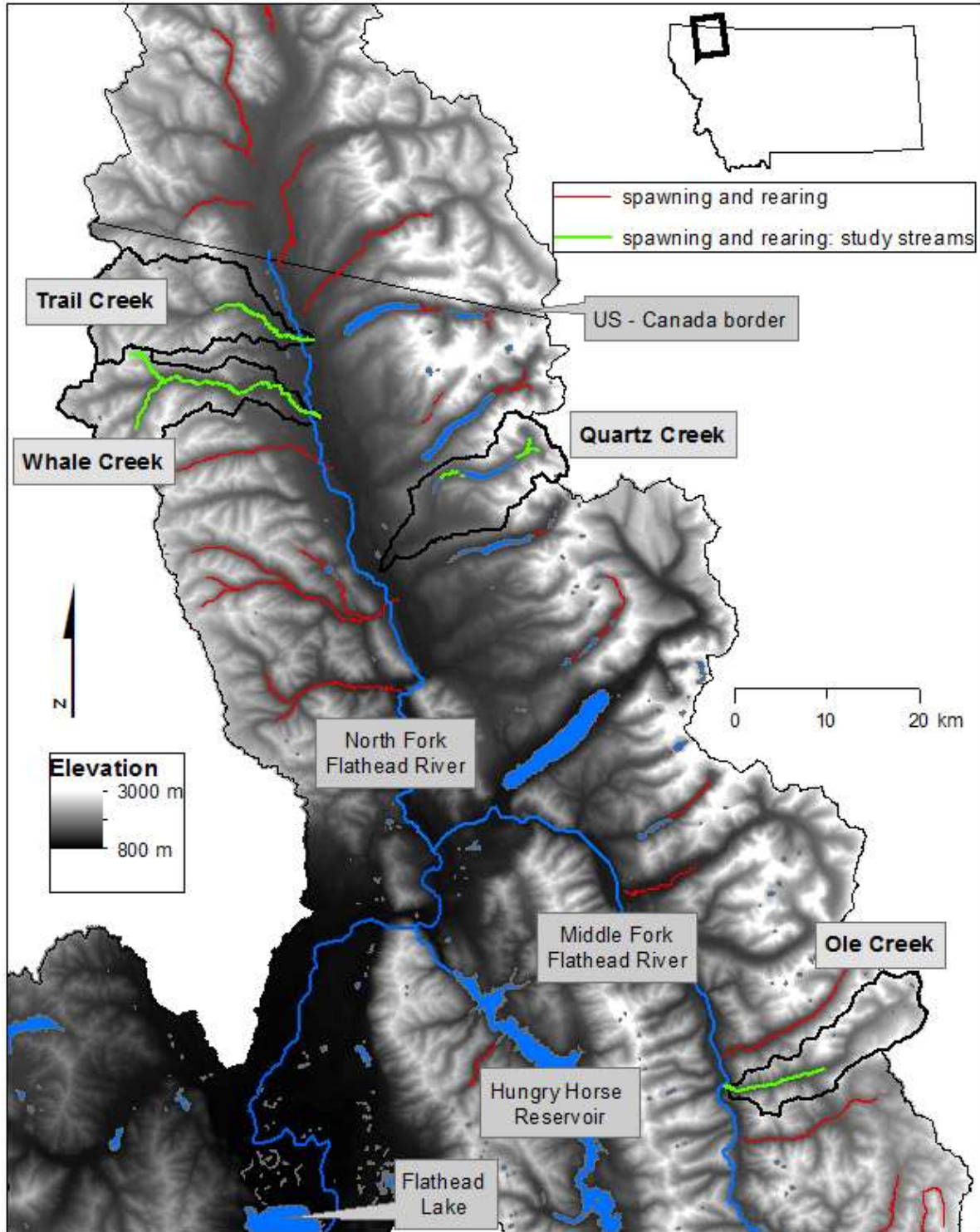
331 Study area

332 The Flathead River Basin is a snowmelt-dominated headwater drainage of the Columbia River
333 and encompasses 18,400 km² of northwestern Montana and southeastern British Columbia (Figure 2).
334 The North and Middle Forks of the Flathead River, in which the study sites described below are located,
335 converge upstream of Flathead Lake and are considered strongholds for native bull trout populations
336 (Fraley and Shepard, 1989; Muhlfeld et al., 2009). Mean annual precipitation in the North and Middle
337 Fork drainages ranges from 55 cm in the valleys to over 215 cm in the highest elevations (Daly and
338 Taylor, 1998). Flow data from 1940 to 2010 indicate that peak annual flows in the North and Middle
339 Fork drainages typically occur in late-May to mid-June (USGS stream gage data, Appendix 1A). Peak
340 annual flows (95th percentiles) occasionally occur while bull trout eggs are incubating in streambed
341 gravels (e.g. in 2007 on November 8; USGS stream gage data, Appendix A). Additionally, the likelihood of
342 fall and winter flood events is increasing (Isaak et al., 2012).

343 The North and Middle Fork basins are underlain by Precambrian Belt Supergroup
344 metasediments (Vuke et al., 2007). Hydrologically, northwestern Montana is characterized by semiarid
345 mountains with permeable soils and low permeability bedrock (Wolock et al., 2004). Shallow hyporheic
346 and groundwater typically transports ~57% of the total catchment outflow whereas overland flow
347 transports ~43% (Santhi et al., 2008).

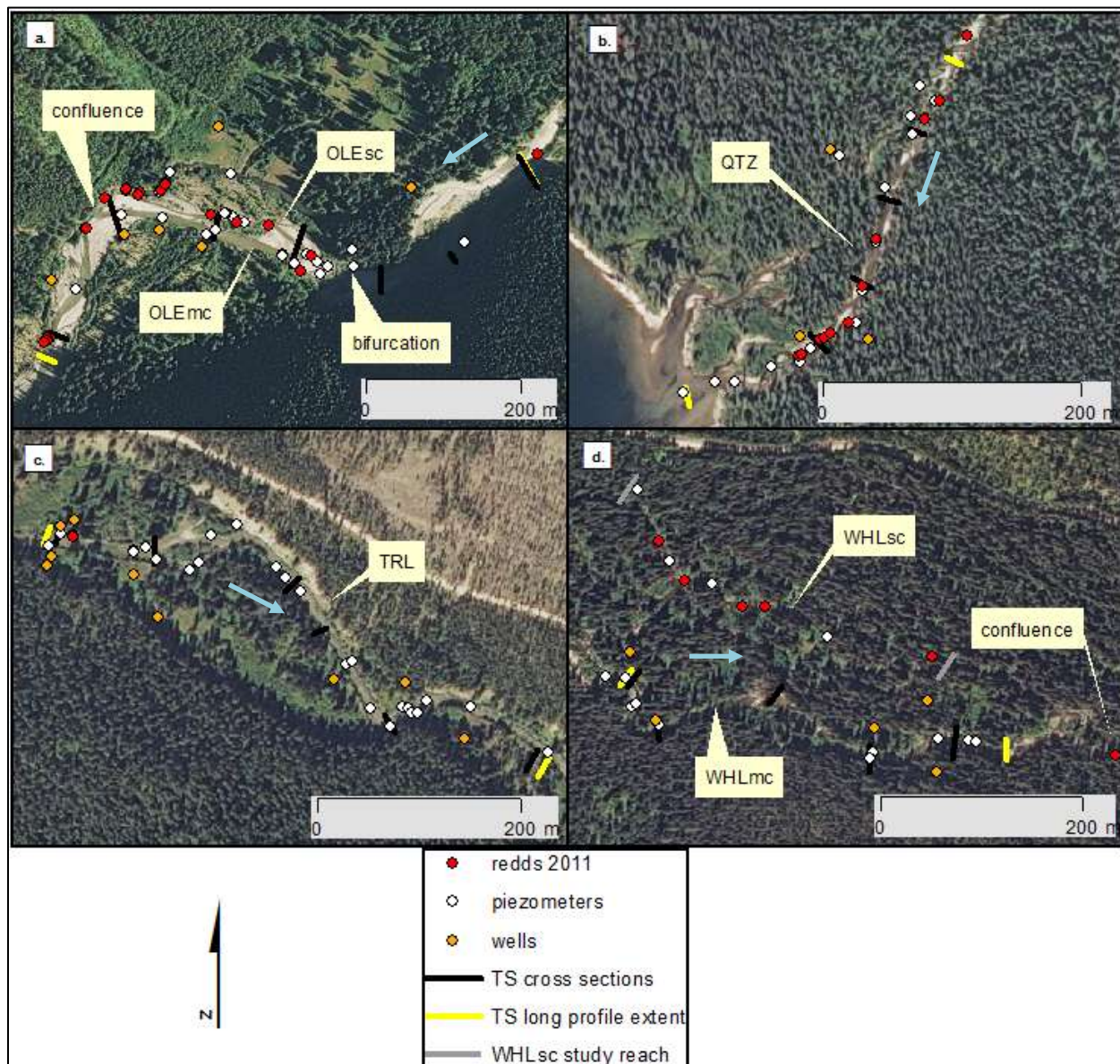
348 For this study, I selected four tributary streams—Ole Creek, Quartz Creek, Trail Creek, and
349 Whale Creek—for field characterization of high-density spawning reaches based on the following
350 criteria: 1) availability of historical bull trout spawning records and active fisheries research and 2) inter-
351 catchment geomorphic variability (Figure 2). Ole and Quartz are within Glacier National Park. Ole is a
352 tributary of the Middle Fork of the Flathead River; Quartz is a tributary of the North Fork and is within
353 the drainage basin of Rainbow Glacier. Draining from the Flathead National Forest, Trail and Whale are
354 also tributaries of the North Fork. Adfluvial bull trout from Flathead Lake spawn in Ole, Trail, and Whale
355 creeks, whereas those spawning in Quartz Creek represent an adfluvial population from Quartz Lake.
356 Bull trout populations in the upper Flathead Lake and River system declined in the early 1990s as a result
357 of community changes related to the invasion of the opossum shrimp (*Mysis diluviana*) in the 1980s into
358 Flathead Lake and the subsequent boom in the non-native lake trout population (Ellis et al., 2011;
359 Muhlfeld et al., 2012). Quartz Lake also hosts a resident lake trout population. Mature, spawning bull
360 trout in the North and Middle Fork drainages are most commonly 6 years old (range 5-8 years old)
361 (Fraley and Shepard, 1989). Focusing my research on headwater snowmelt-dominated streams in the
362 Crown of the Continent ecosystem provided a model to identify natural factors and physical processes
363 influencing bull trout spawning habitat.

364 In evaluating potential study reaches, I first reviewed historical spawning location data and
365 consulted fisheries biologists familiar with the study streams. Secondly, I selected what I estimated to be
366 consistent high density spawning reaches of each study stream for field characterization. All field



367
 368 Figure 2. The study area is part of the Flathead River Basin in northwestern Montana. Stream reaches used by bull
 369 trout for spawning and rearing are highlighted in red and green (USFWS, 2008); green lines indicate the spawning
 370 and rearing reaches of the streams selected for this study. The study catchments are outlined and labeled with
 371 bold text.

372
 373
 374



376
 377 Figure 3. Aerial photographs of the 4 study streams and 6 study reaches. Bull trout redds observed in 2011 are also
 378 shown. Blue arrows show stream flow direction. In the legend, TS means “topographic survey”; WHL_{sc} is the only
 379 study reach not included in the topographic survey. (NAIP (2011) photos)
 380

381 instrumentation and site characterization were completed prior to 2011 spawning because regulatory
 382 constraints prevented direct instrumentation of newly created redds (Figure 3).

383 The selected study reaches in Quartz and Trail contained one primary channel, whereas study
 384 reaches in Ole and Whale contained a main channel and a secondary channel. The secondary channels
 385 of the Ole and Whale study reaches were not connected to the main channels at bankfull discharge. I
 386 treat the secondary channels as separate study reaches. Therefore, there are 4 study streams and 6
 387 study reaches. The 6 study reaches are hereafter referred to as: Ole main channel study reach = OLE_{mc};
 388 Ole secondary channel study reach = OLE_{sc}; Quartz study reach = QTZ; Trail study reach = TRL; Whale
 389 main channel study reach = WHL_{mc}; Whale secondary channel study reach = WHL_{sc} (Figure 3). US Forest
 390 Service roads provided access to the Trail and Whale study sites. The Ole and Quartz sites were

391 accessible only by foot (and boat for Quartz), and site visits required remaining in the backcountry
392 multiple days at a time. Few hydrogeomorphic datasets exist from remote study sites like OLE_{mc}, OLE_{sc},
393 and QTZ.

394 In early October 2011, I assisted fisheries professionals with bull trout redd counts in each of the
395 study streams. In Ole, Quartz, and Trail creeks, I recorded the location of all redds with a handheld
396 Trimble GeoXH 6000 GPS unit. I recorded redd locations in the WHL_{sc} with the same GPS unit; redd
397 locations in WHL_{mc} and throughout the rest of Whale Creek were recorded in paces by fisheries
398 biologists with Montana Fish, Wildlife and Parks.

399

400 1A&B) Reach-scale physical characterization

401 To characterize the geomorphic conditions of the study reaches, I surveyed channel topography,
402 recorded changes in stream stage, measured stream discharge, mapped textural facies, and completed
403 pebble counts (Table 2). I conducted channel topographic surveys with a Leica model TS06 total station
404 (Figure 3). To prepare for the topographic survey, cross section endpoints were staked and their
405 positions recorded with a Trimble GeoXH 6000. Accuracy of these positions was improved by consulting
406 local base station files with the Differential Correction Wizard in GPS Pathfinder Office. These corrected
407 positions were uploaded to the total station to facilitate spatial referencing of the topographic survey.
408 I recorded changes in stream stage in each study stream with Solinst Levellogger Gold Model 3001
409 dataloggers.

410 I used stream discharge measurements and estimations to model the driving forces of stream
411 competence—or the capacity of a flow to mobilize streambed particles. I measured stream discharge in
412 late August (hereafter referred to as the “spawning discharge” or Q_{spawn}) using float test methods (3
413 timed floats over a 20 m distance; velocity correction factor of 0.8) in OLE_{mc}, OLE_{sc}, QTZ, and WHL_{mc} (e.g.
414 Embody, 1927). I did not estimate Q_{spawn} for WHL_{sc}. I estimated Q_{spawn} for TRL as

$$415 \quad (1) \quad Q_{\text{spawn TRL}} = Q_{\text{spawn WHL}_{mc}} * \frac{Q_2 \text{ TRL}}{Q_2 \text{ WHL}_{mc}}$$

416 where Q_2 is a 2-year recurrence interval flood discharge estimate (Equations 2 and 3) (Parrett and
417 Johnson, 2004) (Appendix 1A). Different elements of my analysis required drawing linkages between the
418 Q_2 , for which empirical regional relations are available (Parrett and Johnson, 2004) and which are
419 simulated in the HEC-RAS modeling described below, and field measurements of the bankfull level in the
420 study streams. I adopted a simplifying assumption that Q_2 approximates bankfull discharge (Q_{bf}) (e.g.
421 Woman and Miller, 1960). An assessment of ungaged streams in Montana found that the median ratio
422 of Q_{bf} to Q_2 is 0.84, with considerable variability, across 41 sites (Lawlor, 2004). To estimate Q_2 (Q_{bf}) of
423 the main channels of the study streams, I used the USGS Montana ungaged basin flood-frequency
424 calculator which uses basin and climate characteristics and regression equations to estimate various
425 recurrence interval flood discharges (Parrett and Johnson, 2004; Equations 2 and 3; Table 3). For OLE_{mc},
426 in the Northwest region of Montana, I estimated

$$427 \quad (2) \quad Q_2 = 0.128A^{0.918}P^{1.33}$$

428 and for QTZ, TRL, and WHL_{mc}, in the West region of Montana, I estimated

$$429 \quad (3) \quad Q_2 = 0.268A^{0.927}P^{1.60}(F + 1)^{-0.508}$$

430 where A is drainage area (in mi²), P is mean annual precipitation (in inches), and F is percentage of basin
431 covered by forest (Parrett and Johnson, 2004) (Table 3).

432

433

434 Table 2. Summary of study reach geomorphic field measurements. X's indicate data was collected; -'s indicate data
 435 was not collected.

Study reach	Long profile	Cross sections	Stream	Stream	Textural facies	Pebble counts
			stage change	discharge (Q_{spawn})		
OLE _{mc}	x	7	-	x ^a	x	4
OLE _{sc}	x	3	x	x	x	2
QTZ	x	4	x	x	x	4
TRL	x	6	x	x	x	4
WHL _{mc}	x	5	x	x	x	5
WHL _{sc}	-	-	-	-	x	2

436 ^a I conducted the OLE_{mc} float test discharge measurement adjacent to the OLE_{sc} float test discharge measurement.
 437 Therefore, I estimated the OLE_{mc} discharge upstream of the OLE_{sc} bifurcation (and downstream of the OLE_{sc}
 438 confluence) to be the sum of the OLE_{mc} and OLE_{sc} float test discharge measurements.
 439

440 Table 3. Study reach bankfull discharge (Q_{bf}) estimate input data to the “Basin and climate characteristics model”
 441 of the USGS Montana Ungaged Basin Flood-Frequency Calculator (Parrett and Johnson, 2004).

Stream	Region	Drainage	Mean	Basin	Flood
		area ^a (km ²)	annual precipitation ^b (cm)	forest cover ^c (%)	recurrence interval ^d (yrs)
Ole	Northwest	100	102	NA ^e	2
Quartz	West	30	122	80%	2
Trail	West	140	122	80%	2
Whale	West	130	122	80%	2

442 ^a Calculated at the center of each study reach from 30 m digital elevation models (DEMs).

443 ^b Estimated from mean annual precipitation map provided by the Montana flood frequency calculator; mean
 444 annual precipitation data from the US Soil and Conservation Service (1981).

445 ^c Estimate based on visual field observations.

446 ^d The 2 yr recurrence interval (RI) flood (Q_2) is the lowest RI flood discharge value output by the calculator and is
 447 used as my estimate of bankfull discharge (Q_{bf}) for the study reaches.

448 ^e % basin cover is not included in the Northwest (MT) region flood-frequency regression equation (Equation 2).
 449

450 Textural facies are defined herein as streambed surface patches of distinct grain size (e.g.
 451 Pettijohn, 1975; Kondolf et al., 2003). I created textural facies patch maps (Appendix 1A) from narrated
 452 field video recordings of each study reach in which I walked the study reach and described streambed
 453 grain size and wood distributions. I assigned descriptive grain size codes to each textural facies using the
 454 terminology described by Buffington and Montgomery (1999a). Random-walk pebble counts of the b-
 455 axis of 100 particles (Wolman, 1954) were conducted in the dominant textural facies of each study reach
 456 to estimate the D_{16} (the size for which 16% are finer), D_{50} (median grain size), and D_{84} (the size for which
 457 84% are finer) of each textural facies in each study reach (Kondolf et al., 2003). Particles <2 mm were
 458 recorded as 1 mm (Buffington and Montgomery, 1999b). I did not truncate grain size data collection at 4
 459 or 8 mm as is sometimes recommended (e.g. Wolman, 1954; Kellerhals and Bray 1971; Church et al.,
 460 1987; Bundt and Abt, 2001; Kondolf et al., 2003) because such truncation can distort the size
 461 distribution (Buffington and Montgomery, 1999b). Inclusion of fine particles in pebble count data should

462 not be problematic for characterizing the framework gravel sizes (e.g. Bundt and Abt, 2001; Kondolf et
 463 al., 2003).

464 I assess subreach- and reach-scale streambed mobility of the study reaches at bankfull flows
 465 with calculations of Shields stress (τ^*), a dimensionless measure of stream competence (e.g. Shields,
 466 1936; Church, 2006). The use of a dimensionless parameter allows direct comparisons of stream
 467 competence within and between stream systems. The critical, or threshold Shields stress (τ^*_c) for
 468 streambed particle entrainment in alluvial rivers varies; Buffington and Montgomery (1997) report a
 469 range from 0.03 to 0.086. For this study, I adopt a commonly used τ^*_c value of 0.045 (e.g. Yalin and
 470 Karahan, 1979; Buffington and Montgomery, 1997; Church, 2006; Dingman, 2009). Shields stress (τ^*) is
 471 the ratio of the flow force per unit area (τ_o) to the submerged weight of sediments per unit area
 472 (Church, 2006):

$$473 \quad (4) \quad \tau^* = \frac{\tau_o}{(\rho_s - \rho_w)gD_{50}}$$

474 where

$$475 \quad (5) \quad \tau_o = \rho_w g R S$$

476 and τ_o is total boundary shear stress (in N/m^2), ρ_s is the density of the streambed sediment (estimated as
 477 the density of quartz, 2650 kg/m^3), ρ_w is the density of water (estimated as 1000 kg/m^3), g is the force of
 478 gravity (9.8 m/s^2), D_{50} is median surface grain size (in m), R is hydraulic radius (in m), and S is slope. Total
 479 boundary shear stress (τ_o) is commonly used in the calculation of streambed mobility, although
 480 sediment transport is driven only by the portion of τ_o applied to the streambed – known as bed or grain
 481 shear stress (τ') (e.g. Buffington and Montgomery, 1997). Bed shear stress (τ') is defined as total
 482 boundary shear stress (τ_o) corrected for momentum losses due to hydraulic roughness caused by banks,
 483 bars, and wood debris (e.g. Einstein and Banks, 1950; Einstein and Barbarossa, 1952; Buffington and
 484 Montgomery, 1999b). In gravel-bed rivers, hydraulic roughness due to bedforms alone (e.g. “form drag”)
 485 can cause grain shear stress (τ') to be 10-75% less than total boundary shear stress (τ_o) (e.g. Parker and
 486 Peterson, 1980). Therefore, in order to more accurately calculate streambed mobility in the study
 487 reaches, I calculated an adjusted Shields stress (τ^{**}):

$$488 \quad (6) \quad \tau^{**} = \frac{\tau'}{(\rho_s - \rho_w)gD_{50}}$$

489 I calculate the grain shear stress (τ') using a modified form of an equation suggested by Wilcock et al.
 490 (2009) based on the Strickler relation for grain roughness:

$$491 \quad (7) \quad \tau' = 0.018(SD_{50})^{1/4}U^{3/2}$$

492 where 0.018 represents the density of water, the force of gravity, and the Strickler relation for grain
 493 roughness; and U represents streamflow velocity (in m/s) (Wilcox, 2011).

494 For the Shields stress calculations, I obtained D_{50} values from my textural facies maps and
 495 pebble count data (e.g. Kondolf et al., 2003). Based on visual observations, I grouped the subreaches of
 496 each study reach into textural facies using the classification system of Buffington and Montgomery
 497 (1999a) (Appendix 1). I then conducted pebble counts in each textural facies and used the D_{50} values in
 498 my Shields stress calculations. Additionally, I input channel topography and stream discharge
 499 measurements into the Hydrologic Engineering Center’s River Analysis System (HEC-RAS: Brunner, 2010)
 500 to calculate total boundary shear stress (τ_o), channel slope (S), and streamflow velocity (U) at the
 501 subreach-scale for bankfull conditions (see Appendix 1A for details on HEC-RAS input data and
 502 assumptions). I calculated bankfull Shields stress (τ^*_{bf}) and bankfull adjusted Shields stress (τ^{**}_{bf}) for 20
 503 m long subreach-scale sections in OLE_{mc} , OLE_{sc} , QTZ, TRL, and WHL_{mc} .

504 To characterize the hydrogeologic properties of the study reaches, I installed in-stream mini-
 505 piezometers (hereafter referred to as “piezometers”) and measured vertical hydraulic gradients (VHG),
 506 horizontal hydraulic conductivity (K_h), vertical specific discharge (q_v), vertical hydraulic conductivity (K_v),
 507 and hydraulic conductivity anisotropy ratios (K_h/K_v). Networks of in-stream piezometers were installed

508 by hand throughout each study reach using standard methods at various spatial densities depending on
509 the geomorphic complexity of the reach (Figure 3; Table 4) (Lee and Cherry, 1978; Baxter et al., 2003).

510

511 Table 4. Number of in-stream piezometers per study reach.

Study reach	In-stream piezometers
OLE _{mc}	14
OLE _{sc}	11
QTZ	15
TRL	22
WHL _{mc}	10
WHL _{sc}	4

512

513 All piezometers were 2.54 cm diameter and 152 cm long polyvinyl chloride (PVC) tubes.

514 Piezometers used to characterize streambed horizontal hydraulic conductivity (“slug test piezometers”)

515 had a 20 cm long perforated interval of ~14 drilled holes (~6 mm diameter); this screen section was

516 wrapped with paint strainer nylon mesh. Piezometers not used for horizontal hydraulic conductivity (K_h)

517 characterization had 5-7 cm long perforated intervals of 4 drilled holes (~2 mm diameter). I drove

518 piezometers into the streambed using a similar method to that described by Baxter et al. (2003)

519 (Appendix 1B). Piezometers were installed to an approximate total depth in the streambed of 45 cm,

520 which is below the maximum depth of observed bull trout redd excavation (~25 cm; e.g. Weaver and

521 Fraley, 1991). Characterization of hyporheic flows in spawning reaches allows inferences about the ease,

522 magnitude, and direction of water flows through the streambed prior to redd construction. I made an

523 effort to install piezometers in each textural facies identified in the subreach geomorphic

524 characterization; however some textural facies were too coarse for piezometer installation. Because of

525 literature-supported correlations of spawning with concave-up bedforms (e.g. pool tail-outs: Kondolf,

526 2000; Baxter and Hauer, 2000), I instrumented concave-up bedforms with piezometers more frequently

527 than other bedform types (e.g. mid-riffle). Vertical hydraulic gradient (VHG) measurements were made

528 monthly by hand using a tape measure and water soluble marker. VHG is calculated from the equation

529
$$(8) \quad VHG = \frac{\Delta h}{\Delta l}$$

530 where Δh is the length difference between the water level inside the piezometer to water level of the

531 stream surface, and Δl is the length from the streambed surface to the center of the piezometer

532 perforations at depth.

533 To estimate streambed horizontal hydraulic conductivity (K_h) in OLE_{mc}, QTZ, TRL, and WHL_{mc}, I

534 conducted multiple falling-head slug tests in 4-5 piezometers per study reach by introducing a slug of

535 100 ml of water and measuring head change at 0.5 s or 1 s intervals with a Solinst Levellogger Gold

536 Model 3001. Efforts were made to introduce the slug as instantaneously as possible as recommended by

537 Butler (1998). I attempted to create a streambed surface seal to prevent vertical leakage by stomping

538 and tamping sediment around the piezometer with my wading boots immediately after piezometer

539 installation (e.g. Kondolf et al., 2008). In analyzing my slug test data, I followed the pre-analysis

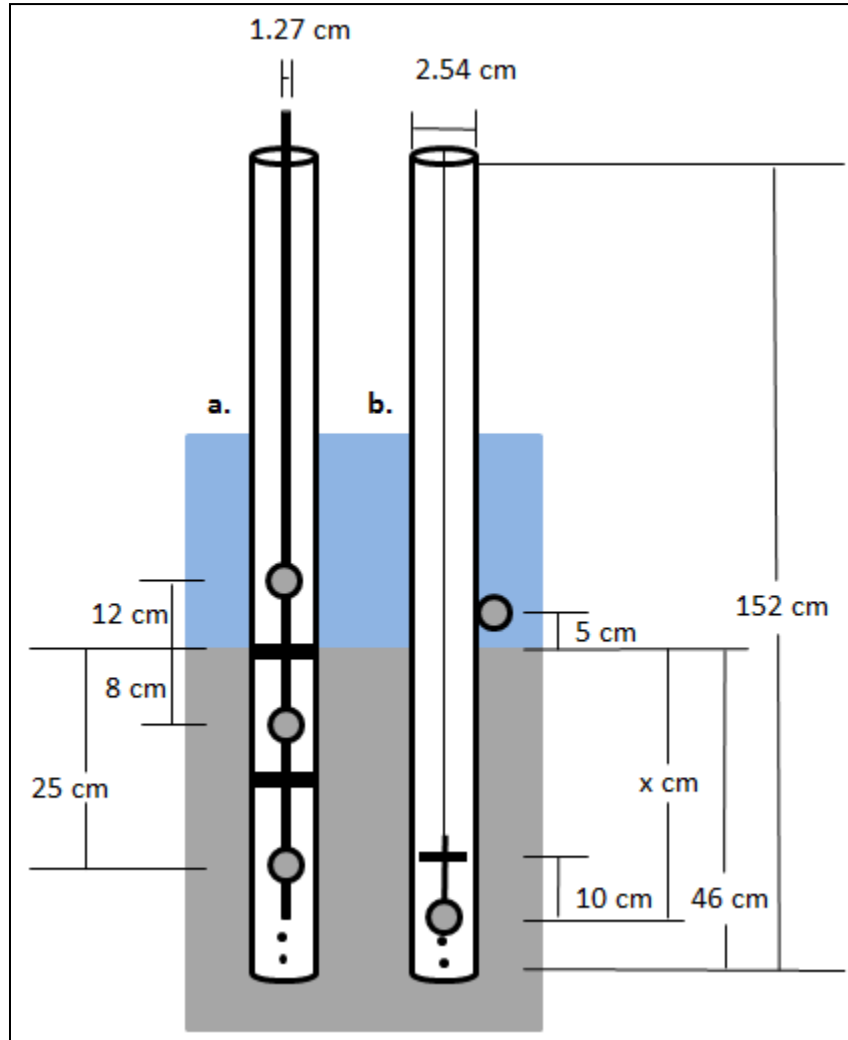
540 processing guidelines of Butler (1998). Because of non-instantaneous slug introduction, I used the

541 translation method (Pandit and Miner, 1986). I normalized water level deviations from static and then

542 used the AquiferTest software package (Schlumberger, 2011) to curve-match the head response data

543 and estimate horizontal hydraulic conductivity (Appendix 1B).

544 To estimate streambed vertical specific discharge (q_v), I installed vertical arrays of Maxim
 545 iButton thermochrons (Part # DS1921Z-F5) inside piezometers (OLE_{mc} n=7; OLE_{sc} n=3; QTZ n=2; TRL n=9;
 546 WHL_{mc} n=5; WHL_{sc} n=2). iButton calibration and vertical array installation procedures were similar to
 547 methods described by Johnson et al. (2005); expected error in the calibrated temperature datasets is
 548 <0.25°C (Johnson et al., 2005). I tested various waterproofing techniques and witnessed occasional
 549 failures of both “waterproofed” and “non-waterproofed” (unaltered) iButtons. To reduce the possibility
 550 of data loss, I deployed all iButtons as pairs. In an attempt to “waterproof” the iButtons, I wrapped each
 551 with parafilm and then covered each with liquid electrical tape. I employed two different vertical array
 552 designs (Figure 4). To analyze the vertical streambed temperature datasets, I first qualitatively described
 553



554 Figure 4. Illustrations of the vertical iButton array designs. iButtons were installed as pairs to reduce the possibility
 555 of data loss if one instrument failed. As stream stage lowered during the field season, I lowered the stream
 556 temperature iButton in design (a) to 6 cm above the streambed. The center rod hosting the iButton pairs in design
 557 (a) was a 1.27 cm diameter PVC tube. The baffles consisted of closed cell foam that was duct taped in place. In
 558 design (b), the stream iButton pair was duct taped to the outside edge of the piezometer on the north side to
 559 minimize solar exposure and potential artificial heat signatures. The inside iButton pair was taped near the bottom
 560 of a 14 cm long bolt that was hung from the top of the piezometer with fishing line. The hanging length varied
 561 from piezometer to piezometer but the iButton pair was intended to be positioned about 10 cm above the bottom
 562 of the piezometer. About 10 cm up from the hanging iButton pair, two 2.5 cm diameter galvanized washers
 563 separated by a nut acted as a baffle to isolate the iButtons.
 564

565 differences between the stream water temperature signal and subsurface water temperature signals
566 using any combination of the metrics coined by Arrigoni et al. (2008): buffered (decrease in amplitude),
567 lagged (difference in phase), or cooled/warmed (difference in mean). Next, for vertical temperature
568 datasets with the most substantial differences, I calculated daily averaged q_v with the MATLAB program
569 Ex-Stream primarily employing the Keery et al. (2007) amplitude ratio method (Swanson and Cardenas,
570 2011). For all designs, I assumed the temperature recorded by the in-stream iButtons to be
571 representative of the water temperature at the stream – streambed interface.

572 At locations where q_v was estimated, I used vertical hydraulic gradient (VHG) measurements
573 from the same piezometer (obtained directly before, during, or after vertical array emplacement) and
574 Darcy's Law to estimate vertical hydraulic conductivity (K_v) (Darcy, 1856):

$$575 \quad (9) \quad K_v = \frac{q_v}{VHG}$$

576 where K_v is in (m/d), q_v is in ($m^3/(m^2d)$), and VHG is dimensionless ($\Delta h/\Delta l$). At sites where both K_h and K_v
577 were determined I calculated the hydraulic conductivity anisotropy ratio (K_h/K_v). Where possible, I
578 compare and contrast conditions within a study reach; however, much of my analysis focused on inter-
579 study reach comparisons of reach-averaged hydrogeologic variables.

580

581 2A&B) Valley-scale physical characterization

582 At the valley-scale (Figure 1d), I evaluated the influence of valley confinement on spawning
583 occurrence. Delineations of unconfined and confined valleys were conducted for all tributary
584 catchments of the Flathead River Basin by Wenger et al. (2011) using ground slope and convolution
585 filtering methods of 30 m digital elevation models (DEMs) and NHDPlus streamlines (Wenger et al.,
586 2011). Unconfined valley inclusion criteria included maximum ground slope of 8%, maximum valley
587 width of 500 m, minimum stream length of 1500 m, and minimum valley area of 3700 m^2 (Nagel et al., *in*
588 *press*). Field validation by Wenger et al. (2011) indicated that the valley confinement algorithm
589 successfully distinguished unconfined and confined valley segments in the interior Columbia River Basin.
590 Occasionally, the Wenger et al. (2011) valley confinement algorithm mistakes terraces for valley
591 bottoms (David Nagel, 2012, personal communication). A new version of the algorithm (Nagel et al., *in*
592 *press*) fixes this problem with a flooding routine (David Nagel, 2012, personal communication)) but was
593 not applied here. I edited unconfined valley delineations of each study catchment in ArcMap 10.0 based
594 on field and DEM observations (Appendix 2A).

595 I characterized valley confinement of the study reaches using the valley confinement ratio (VCR)

$$596 \quad (10) \quad VCR = \frac{\text{unconfined valley width}}{\text{active channel width}}$$

597 I estimated unconfined valley width (in m) of each study reach from the Wenger et al. (2011) unconfined
598 valley polygons as the average valley width at the upstream end, center, and downstream end of each
599 study reach. I estimated valley width of confined valley sections as 30 m (because 30 m DEMs were used
600 to create the unconfined valley polygons). I estimated study reach active channel width (in m) as reach-
601 average bankfull channel width. I obtained reach-average bankfull channel widths for OLE_{mc} , OLE_{sc} , QTZ,
602 TRL, and WHL_{mc} from the channel cross sections surveys. I visually estimated reach-average bankfull
603 channel width for WHL_{sc} . Unconfined valleys are generally described by VCRs > 2.5-5.0; VCRs < 2.5-5.0
604 indicate confined valleys (e.g. Hall et al., 2007; Nagel et al., *in press*).

605 To characterize valley confinement characteristics near bull trout redds observed throughout
606 the study catchments in the 2011 count, I first recorded whether or not each redd was located in an
607 unconfined valley using the edited Wenger et al. (2011) unconfined valley delineations. For redds
608 located in unconfined valleys, I made general observations of valley narrowing, broadening, or
609 remaining constant in the downstream direction. Representations of these qualitative assessments of
610 rate of change in valley width are presented in the results. Due to the coarse scale of the unconfined
611 valley delineations and the error associated with their creation, broad qualitative observations were

612 more appropriate than quantitative measurements of change in valley width at redd locations.
613 Quantitative measurements of change in valley width at redd clusters were attempted, but the
614 differences in spatial resolution of the unconfined valley delineations (coarse) and redd clusters (fine)
615 limited the utility of these assessments.

616 To characterize the valley-scale (Figure 1d) hydrogeology and surface water – groundwater
617 interactions, I installed a limited network of shallow floodplain wells adjacent to each study reach to
618 determine floodplain water table elevations and floodplain water temperatures (Figure 3). These wells
619 were the same dimensions and material as the in-stream piezometers and were installed to a maximum
620 depth of 140 cm. Each floodplain well was paired with an in-stream piezometer positioned on the same
621 perpendicular line from the stream channel to act as a staff gage. I surveyed the elevations of the tops
622 of the wells and staff gage piezometers to compare water level elevations between the floodplain and
623 stream. I measured water table elevations monthly by hand per stream section on the same day that I
624 measured VHGs of the in-stream piezometers. Using monthly water table and stream stage
625 measurements in August, September, and October, I created potentiometric surface maps by plotting
626 the floodplain wells and in-stream staff gages spatially in ArcMap 10.0 and hand drawing contour lines
627 of water table elevation. Taking into account the valley confinement polygons, I drew floodplain alluvial
628 subsurface water flow lines perpendicular to the water table contour lines (Appendix 2B) (Fetter, 2001).

629 I assessed the influence of hyporheic exchange and valley-scale groundwater system discharges
630 associated with spawning reaches using shallow floodplain water temperature datasets from the study
631 reaches and catchment-wide stream temperature datasets. I instrumented at least one floodplain well
632 in each study reach with a pair of iButton thermochrons to measure floodplain water temperature
633 through time. I obtained the stream temperature datasets from upstream and downstream of my study
634 reaches from the USGS and the Flathead National Forest (Appendix 2B). I compared floodplain water
635 temperature data to stream water temperature in the study reaches to evaluate hyporheic mixing
636 processes and rates. I also estimated the temperature of theoretical regional groundwater at 10-25 m
637 depth as 1-2°C higher than average annual air temperature (Kaselow, 2001). I estimated average annual
638 air temperature of the study area as the average air temperature from 2007-2011 recorded by the 3
639 most proximal SNOTEL stations (Appendix 2B). The SNOTEL station elevations are within 150 m of the
640 study reach elevations (Appendix 2B).

641 Water temperature metrics calculated for various durations included average, standard
642 deviation, rate of change (dT/dt), and coefficient of variation (C_v). Coefficient of variation (C_v) is a
643 dimensionless measure of the extent of variability in relation to the average of a sample population:

$$644 \quad (11) \quad C_v = \frac{\sigma}{\bar{T}}$$

645 where σ is the standard deviation in water temperature (in Kelvin), and \bar{T} is the average water
646 temperature (in Kelvin). Kelvin temperatures must be used because C_v is computed from a ratio scale
647 rather than an interval scale, such as Celsius. In analyzing the stream temperature datasets, I considered
648 sensor distribution in relation to the valley confinement delineations.

649

650 Statistical analyses

651 I statistically tested relationships between physical factors and redd density of the study reaches
652 using linear, exponential, and power function regressions (using SigmaPlot 12.3). For each pair of
653 independent and dependent variables, I present the regression with the strongest explanatory power.
654 At the subreach-scale, I tested the dependence of redd density on subreach bankfull and adjusted
655 bankfull Shields stress (τ_{bf}^* , τ_{bf}^{**}) within and among the study reaches. To satisfy statistical test
656 assumptions of normal distribution (Shapiro and Wilk, 1965) and constant variance, I log transform
657 subreach-scale redd density. For subreach channel sections, I calculate redd density as

$$658 \quad (12) \quad \text{subreach redd density} = \frac{\text{redds}}{(20 \text{ m}) * (\bar{w})}$$

659 where 20 m represents the longitudinal subreach section length and \bar{w} represents average channel
660 width (in m) per study reach at the time of spawning.

661 At the reach-scale, I tested the dependence of reach-average redd density on reach-averaged
662 physical variables (D_{16} , D_{50} , D_{84} , τ_{bf}^* , τ_{bf}^{**} , slope, VCR, VHG, K_h , q_v , K_v , average stream temperature
663 during spawning, standard deviation in stream temperature, and stream temperature C_v). I calculated
664 reach-average redd density as:

$$665 \quad (13) \quad \text{reach average redd density} = \frac{\text{redds}}{(L_{sr}) * (\bar{w})}$$

666 where L_{sr} was study reach length (in m).

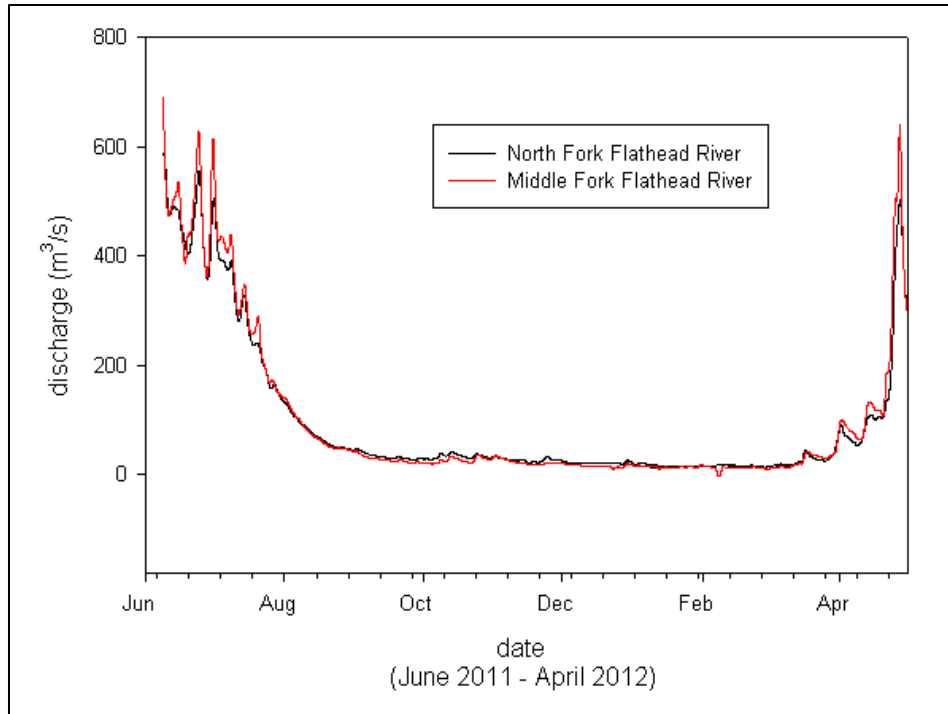
667 I also tested statistical relationships among reach-average physical variables, including the
668 dependence of (1) reach-average D_{50} on reach-average slope and reach-average VCR, (2) reach-average
669 slope on VCR, and (3) various reach-averaged hydrogeologic variables (VHG, K_h , q_v , and K_v) on reach-
670 averaged geomorphic variables (D_{50} , τ_{bf}^{**} , and VCR). Multiple regression analyses of reach-average redd
671 density dependence on physical variables were attempted but were limited by collinearity of physical
672 variables and dataset size.

673

674 RESULTS

675 Flow data from gages on the North Fork and Middle Fork Flathead Rivers, which were used to
676 infer flow conditions in the study reaches, show that in the spring runoff period preceding my data
677 collection (i.e., spring 2011), peak flow magnitudes were above average, with a 3 year recurrence
678 interval (RI) on the North Fork and a 5 year RI on the Middle Fork (USGS gage data; Figure 5; Appendix
679 1A). Peak flows occurred on June 8 at these gages, within the normal May to June time range of peak
680 discharges in these rivers. Baseflow conditions characterized the majority of the 2011-2012 spawning
681 and incubation period (Figure 5). September (spawning) stream stage in each of study reaches
682 fluctuated less than +/-0.15 m (Appendix 1A).

683 In October 2011, the number of redds observed in the Ole, Quartz, and Whale drainages, 40, 35,
684 and 42, respectively, was in the range of redds observed over the previous decade (Table 5). In Trail, the
685 8 redds counted in 2011 was the lowest since 1996 (also 8 redds; Fraley, 2010). Redd densities in the
686 study reaches in 2011 ranged from 0 redds/m² in WHL_{mc} to 0.004 redds/m² in OLE_{sc} (Table 6).



687
 688 Figure 5. USGS stream gage data for the North and Middle Forks of the Flathead River (USGS gage numbers: North
 689 Fork 12355500; Middle Fork 12358500) from the 2011 peak flow (June 8) through spawning (August through
 690 October; e.g. Fraley and Shepard, 1989) and emergence (February through April; e.g. Baxter and Hauer, 2000).

691
 692 Table 5. Historical redd numbers in the index sections of the study streams.

Year	Ole ^a	Quartz ^a	Trail ^b	Whale ^b
2000	33		42	68
2001	29		27	77
2002	21		26	71
2003	21	31	14	34
2004	14	46	34	41
2005	16 ^c	4 ^c	30	39
2006	31	36	34	56
2007	29	14 ^d	51	27
2008	42	51	49	34
2009	34	34	19	43
2010	32	27	11	31
2000-2010 Avg.	27	30	31	47
2011	40 ^e	35 ^f	8 ^g	42 ^h
2011 % of 2000-2010 Avg.	148%	117%	25%	89%

693 ^a Data from Downs et al. (2011). The Quartz index section does not include Rainbow Creek (from the mouth of
 694 Cerulean Lake downstream to the confluence with Quartz Creek).

695 ^b Data from Fraley (2010).

696 ^c High flows may have obliterated some redds – minimum count (Downs et al., 2011).

697 ^d Weir at mouth of Quartz Creek likely inhibited spawning activity (Tennant, 2010; Downs et al., 2011).

698 ^e Redd count by John Fraley, Chris Downs, and Jared Bean.

699 ^f Redd count by Clint Muhlfeld and Jared Bean. Does not include the 8 additional redds observed in Rainbow Creek
 700 near the Mouth of Cerulean Lake.

701 ^g Redd count by Mark Deleray, Clint Muhlfeld, and Jared Bean.

702 ^h Redd count by Mark Deleray and Gary Michael.

703

704 Table 6. Study reach geomorphic characteristics and 2011 redd numbers per study reach.

Study reach	Channel length (m)	W_{spawn}^b (m)	Slope	Reach-avg. D_{50} (mm)	2011 Q_{spawn} (m^3/s)	2011 Q_{bf} (m^3/s)	Redds in study reach (2011)	Reach-avg. redd density (redds/m^2)
OLE _{mc}	890	11	1.1%	49	3.4 ^c	14	7	0.0007
OLE _{sc}	360	7	1.2%	18	1.6	-	9	0.004
QTZ	400	8	0.74%	22	2.4	4.1	10	0.003
TRL	620	16	1.0%	76	3.9	16	1	0.0001
WHL _{mc}	490	13	0.36%	45	3.5	15	0	0
WHL _{sc}	390 ^a	6	-	16	-	-	5	0.002

705 ^a All study reaches were topographically surveyed except WHL_{sc}; 390 m is the observed channel length for WHL_{sc}.

706 ^b Reach-average channel width at Q_{spawn} .

707 ^d Discharge of OLE_{mc} upstream of OLE_{sc} bifurcation.

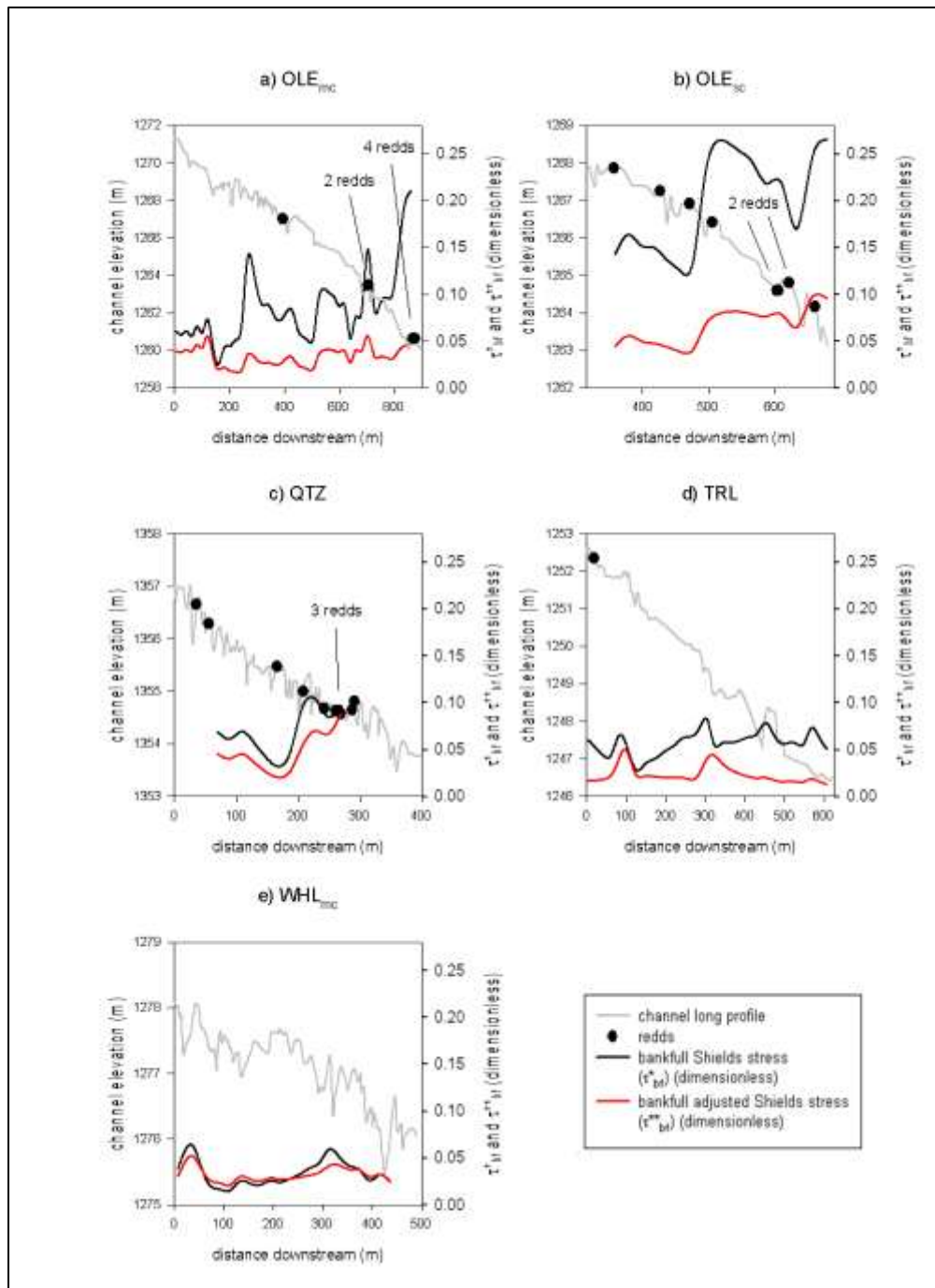
708

709 1A) Reach-scale fluvial geomorphology

710 Redds in the study reaches tended to be located in concave-up bedforms (Figure 6, Figure 7) and
 711 the finest textural facies of the study reaches (Figure 6, Figure 8, Appendix 1A). At the subreach-scale,
 712 considering all study reaches, redd density was significantly ($\alpha=0.05$) positively correlated with subreach
 713 bankfull Shields stress (τ_{bf}^* , $p=0.04$) and bankfull adjusted Shields stress (τ_{bf}^{**} , $p=0.02$) (Figure 9a,b).
 714 Within individual study reaches, subreach-scale redd density was not significantly related to subreach
 715 bankfull or bankfull adjusted Shields stress (Figure 9c).

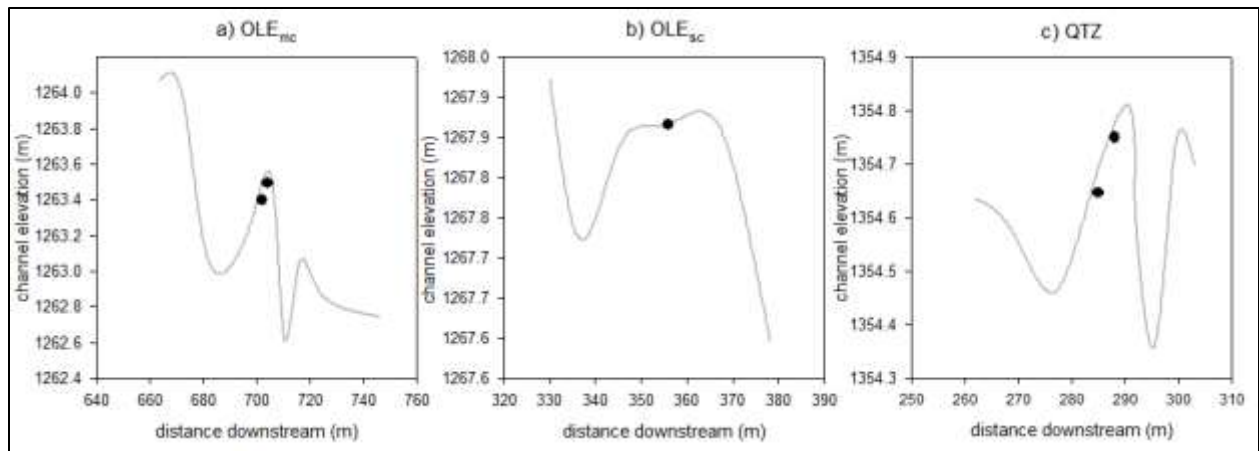
716 At the reach-scale, study reach redd density was significantly negatively correlated with reach-
 717 averaged D_{16} ($p=0.01$), D_{50} ($p=0.02$), and D_{84} ($p=0.02$) (Figure 10, Table 7). Reach-average redd density
 718 was significantly positively correlated with τ_{bf}^{**} ($p=0.02$) (Figure 11, Table 7). There was no relationship
 719 between reach-average slope and D_{50} ($R^2=0.00$; $p=1.0$; Figure 12. Modeled bankfull adjusted Shields
 720 stresses (τ_{bf}^{**}) in the majority of subreach streambed sections in OLE_{sc}, the study reach with the highest
 721 redd density, are above the 0.045 value of critical Shields stress (τ_c^*) that is often considered the
 722 threshold for particle entrainment (Figure 13). Based on visual observations and patch maps, median
 723 surface grain size (D_{50}) of spawning sites in OLE_{sc}, QTZ, and WHL_{sc} were ~16-18 mm; in OLE_{mc}, D_{50} of
 724 spawning sites was ~35 mm. Variation in D_{50} of dominant textural facies is most prominent in OLE_{mc},
 725 TRL, and WHL_{mc} (Figure 6, Figure 8). Streambed grain size distributions in OLE_{sc}, QTZ, and WHL_{sc} are
 726 relatively consistent (Figure 5, Figure 8). Based on qualitative visual assessment, I rank the study reaches
 727 in terms of relative hydraulic roughness (e.g. bar, bank, and wood roughness) from highest to lowest as
 728 WHL_{sc}, QTZ, WHL_{mc}, OLE_{sc}, OLE_{mc}, and TRL.

729

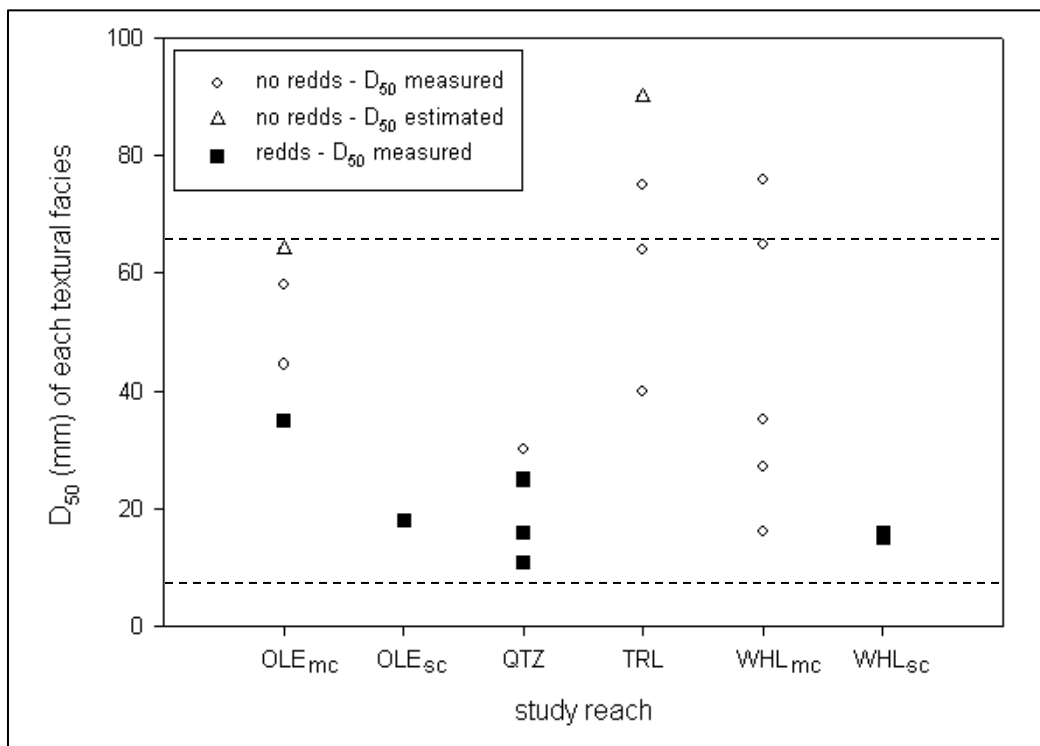


730
731
732
733

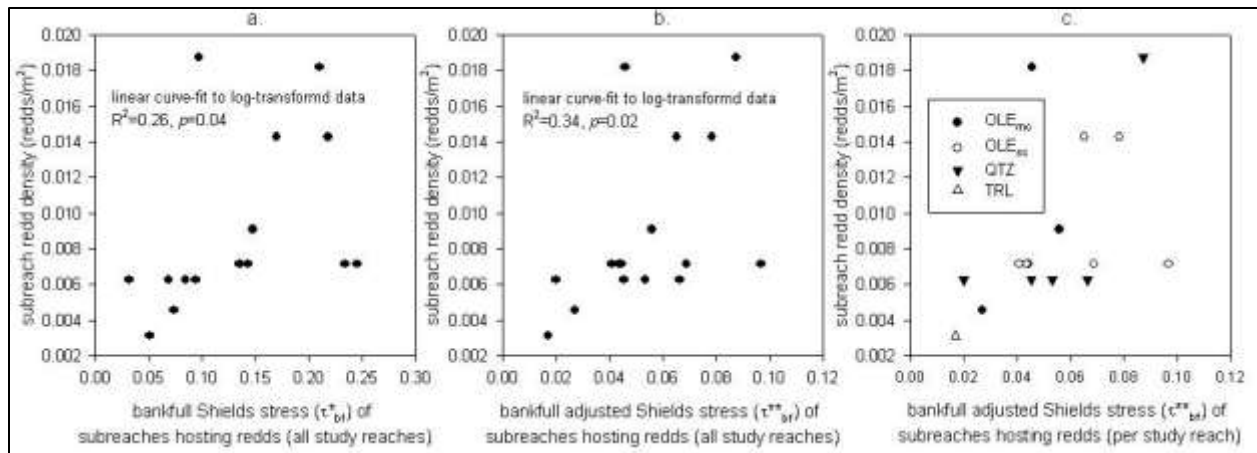
Figure 6. Redd locations in relation to study reach channel long profile, bankfull Shields stress, and bankfull adjusted Shields stress. WHL_{sc} is not included in these plots because it was not topographically surveyed. Finer-scale examples of redd location in relation to bedform curvature are presented in Figure 7.



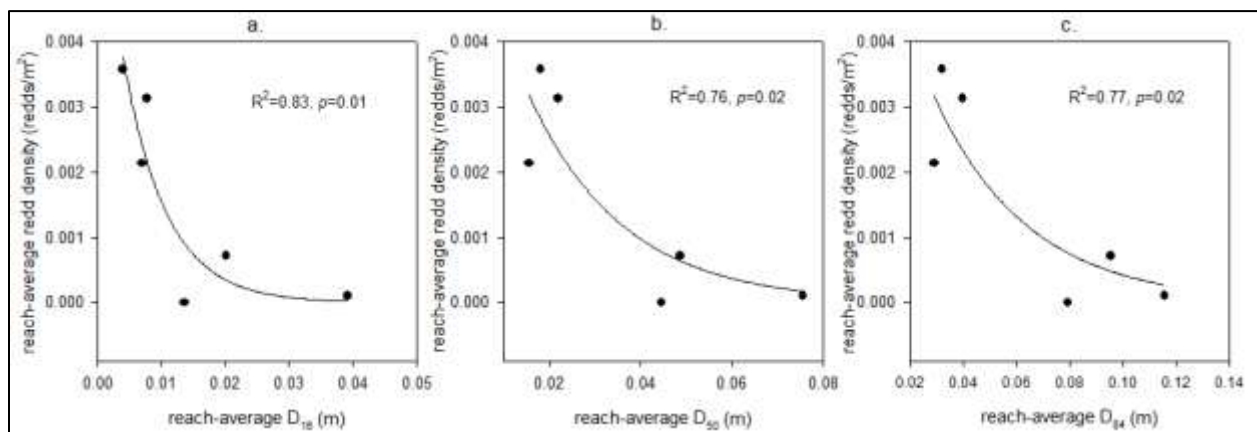
734
735 Figure 7. Examples of redds (black dots) in concave-up bedforms. Gray lines represent streambed long profile.
736



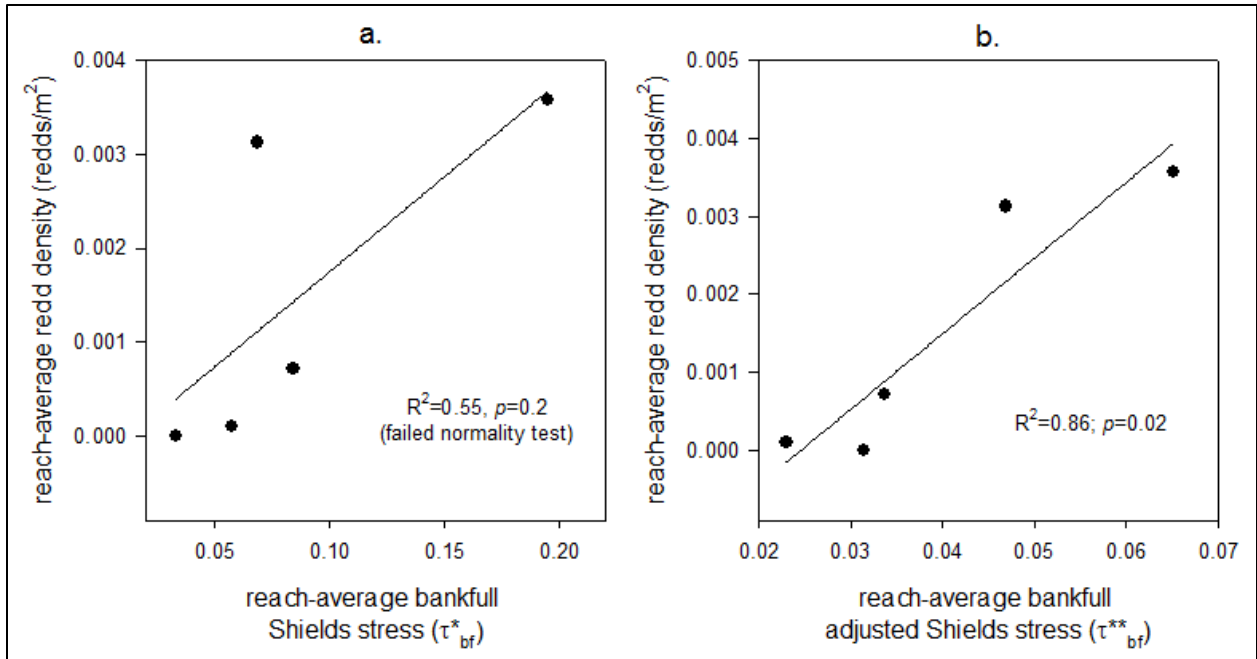
737
738 Figure 8. Median surface grain size (D_{50}) of the primary textural facies of each study reach, based on pebble counts
739 that were used to characterize the textural facies. D_{50} values of the coarsest textural facies in Ole and Trail were
740 visually estimated (Appendix 1A). Textural facies observed hosting 2011 redds are indicated with black boxes. The
741 dashed lines indicate the lower (8 mm) and upper (64 mm) bounds of the reported range of suitable spawning
742 gravel D_{50} for bull trout (Baxter and McPhail, 1996; Dunham et al., 2001).
743
744



745
 746 Figure 9. Subreach-scale bankfull and bankfull adjusted Shields stress (τ_{bf}^* , τ_{bf}^{**}) versus redd density: (a) and (b)
 747 show subreach sections hosting redds from all study reaches, and (c) shows subreach sections hosting redds per
 748 study reach. Linear curve-fits to log transformed data in (a) and (b) satisfy statistical assumptions (normality and
 749 constant variance) and describe statistically significant relationships. Regression equations: (a) $y = -2.3169 + 1.6254x$;
 750 (b) $y = -2.3893 + 5.4154x$; (c) $OLE_{mc}: y = -2.6050 + 13.158x$ ($R^2 = 0.41$, $p = 0.6$, failed constant variance test); $OLE_{sc}: y =$
 751 $-2.1921 + 2.1086x$ ($R^2 = 0.09$, $p = 0.5$, failed constant variance test); $QTZ: y = -2.4513 + 6.2901x$ ($R^2 = 0.54$, $p = 0.2$).
 752

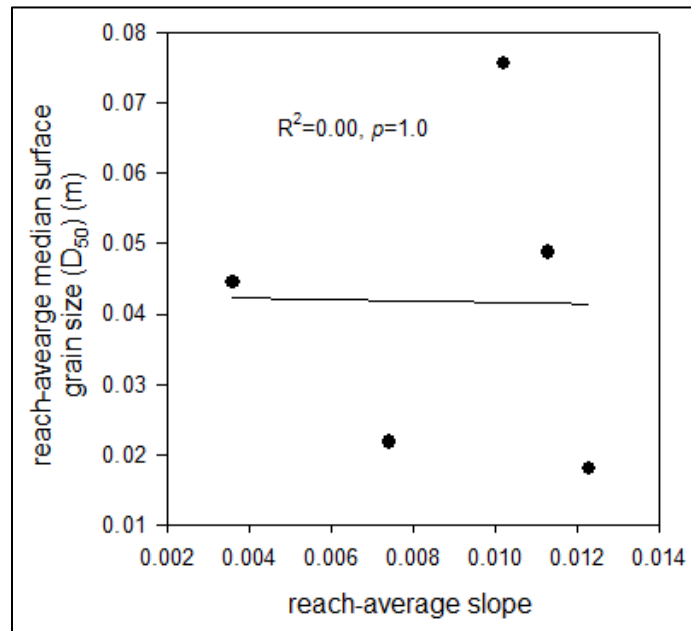


753
 754 Figure 10. Reach-averaged grain size metrics (D_{16} , D_{50} , D_{84}) versus reach-averaged redd density. Regression
 755 equations: (a) $y = 0.0068 * \exp(-148.2543x)$; (b) $y = 0.0068 * \exp(-48.4346x)$; (c) $y = 0.0072 * \exp(-28.3850x)$.
 756



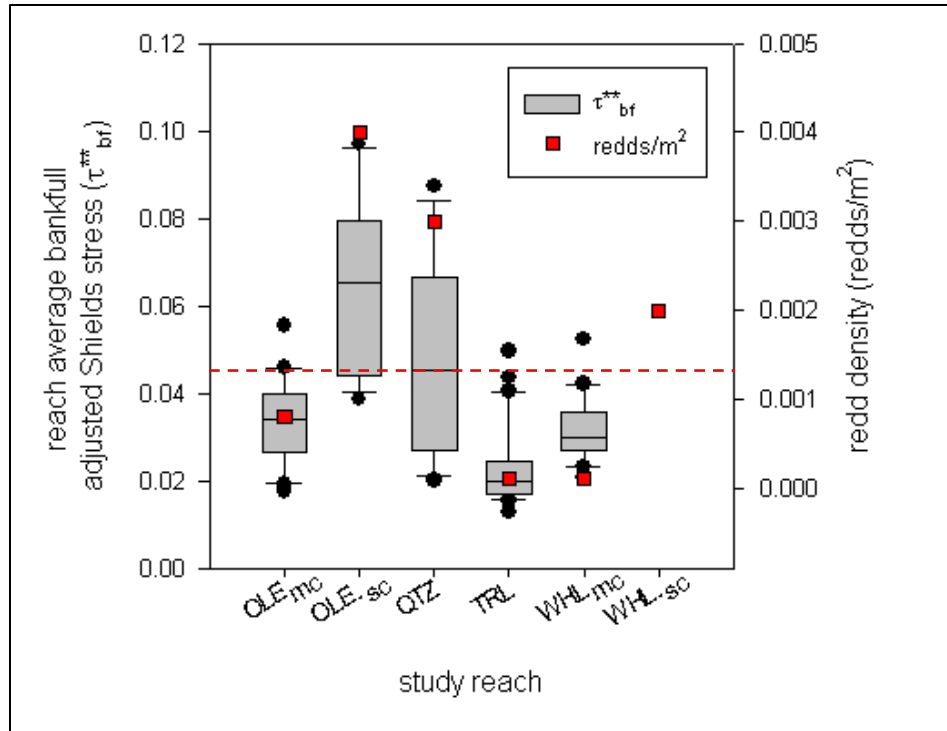
757
758
759
760
761

Figure 11. Reach-averaged (a) bankfull and (b) bankfull adjusted Shields stress (τ_{bf}^* , τ_{bf}^{**}) versus reach-averaged redd density (for all study reaches except WHL_{sc}). Regression equations: (a) $y = -0.0003 + 0.0202x$; (b) $y = -0.0024 + 0.0969x$.



762
763
764

Figure 12. Study reach streambed slope versus reach-averaged median surface grain size (D_{50}).



765 Figure 13. Distribution of subreach-scale bankfull adjusted Shields stress (τ^{**}_{bf}) in each study reach. Study reach-
 766 average redd density is also plotted. WHL_{sc} was not topographically surveyed, therefore I did not model shear
 768 stress distributions in that study reach. The dashed red line represents critical Shields stress ($\tau^*_c=0.045$), an often-
 769 cited threshold for streambed particle entrainment in alluvial rivers (e.g. Yalin and Karahan, 1979). Solid lines
 770 within the box plots represent medians; boxes bound the upper and lower quartiles; whiskers illustrate upper and
 771 lower tenths; solid dots represent extrema. (OLE_{mc} n=42; OLE_{sc} n=17; QTZ n=11; TRL n=30; WHL_{mc} n=21.)
 772
 773

774 Table 7. Reach-average correlations between measured physical variables and redd density. Reach-average redd
 775 density is the y variable for all regressions. Statistically significant relations are bold ($p < 0.05$).

x variable	n	R ²	p	Equation
D₁₆	6	0.83	0.01	y=0.0068*exp(-148.2543*x)
D₅₀	6	0.76	0.02	y=0.0068*exp(-48.4346*x)
D₈₄	6	0.77	0.02	y=0.0072*exp(-28.3850*x)
τ* _{bf}	5	0.55	0.2 ^a	y=-0.0003+0.0202*x
τ**_{bf}	5	0.86	0.02	y=-0.0024+0.0969*x
slope	5	0.14	0.5	y=-0.0001+0.1794*x
VCR	6	0.08	0.6	y=0.0009+0.0000356*x
VHG	6	0.00	0.9	y=0.0017+0.0006*x
K _h	4	0.02	0.8 ^b	y=0.0015-0.0000035156*x
q _v	5	0.00	1.0	y=0.0012-0.00003555*x
K _v	5	0.14	0.5	y=0.0004+0.00004953*x
Stream temperature (9/27/11-10/10/11)				
Avg.	6	0.38	0.2	y=-0.0064+0.0012*x
σ	6	0.02	0.8	y=0.0008+0.0015*x
C _v	6	0.02	0.8	y=0.0026-0.0119*x

776 ^a Shapiro-Wilks normality test failed.

777 ^b Constant variance test failed.

778

779 1B) Reach-scale hydrogeology

780 Of the subreach-scale physical hydrogeologic variables measured (VHG, K_h, q_v, and K_v), reach-
 781 averaged values were not significantly related to reach-average redd density between the streams
 782 (Table 7, Figure 16). Streambed water temperature data in the study reaches tended to mimic stream
 783 water diurnal cycles. In late September, during the spawning period, average streambed temperatures
 784 at ~25 cm depth were <2% different from stream temperatures (Table 8). Stream and streambed
 785 temperatures in OLE_{mc} and QTZ were warmer than the reported 7°C threshold of spawning appropriate
 786 water temperature, whereas water temperatures in TRL and WHL_{mc} were below the threshold (Table 8)
 787 (streambed temperatures for WHL_{sc} were not measured in this time window) (e.g. Goetz, 1989; Fraley
 788 and Shepard, 1989; Sauter et al., 2000). Additional water temperature data are presented in Results
 789 section 2B.

790 In September and October, during the spawning and early incubation period, streambed vertical
 791 hydraulic gradients (VHG) for all study reaches were dominantly downward indicating overall movement
 792 of stream water into the streambed (Figure 14). Vertical hydraulic gradients (VHGs) within the study
 793 reaches exhibited little change from September to October (Figure 14).

794 Horizontal hydraulic conductivity (K_h) measurements in the study reaches ranged from 35-660
 795 m/d (Figure 15a). Reach-average K_h showed no correlation with redd density (R²=0.02, p=0.8; Table 7;
 796 Figure 16a). The falling-head slug test responses ranged from over-damped to critically-damped to
 797 under-damped and tended to equilibrate within 5-10 seconds (Appendix 1B). Horizontal hydraulic
 798 conductivity (K_h) values reported here have substantial uncertainty as differences in estimated K_h values
 799 where the datalogger was measuring head change at the 1 s intervals ranged from 0%-160%; at 0.5 s
 800 intervals, differences in K_h derived from repeat slug tests ranged from 0%-90% (Appendix 1B).

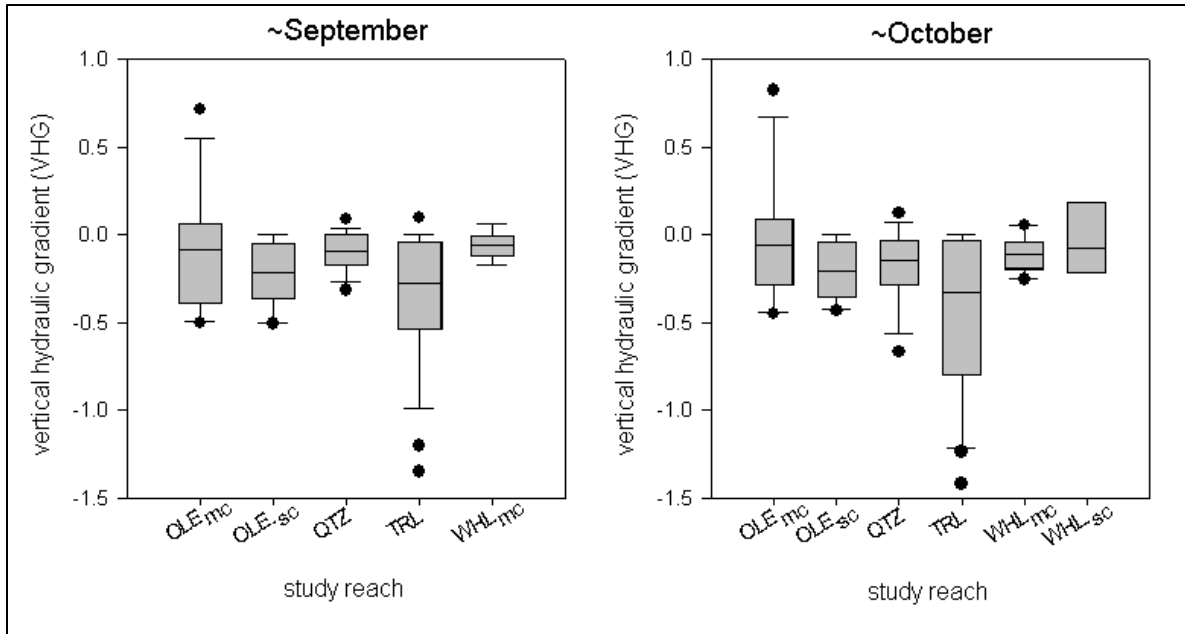
801 Comparing K_h values derived from 1 s and 0.5 s curves at a single piezometer, differences ranged from
 802 0%-440% (Appendix 1B). However, 0.5 s interval tests did not consistently compute higher or lower K_h
 803 values than 1 s interval tests. Considering error margins and sample sizes, there is no distinguishable
 804 difference in K_h between the study reaches.

805 In agreement with the VHG data, vertical streambed temperature arrays in each study reach
 806 indicate streambed water vertical flux (q_v) is dominantly downward throughout the study period (Figure
 807 15b). Vertical thermochron datasets analyzed in Ex-Stream indicated q_v ranged from $+1.6 \text{ m}^3/(\text{m}^2\text{d})$
 808 (upward) to $-2.5 \text{ m}^3/(\text{m}^2\text{d})$ (downward) with median values per study reach varying between -2.0 to -0.5
 809 $\text{m}^3/(\text{m}^2\text{d})$ (Figure 15b). Reach-average q_v showed no correlation with redd density ($R^2=0.02$, $p=0.8$; Table
 810 7; Figure 16b). Due to uncertainty and error in the q_v estimates as well as the low sample numbers in
 811 each study reach, comparisons of inter-stream q_v beyond the general range of values are not presented.
 812 Although downward streambed flux dominated the study reaches, spawning preference for downward
 813 or upward streambed flux was not detected as redds were observed <2 m from piezometers of both
 814 downwelling and upwelling flux signatures. Vertical streambed streambed flux (q_v) datasets typically
 815 ranged in extent from 36-40 days; total rate of change in flux over this time period ranged from 0.02% -
 816 7% with an average of 3% (Appendix 1B). Vertical hydraulic conductivity (K_v) values in the study reaches
 817 ranged from 3 m/d to 58 m/d and cluster in the range of 3 m/d to 15 m/d (Figure 15c). Reach-averaged
 818 K_v exhibited the strongest correlation (positive) to reach-average redd density of all streambed
 819 hydrogeologic properties measured (Table 7, Figure 16). Again, due to the low sample numbers in each
 820 study reach, comparisons of inter-study reach K_v beyond the general range of values is not warranted.
 821 Hydraulic conductivity anisotropy ratios (K_h/K_v) in the study reaches ranged from 3-150 (Figure 15d).

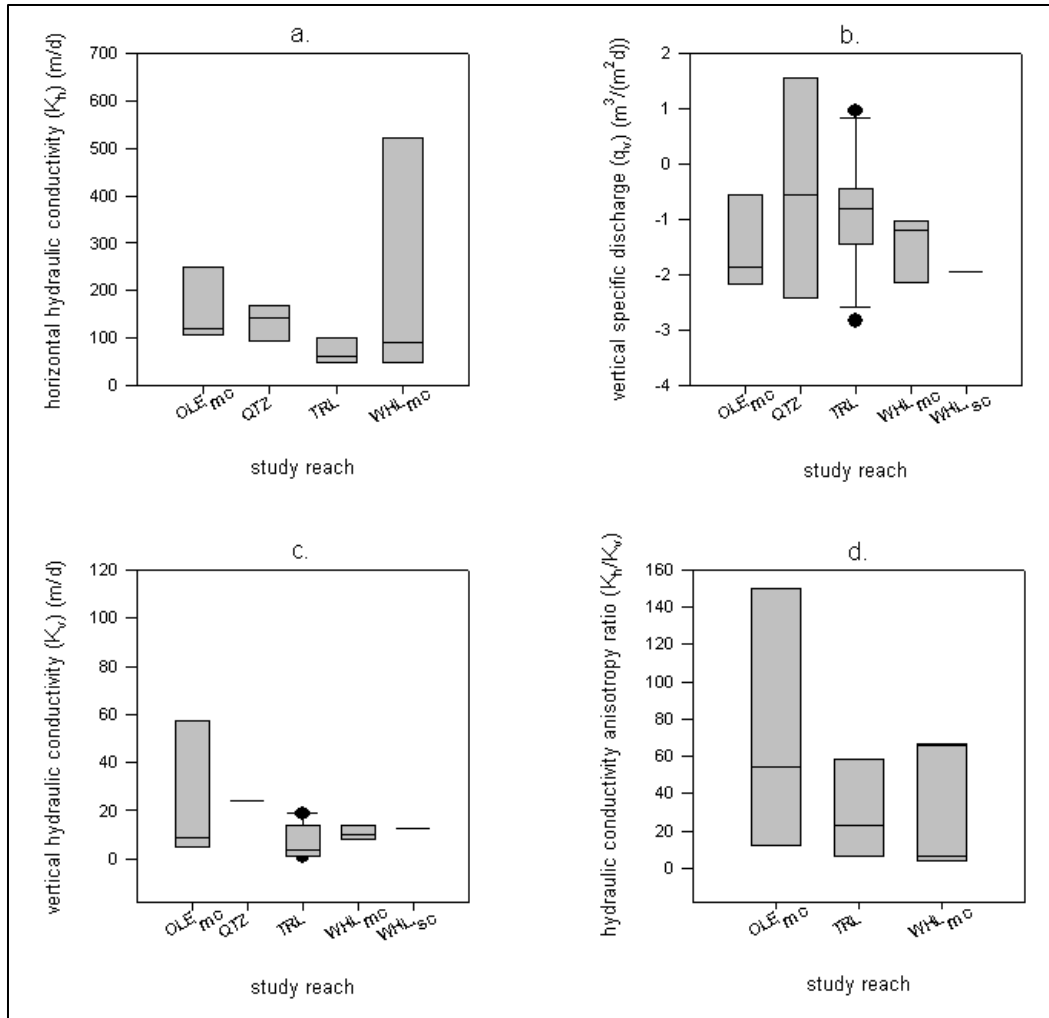
822
 823 Table 8. Average channel and streambed water temperature from 9/19/11-9/30/11 (during the spawning period).
 824 (The number of temperature dataloggers contributing to these average values are: OLE_{mc} $n=4$; OLE_{sc} $n=1$; QTZ $n=1$;
 825 TRL $n=4$; WHL_{mc} $n=4$.)

Average spawning water temperature (°C) (9/19/11-9/30/11)			
study reach	channel	subsurface (~25cm)	% difference
OLE_{mc}	7.6	7.6	0.0%
OLE_{sc}	7.7	7.7	0.0%
QTZ	8.1	8.2	1.2%
TRL	6.1	6.1	0.0%
WHL_{mc}	6.3	6.4	1.6%

826

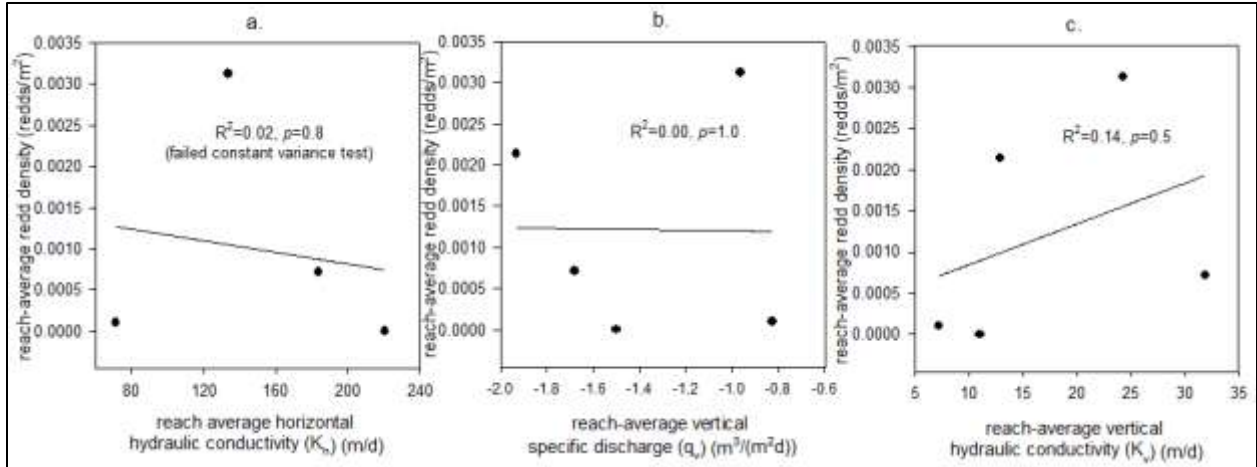


827
 828 Figure 14. Range of vertical hydraulic gradient (VHG) measurements in each study reach for September and
 829 October. Piezometers in WHL_{sc} were installed on 10/12/11, therefore there is no WHL_{sc} VHG data for September.
 830 (September plots: OLE_{mc} n=14; OLE_{sc} n=14; QTZ n=15; TRL n=25; WHL_{mc} n=9.) (October plots: OLE_{mc} n=13; OLE_{sc}
 831 n=13; QTZ n = 13; TRL n=21; WHL_{mc} n=10; WHL_{sc} n=4.)
 832
 833
 834



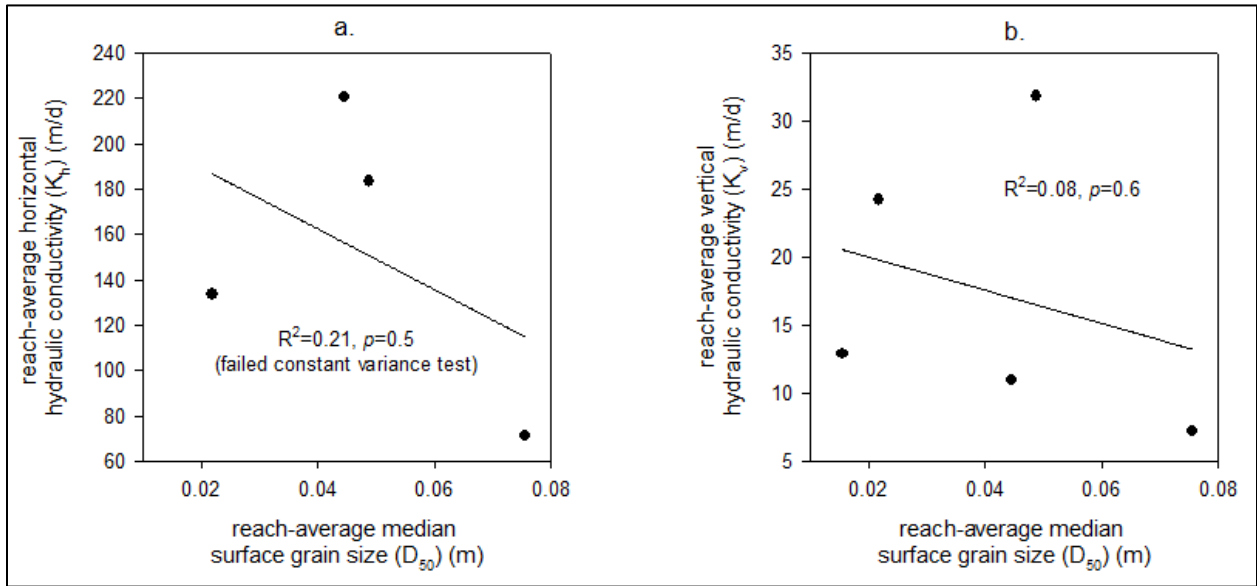
835
 836 Figure 15. Summary plots of hydrogeologic variables measured in the study reaches. (a) Horizontal hydraulic
 837 conductivity (K_h) of streambed sediments at ~40 cm depth measured in each of the study stream sections. Input
 838 for each K_h box plot is the average K_h value derived from each slug test piezometer in a given study reach (OLE_{mc} n
 839 = 6; QTZ n = 5; TRL n = 5; WHL_{mc} n = 4). (b) Ex-Stream estimated vertical specific discharge (q_v) magnitude and
 840 direction. Negative values represent downward flow; positive values represent upward flow. Input values for the
 841 plot are the average value of the daily averaged q_v computed for each thermochron instrumented piezometer
 842 (OLE_{mc} n=5; QTZ n=3; TRL n=11; WHL_{mc} n=5; WHL_{sc} n=1). (c) Vertical hydraulic conductivity (K_v) estimates in each
 843 study reach (OLE_{mc} n=5; QTZ n=1; TRL n=10; WHL_{mc} n=5; WHL_{sc} n=1). (d) Hydraulic conductivity anisotropy ratio
 844 ranges in the streambed sediments (OLE_{mc} n=3; TRL n=7; WHL_{mc} n=3).

845
 846
 847

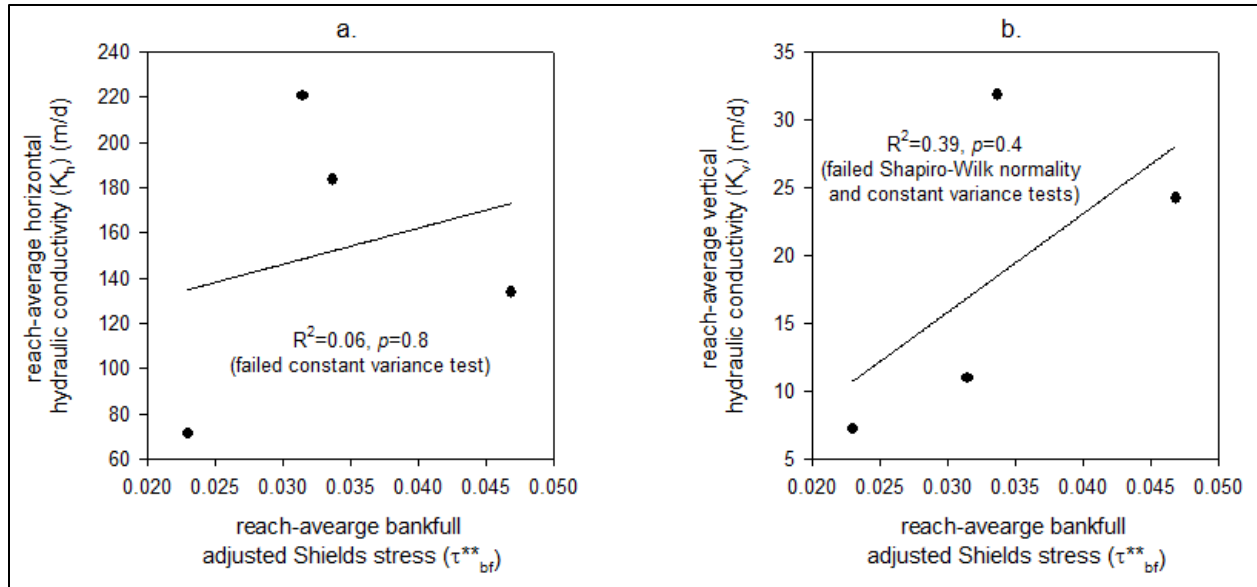


848 Figure 16. Reach-average hydrogeologic variables versus reach-average redd density. Regression equations are
 849 presented in Table 7.
 850
 851

852 No relationships between reach-average geomorphic and hydrogeologic variables were
 853 significant, although weak trends were evident (Figure 17, Figure 18; Table 9). Reach-average D_{50} was
 854 negatively correlated with K_h and K_v (Figure 17; Table 9). Reach-average τ^{**}_{bf} was positively correlated
 855 with K_h and K_v (Figure 18, Table 9).
 856



857 Figure 17. Reach-average median surface grain size (D_{50}) versus reach-average (a) horizontal hydraulic conductivity
 858 (K_h) and (b) vertical hydraulic conductivity (K_v). Regression equations are presented in Table 9.
 859



860
861 Figure 18. Reach-average bankfull adjusted Shields stress (τ^{**}_{bf}) versus reach-average (a) horizontal hydraulic
862 conductivity (K_h) and (b) vertical hydraulic conductivity (K_v). Regression equations are presented in Table 9.
863

864 Table 9. Dependency of reach-average hydrogeologic variables on reach-average geomorphic variables.

(x) v (y)	n	R ²	p	Equation
D ₅₀ v VHG	6	0.25	0.3	y=-0.0522-2.9293x
D ₅₀ v K _h	4	0.21	0.5 ^b	y=216.0898-1339.6806x
D ₅₀ v q _v	5	0.25	0.4	y=-1.7848+9.7963x
D ₅₀ v K _v	5	0.08	0.6	y=22.4603-121.9581x
τ^{**}_{bf} v VHG	5	0.01	0.9	y=-0.2101+0.6016x
τ^{**}_{bf} v K _h	4	0.06	0.8 ^b	y=98.2559+1597.4226x
τ^{**}_{bf} v q _v	4	0.00	1.0 ^b	y=-1.2225-0.5994x
τ^{**}_{bf} v K _v	4	0.39	0.4 ^{a,b}	y=-5.954+726.3009x
VCR v VHG	6	0.47	0.1	y=-0.3012+0.0074x
VCR v K _h	4	0.61	0.2 ^b	y=81.5863+4.8356x
VCR v q _v	5	0.48	0.2	y=-0.9270-0.0234x
VCR v K _v	5	0.01	0.9	y=18.8972-0.0759x

865 ^a Shapiro-Wilks normality test failed.

866 ^b Constant variance test failed.

867

868 2A) Valley-scale geomorphology

869 At the valley-scale, according to the edited unconfined valley delineations of Wenger et al.
870 (2011), 74% of the 133 redds observed in the 4 study catchments were within unconfined valleys and
871 26% were within confined valleys (Figure 19, Table 10). The Ole and Quartz catchment unconfined valley
872 delineations of Wenger et al. (2011) appropriately represented landscape conditions (Figure 19a,b). In
873 the Trail and Whale Creek catchments (Figure 19c,d), I removed unconfined valley polygon sections that
874 I deemed to include terraces above the active valley bottom (Appendix 2A). According to my unconfined

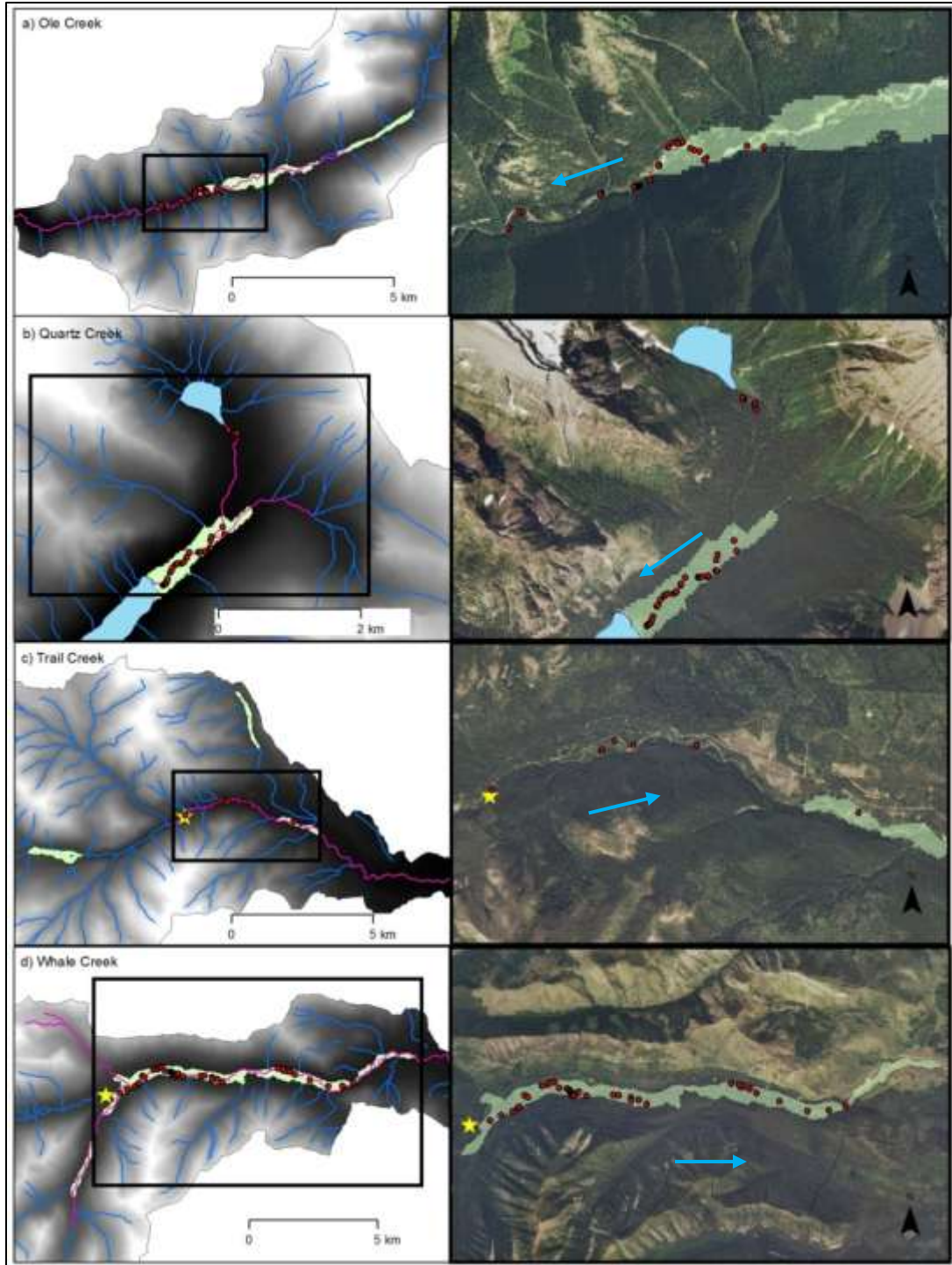
875 valley delineations, rate of change in valley width is not related to redd density, except for in the Ole
876 drainage. Of the 40 redds observed in Ole in 2011, 53% were clustered in the downstream extent of a
877 narrowing unconfined valley (Figure 19a). All other redds in the study catchments were located either in
878 unconfined valley segments of relatively constant width or in confined valley segments.

879 In the Ole catchment, the furthest downstream 3 km of Ole Creek is coarser and steeper and has
880 narrower valley walls than the rest of the drainage of the highlighted spawning and rearing area (Figure
881 19a). Redds are rarely observed in this section (John Fraley, 2011, personal communication). In the
882 Quartz catchment, the base level created by Quartz Lake is a confining factor of the valley-scale
883 geomorphic and hydrogeologic processes.

884 In the Trail catchment, migratory spawning bull trout are unable to access much of the drainage
885 because of an intermittent stream section that acts as a migration barrier during late summer and fall
886 baseflow conditions (the downstream extent of the intermittent stream section is indicated by the
887 yellow star in Figure 19c). In the Whale catchment, Whale Creek Falls (indicated by the yellow star in
888 Figure 19d) is a migration barrier. However, bull trout can and do migrate up the adjacent tributaries
889 near the upstream extent of the large alluvial valley in Whale (Figure 19d). These adjacent tributaries are
890 not included in the annual "index stream" redd count surveys (Table 5). However, the southern
891 tributary, Shorty Creek, which hosts a ~2 km long unconfined valley, is known to annually host spawning
892 bull trout (Tom Weaver, 2012, personal communication) (Figure 19d).

893 Reach-average VCRs of the study reaches range from 38 in WHL_{sc} to 2 in TRL (Table 11). Reach-
894 average VCR was negatively correlated with reach-average D_{50} and S (Figure 20a,b) and positively
895 correlated with reach-average τ_{bf}^{**} but the relationships were not significant (Figure 20c). Reach-
896 average VHG trended towards zero as VCR increased; VCR and K_n were positively correlated; q_v trended
897 towards larger negative values as VCR increased; and K_v exhibited no correlation with VCR; all of these
898 relationships were non-significant (Figure 21).

899



900
 901 Figure 19. Valley confinement and 2011 bull trout redd occurrence in each study stream. Left panel maps are
 902 digital elevation models (DEMs) of the study catchments, and right panel maps are air photos of the 2011 bull trout
 903 spawning sections in each study catchment. Blue arrows indicate streamflow direction. Redd dots indicate 2011
 904 redds. Green polygons indicate the edited unconfined valley delineations (originals created by Wenger et al.,
 905 2011)). In the left panel maps, blue lines are NHDPlus streamlines; pink lines are spawning and rearing reaches
 906 (USFWS, 2008). The southernmost lake in b) is Quartz Lake and the northernmost is Cerulean Lake. Rainbow Creek
 907 connects Cerulean Lake to Quartz Creek and Quartz Lake. Yellow stars in c) and d) maps indicate barriers to
 908 upstream fish migration. (NAIP (2011) air photos)

909
910

Table 10. Bull trout 2011 redd distribution in relation to valley type per study catchment.

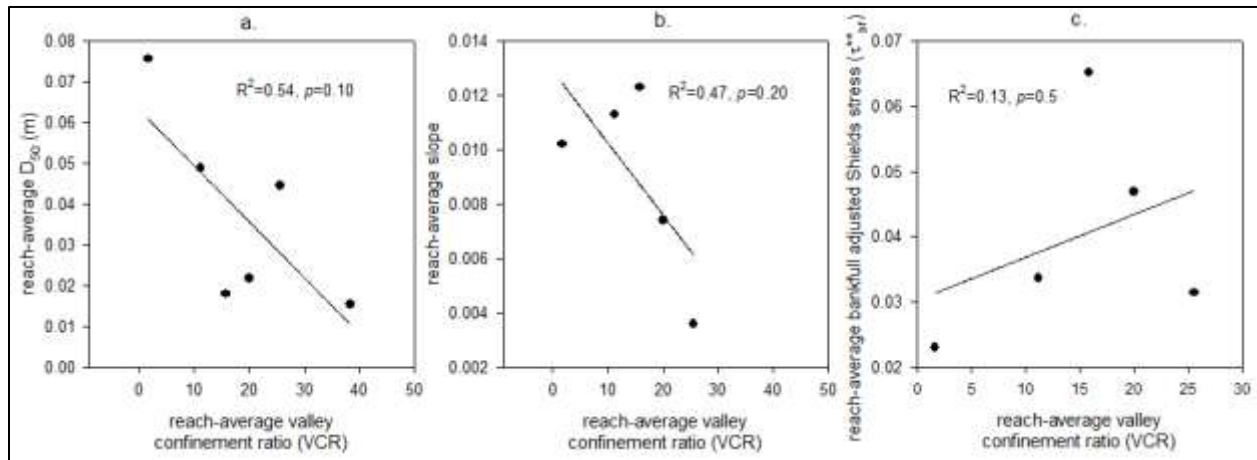
Study stream	Unconfined valley redds (n=99) (74%)	Confined valley redds (n=34) (26%)
Ole	21 (52.5%)	19 (47.5%)
Quartz	35 (81%)	8 (19%)
Trail	1 (12.5%)	7 (87.5%)
Whale	42 (100%)	0 (0%)

911
912

Table 11. Valley confinement ratios (VCR) per study reach.

Study reach	Average valley width (m)	Bankfull channel width (m)	Valley confinement ratio -
OLE _{mc}	190	17	11
OLE _{sc}	190	12	16
QTZ	340	17	20
TRL	30	18	2
WHL _{mc}	460	18	26
WHL _{sc}	460	12	38

913



914
915
916
917

Figure 20. Reach-average valley confinement ratio (VCR) versus other reach-average geomorphic variables. Regression equations: (a) $y=0.0129-0.0003x$; (b) $y=0.0631-0.0014x$; (c) $y=0.0303+0.0007x$.

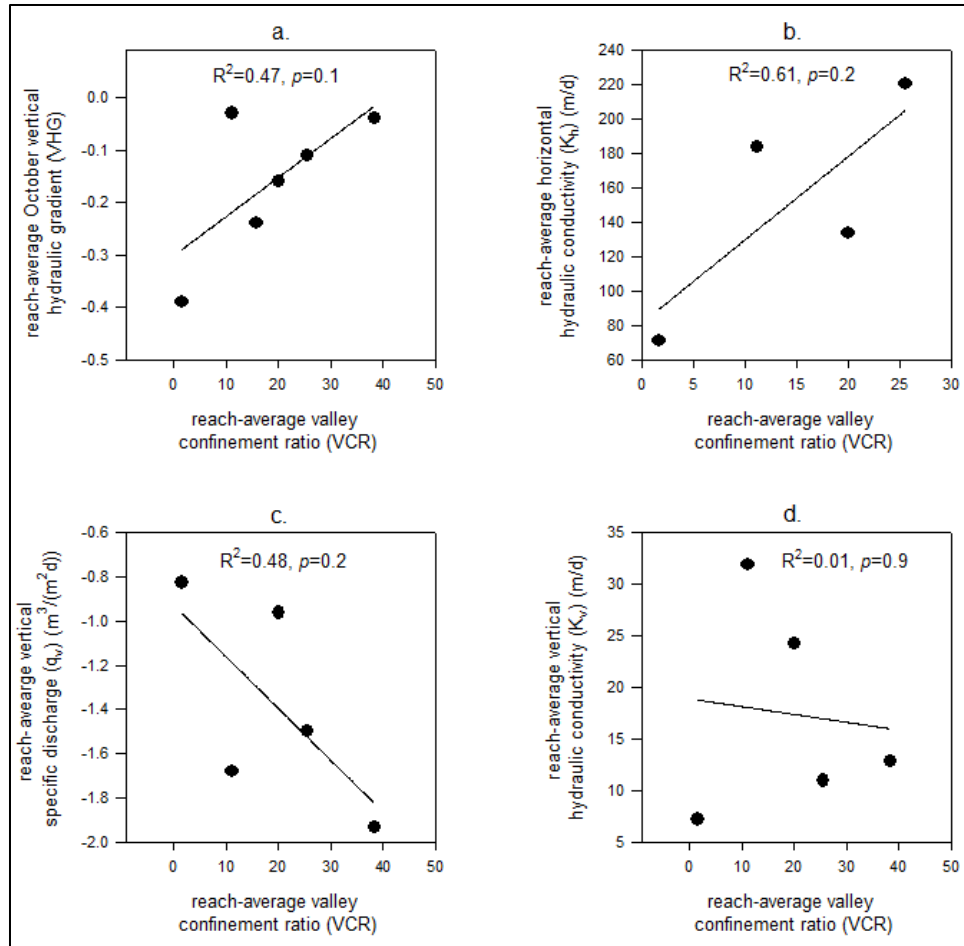


Figure 21. Reach-average valley confinement ratio (VCR) versus reach-average hydrogeologic variables. Regression equations: (a) $y = -0.3012 + 0.0074x$; (b) $y = 81.5863 + 4.8356x$; (c) $y = -0.9270 - 0.0234x$; (d) $y = 18.8972 - 0.0759x$.

2B) Valley-scale hydrogeology

Flownets based on floodplain water level and stream stage data indicate a general down-valley flow direction of floodplain subsurface water in all study reaches (Appendix 2B). Water table maps of the Ole study reaches indicated apparent flow line convergence where the unconfined valley narrows, suggesting valley-scale groundwater was discharging to the stream channel during the study period (Figure 22).

Mean annual air temperature recorded by the 3 most proximal SNOTEL stations was 4.3°C (Appendix 2B). Therefore, I estimated groundwater temperature at 10-25 m depth in all of the study catchments to be ~ 5.3 - 6.3°C (Kasenow, 2001). Although streambed water temperatures tended to mimic stream water diurnal cycles, one Ole upward flux (VHG measurements were positive or 0) piezometer recorded constant streambed water temperatures of 5.3°C in August at 8 and 25 cm depth below the streambed. During this time, the stream water temperature sensor varied diurnally from ~ 6 - 9.5°C (Figure 26: subsurface temperature signal representative of groundwater = O-gw; stream temperature signal = O-5sc).

September shallow floodplain water temperatures in Ole, Trail, and Whale also exhibit near constant temperature signals (Figure 24, Figure 26). In Ole, the shallow floodplain water temperature ($\sim 8^\circ\text{C}$, sensor O-2fp) plotted near the average of the stream water diurnal cycle ($\sim 2^\circ\text{C}$ warmer than computed groundwater temperature) (Figure 24, Figure 26). In Trail and Whale, the shallow floodplain

940 water temperature was $\sim 7^{\circ}\text{C}$ ($\sim 1^{\circ}\text{C}$ + warmer than average stream water temperature and expected
941 groundwater temperature) (Figure 24).

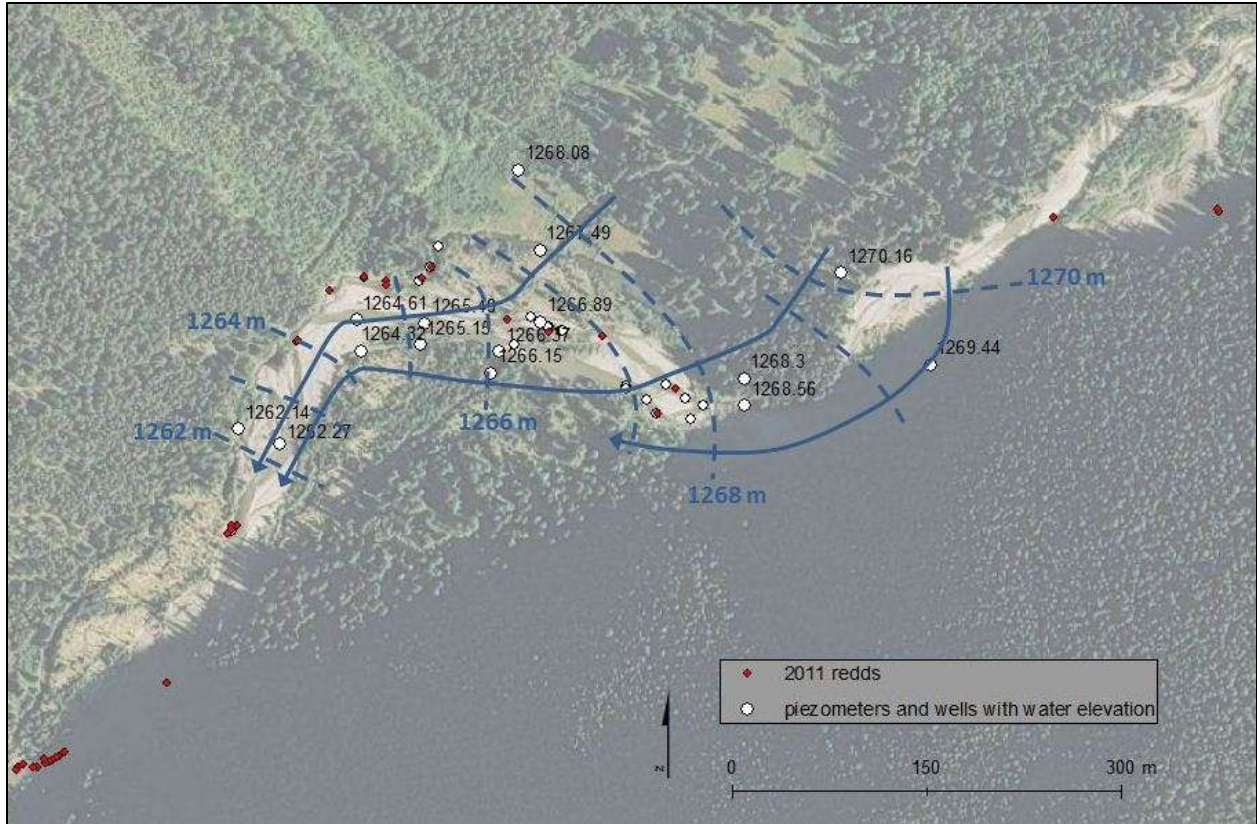
942 The catchment-wide stream water temperature sensors in each study catchment (Figure 23)
943 show Trail and Whale average September stream temperatures (~ 5.6 - 6.5°C) approximately within the
944 range of expected groundwater temperature (~ 5.3 - 6.3°C), whereas average stream temperatures in Ole
945 and Quartz (~ 7.1 - 8.6°C) are warmer (Figure 24). Spawning reaches in all streams were characterized by
946 stream temperatures with coefficients of variation (C_v) of ≤ 0.004 that decreased during the spawning
947 and early incubation period (September and October) (Figure 25); spawning was not observed where
948 stream temperature C_v was > 0.004 and increased during the spawning and early incubation period
949 (Figure 25a).

950 In the Ole drainage, during the spawning and early incubation period (September and October),
951 stream temperature in the spawning area was colder and less variable (sensors O-4mc and O-5sc) than
952 stream temperature upstream and downstream of the spawning area (sensors O-1mc and O-6mc)
953 (Figure 24, Figure 25, Figure 26). Furthermore, variation of the spawning area water temperature (O-
954 4mc and O-5sc) decreased over time whereas variation upstream and downstream (O-1mc and O-6mc)
955 increased over time (Figure 25).

956 In the Quartz drainage, spawning (September) stream temperature 200 m upstream of Quartz
957 Lake (Q-2mc) warmed $\sim 0.4^{\circ}\text{C}$ but was not buffered compared to Rainbow Creek stream temperature
958 200 m downstream of Cerulean Lake (Q-1mc) (Figure 24, Figure 25). Both stream temperature sensors
959 indicate decreasing variability in stream water temperature over the spawning and early incubation
960 period (September through October) (Figure 25).

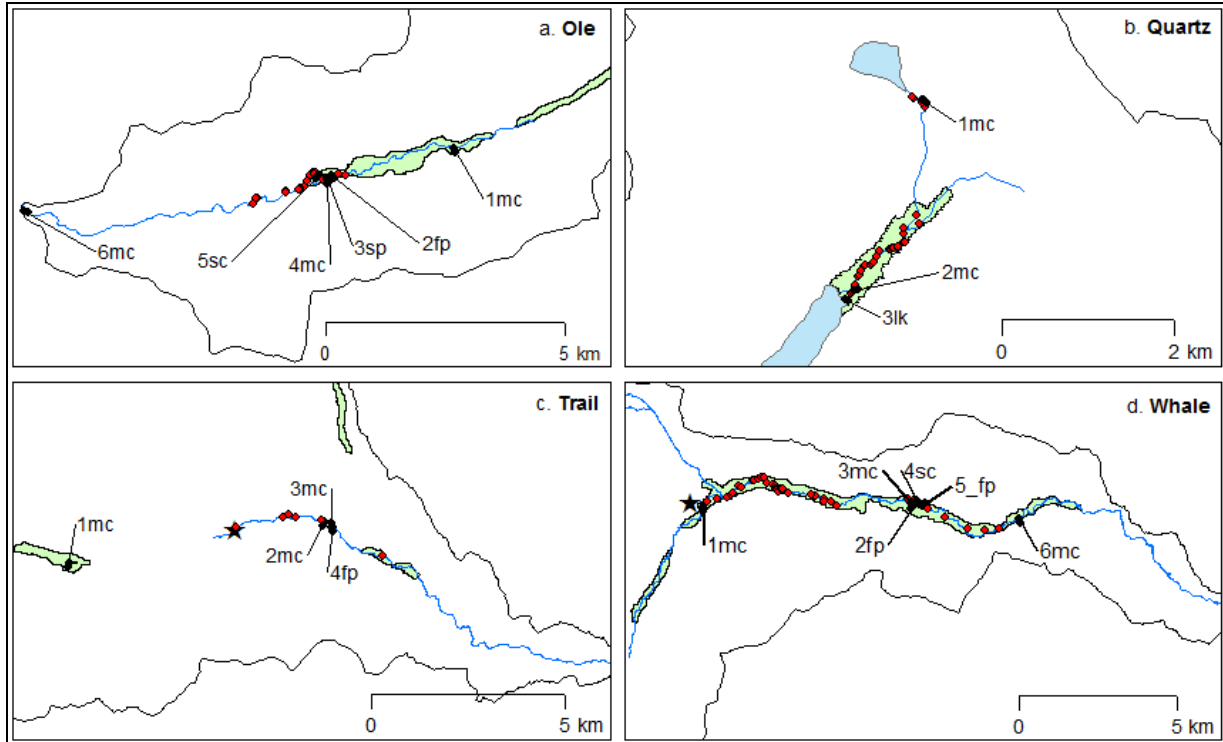
961 In Trail, stream temperature above the intermittent section (T-1mc) was colder and more
962 variable than stream temperature below the intermittent section (T-2mc, T-3mc) (Figure 24, Figure 25).
963 In Whale, stream temperatures are coldest at the upstream extent of the ~ 20 km long alluvial valley, but
964 stream temperatures appear to exhibit similar diurnal variations throughout the valley (Figure 24, Figure
965 25). All Trail and Whale stream temperatures dataloggers indicated a decrease in variation in stream
966 temperature through the spawning and early incubation period (Figure 25). Average September air
967 temperature in the study reaches ranged from 12°C in Ole to 8°C Whale (Figure 27). Daily diurnal
968 fluctuations in air temperature between the study catchments were similar in trend and phase (Figure
969 27).

970
971
972

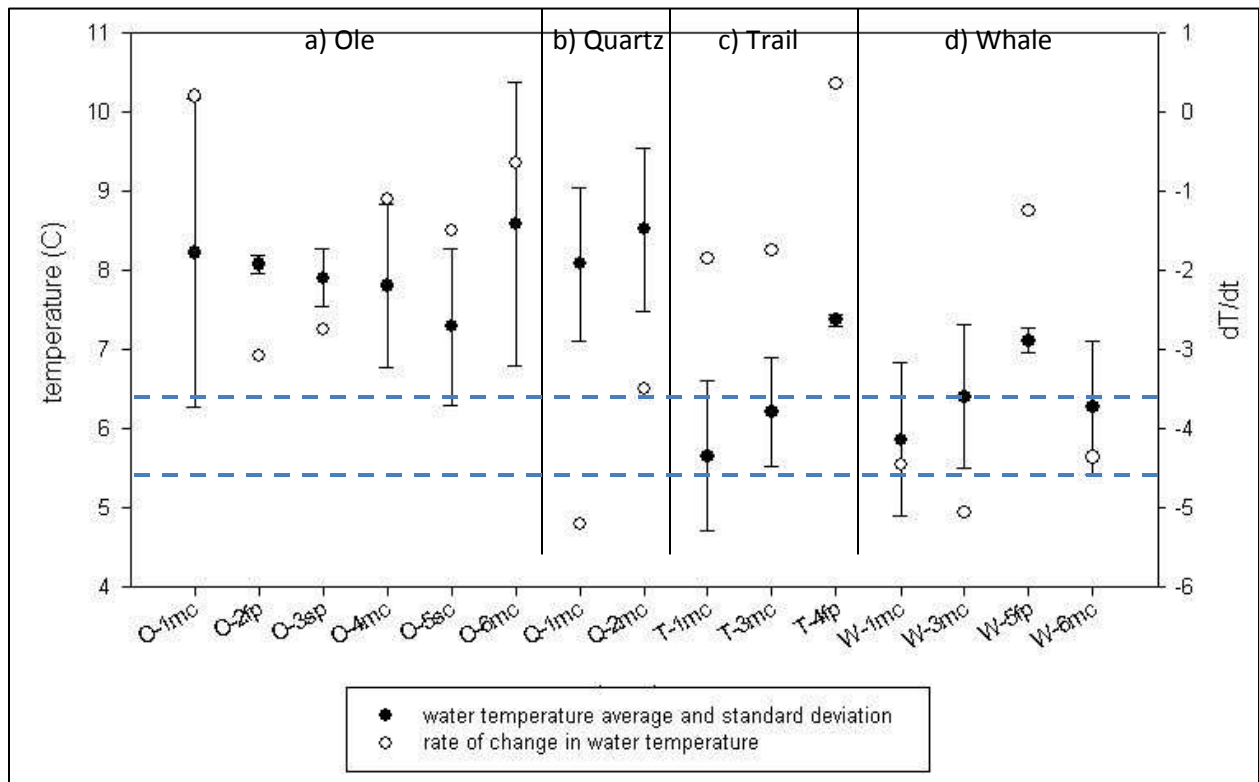


973
 974
 975
 976
 977
 978

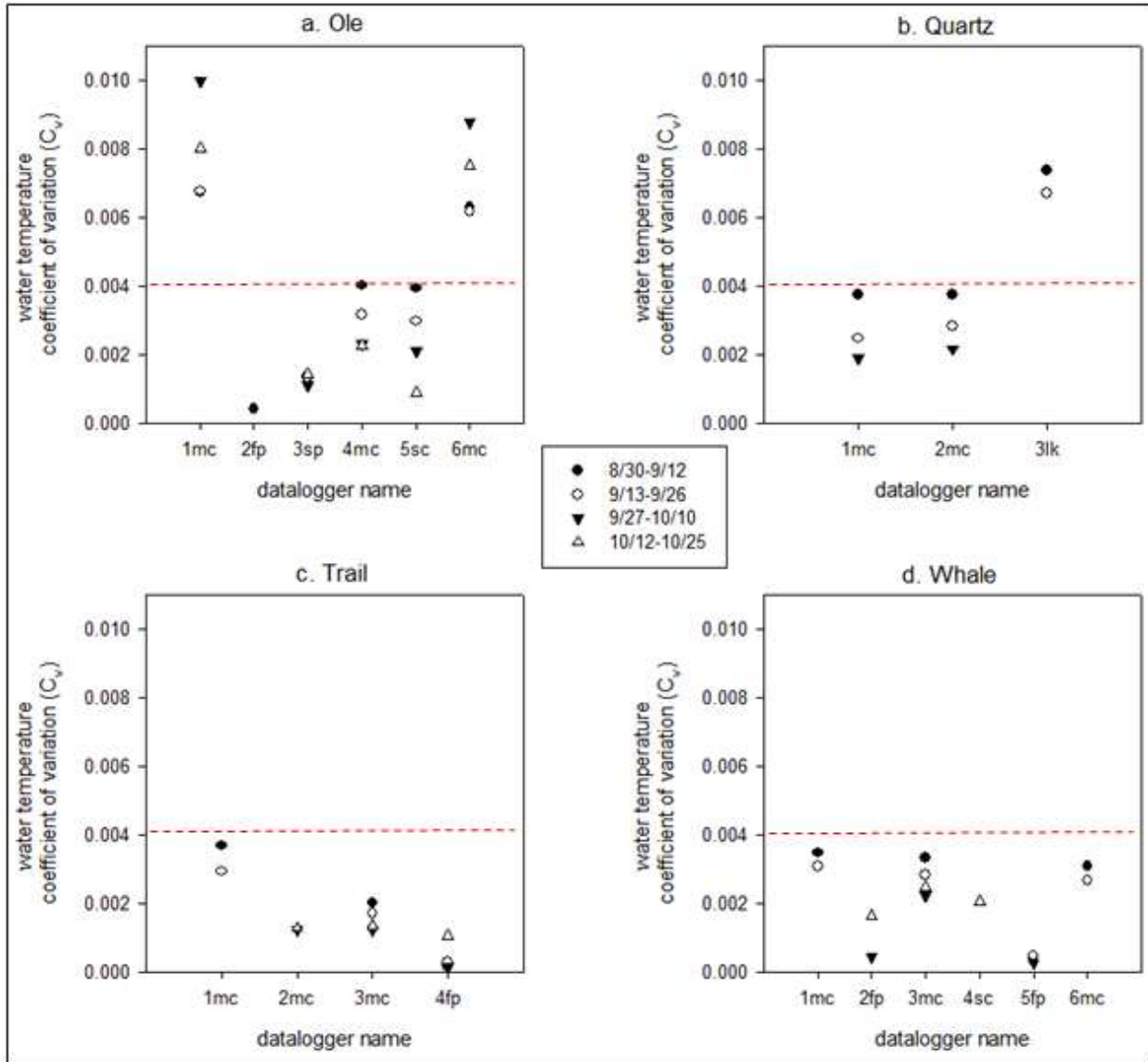
Figure 22. Ole Creek water table contour map encompassing OLE_{mc} and OLE_{sc} on 9/11/11. Dashed blue lines are water table contours with blue elevation numerical labels. Solid blue lines are inferred subsurface flow direction lines. (NAIP (2011) photos)



979
 980 Figure 23. Location of catchment-scale water temperature dataloggers (black dots) and 2011 bull trout redds (redd
 981 dots). Numerically, prefixes of the sensor names in each drainage increase in the downstream direction (e.g. 1 =
 982 furthest up stream). Suffixes indicate the lateral location of the sensor in relation to the stream channel: mc = main
 983 channel stream water temperature sensor; sc = secondary channel stream water temperature sensor; sp = spring
 984 channel stream water temperature sensor; fp = floodplain well water temperature sensor.
 985
 986

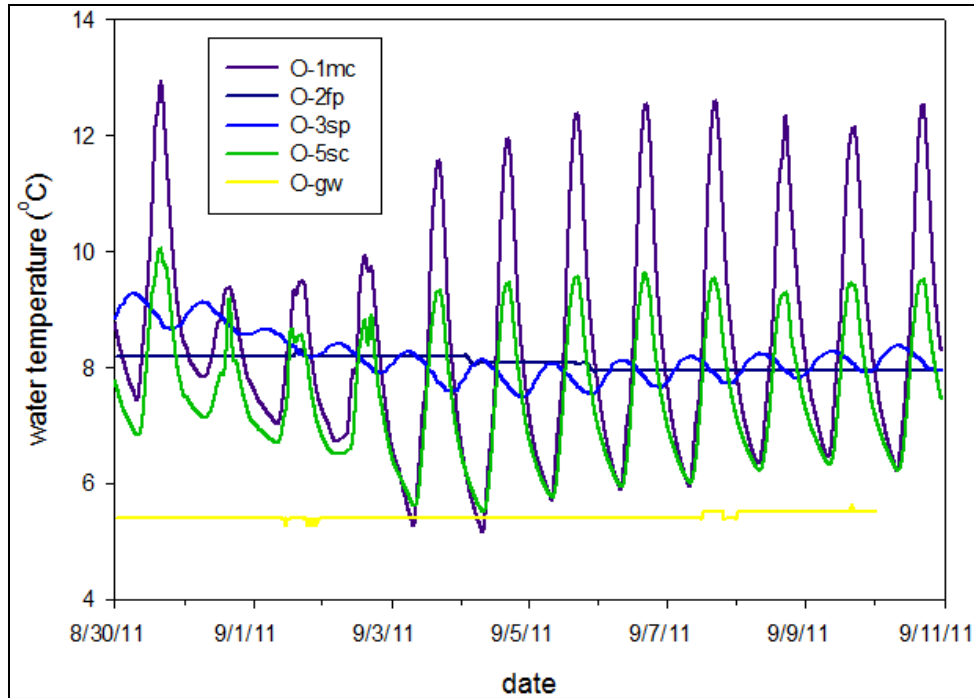


988
 989 Figure 24. Comparison of the average (dark dots), standard deviation (whiskers), and rate of change in stream
 990 temperature (white dots) in September for various longitudinal locations in each study stream. The x-axis indicates
 991 datalogger names and locations: label prefixes indicate the stream (e.g. O = Ole); suffixes indicate the longitudinal
 992 stream location as shown in Figure 23. Sensor naming codes are further explained in the Figure 23 caption. The
 993 blue dashed lines encompasses the estimated temperature of long residence time groundwater at 10-25 m depth
 994 for the study area latitude and elevation.
 995



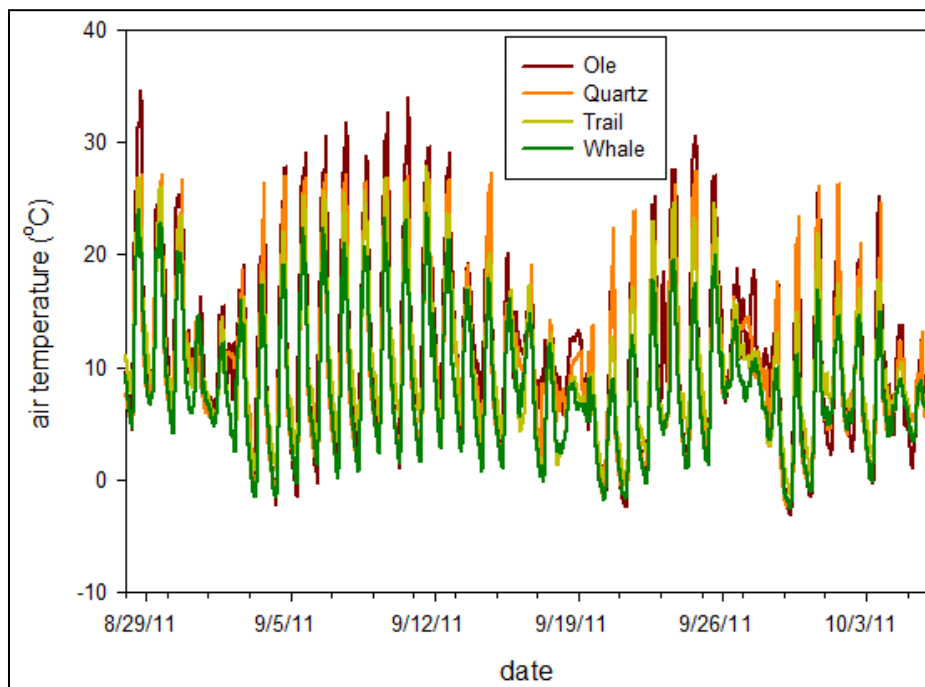
996
 997
 998
 999
 1000

Figure 25. Coefficient of variation (C_v) in water temperature of the catchment-wide temperature sensors for the time windows indicated. Stream temperature sensors in spawning reaches plot below the red dashed line at $C_v=0.004$. Sensor locations are shown in Figure 17. Sensor naming codes are further explained in the Figure 23 caption.



1001
1002
1003
1004
1005

Figure 26. Spatial comparison of diurnal water temperature oscillations in the Ole Creek catchment. Temperature sensor locations are shown in Figure 18a-d. All sensors in this plot measured surface water temperatures except O-gw, which was located 8 cm below the streambed in OLE_{sc} – about 100 m downstream from O-5sc.



1006
1007
1008
1009
1010
1011
1012

Figure 27. Air temperature in each of the study reaches ~1-2 m above the ground or water surface. From 8/28/11 – 10/6/11, the average air temperature in the study reaches was: Ole 12°C, Quartz 10°C, Trail 10°C, and Whale 8°C.

DISCUSSION

Whereas 2011 redd counts in Ole, Quartz, and Whale are within the annual range of 2000-2010 redd counts, the Trail redd count was lower than any recorded in the previous decade. Some of the year

1013 to year variability in redd counts is attributable to observer error (e.g. Muhlfeld et al., 2006). All of the
1014 redd counts reported here may be low compared to historical levels as a result of the change in
1015 community dynamics of the Flathead Lake and river system related to the opossum shrimp invasion and
1016 the lake trout population surge of the 1980s and 1990s (e.g. Ellis et al., 2011; Muhlfeld et al., 2012).

1017
1018 1A) Reach-scale fluvial geomorphology

1019 Hypothesis 1A, which related spawning occurrence at the subreach- and reach-scales to areas of
1020 low mobility of spawning appropriate sediment at bankfull flows, was not supported (e.g. Figure 9,
1021 Figure 11). This hypothesis was based on the premise that because high flows (e.g. bankfull) can occur
1022 while eggs are incubating in the streambed, salmonids may select redd sites with low streambed
1023 mobility at high flows (e.g. Moir et al., 2009). In my highest redd density study reach, OLE_{sc}, bankfull
1024 Shields stress and bankfull adjusted Shields stress typically exceeded 0.045, a commonly cited threshold
1025 for streambed particle entrainment (e.g. Buffington and Montgomery, 1997) (Figure 6a,b, Figure 9,
1026 Figure 11, Figure 13). Furthermore, subreach and reach-average redd density of all study reaches was
1027 positively correlated with bankfull adjusted Shields stress (τ^{**}_{bf}) and the relationships were significant
1028 ($p=0.02$) (Figure 9b; Figure 11b). Bull trout may choose to spawn in subreach- and reach-scale channel
1029 sections of higher Shields stresses and sediment mobility because these sediments should be easiest to
1030 move and excavate a redd. Additionally, high Shield stresses may be indicative of dynamic stream
1031 sections in which reworking of the shallow streambed sediments by bankfull flows decreases the
1032 amount of fine sediment accumulation in the streambed, thus allowing hyporheic water to more freely
1033 circulate. The positive (albeit non-significant) correlation between reach-average τ^{**}_{bf} and K_v ($R^2=0.39$,
1034 $p=0.4$; Figure 18b) supports this notion.

1035 Subreach- and reach-average Shields stress results in the study reaches (e.g. Figure 13) indicate
1036 that bankfull flows likely mobilize and sort the dominant textural facies of OLE_{sc} and QTZ as well as
1037 certain portions of OLE_{mc} (the study reaches with the highest redd density in 2011). The dominant
1038 textural facies of TRL and WHL_{mc} (the study reaches with the lowest redd density in 2011) are likely not
1039 mobilized by bankfull flows (Figure 13).

1040 In contrast to my findings, Moir et al. (2009) found the spawning frequency of Atlantic salmon at
1041 the subreach-scale in a gravel-bed Scottish mountain stream to be negatively correlated with streambed
1042 mobility. These conflicting results are likely due to several factors. First, my study has the potential for
1043 including redds in the analyses that were constructed in isolated, seasonally transient patches of
1044 sediment that are not accurately described by subreach-scale physical characteristics (e.g. subreach-
1045 scale τ^{**}), because my study used only 1 year of direct redd location observations. In contrast, Moir et
1046 al. (2009) assessed spawning subreaches consistently used by spawning salmon over a 5 year period.
1047 Secondly, Moir et al. (2009) only consider mobility of a single D_{50} , whereas I used the observed dominant
1048 D_{50} of each subreach channel section. Because the competence of a given flow is dependent on
1049 streambed grain size (e.g. Montgomery et al., 2009), and salmonid species are known to spawn in a
1050 range of D_{50} (e.g. bull trout 8 mm – 64 mm: Baxter and McPhail, 1996), interpretations of spawning
1051 sediment mobility are dependent on choices about the representative grain size in calculations,
1052 including whether true grain size or a constant, average grain size is used. Finally, Moir et al. (2009)
1053 used total boundary shear stress (τ_o), whereas I used grain stress (τ') in an effort to account for form
1054 drag from bank, bar, and wood roughness, which can be substantial in my study reaches.

1055 My work on streambed mobility is anchored to the recognition that availability of appropriate
1056 spawning gravels is a primary control on the spatial distribution of salmonid spawning habitat (e.g.
1057 Buffington et al., 2004; Moir et al., 2006). Similarly, my results indicate that the spatial distribution of
1058 spawning appropriate gravels in the study reaches plays a major role in bull trout redd distributions and
1059 densities. In all of my study reaches, bull trout spawned only the finest of the dominant textural facies
1060 (Figure 6, Figure 8, Figure 10).

1061 Salmonids can spawn in substrate with a D_{50} up to 10% of their body length (Kondolf and
1062 Wolman, 1993). The D_{50} values of textural facies used by spawning bull trout in my study tend to be
1063 smaller than those reported by others (e.g. Baxter and McPhail, 1996; Dunham et al., 2001). Because
1064 Flathead River bull trout are among the largest in their native range (Clint Muhlfeld, 2012, personal
1065 communication), it appears that the bull trout in my study reaches were large enough to excavate redds
1066 in larger substrate, but they preferentially chose to spawn in the finer textural facies. Because fish length
1067 can be approximated from redd dimensions (e.g. Crisp and Carling, 2006), these speculations could be
1068 tested from redd dimension measurements.

1069 Potential error in my Shields stress values arise from many sources. Streambed grain size
1070 distributions relied on simplified visual observations of dominant textural facies. HEC-RAS flow modeling
1071 used measured cross sections of approximately 100 m spacing and therefore involve substantial
1072 interpolation, simplification, and uncertainty. Furthermore, there are additional physical factors
1073 reported to influence bull trout spawning site selection, such as proximity to cover, that are not
1074 incorporated in my study.

1075 Additional statistical analyses would help describe the relationship between streambed
1076 competence and redd occurrence and density. For example, a logistic regression model describing
1077 trends in presence or absence of redds may further explain the degree to which bull trout select or avoid
1078 streambed sections of high competence. Additionally, due to my low sample sizes, the use of simple,
1079 non-parametric correlations may be more appropriate than the regression analyses I performed as part
1080 of this study.

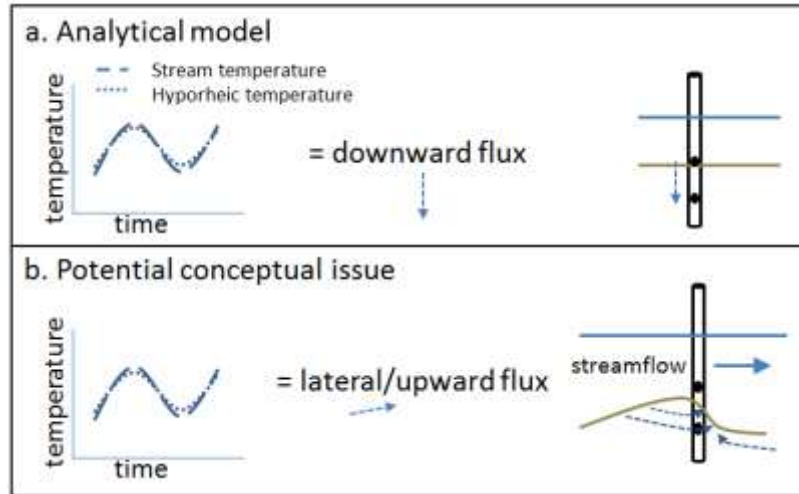
1081

1082 1B) Reach-scale hydrogeology

1083 Hypothesis 1B, which related spawning occurrence at the subreach- and reach-scale to
1084 extensive vertical and lateral hyporheic exchange, was supported. Streambed water temperature data
1085 indicated rapid hyporheic mixing of stream water into the streambed for all study reaches. Other
1086 researchers have observed similar streambed conditions in potential salmon spawning areas (e.g.
1087 Alexander and Cassie, 2003). Additionally, reach-average redd density was positively correlated with
1088 streambed K_v (Figure 16c). In salmonid spawning habitat studies, measurements of streambed hydraulic
1089 conductivity often include only the measurement of the horizontal component (K_h) (e.g. Baxter and
1090 Hauer, 2000). Sediment sorting processes often produce stratified beds (e.g. Marion et al., 2008b), and
1091 vertical hydraulic conductivity (K_v) values are generally one or two orders of magnitude less than K_h
1092 (Chen, 2000). All of the study reaches exhibited K_h values representative of a mix of well-sorted gravel
1093 and sand and glacial outwash (Fetter, 2001).

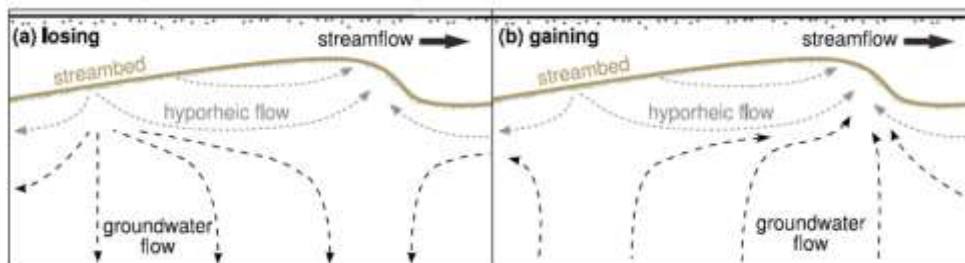
1094 Whereas vertical hydraulic gradients (VHG) in all study reaches were dominantly negative, most
1095 piezometers were installed in concave-up bedforms where negative VHG was to be expected (e.g. Keller
1096 and Kondolf, 1990; Tonina and Buffington, 2011; Bhaskar et al., 2012). Hydrogeologic conditions during
1097 the spawning period appeared stable because stream stage, VHG, and q_v were relatively constant
1098 (Janssen et al., 2012; Tonina and Buffington, 2009a). Use of streambed temperature signals to
1099 compute q_v values in site conditions similar to mine (lack of buffering, lagging, or cooling/warming of
1100 shallow (<25 cm deep) streambed temperatures) should be done with caution. I recommend, as a first
1101 order check on specific discharge direction estimation by an analytical heat and fluid flow model, VHG
1102 should be measured periodically along with the vertical temperature time series (Figure 28). This
1103 provides a second set of flow direction data. Conceptually, using only temperature data, it appears that
1104 certain temperature signals can be calculated as downward when they are in fact parallel to the
1105 streambed or even upward (Figure 28). For this study, I assumed temperature signals indicated upward
1106 or downward flow; I did not account for horizontal streambed flow conditions.

1107



1108
 1109 Figure 28. Illustration of potentially inaccurate heat and fluid flow analytical model calculation of specific discharge
 1110 magnitude and direction from vertically spaced streambed temperature time series data. (a) represents potential
 1111 input and output from the analytical model; (b) represents a physical conditions creating the same temperature
 1112 curves but with an entirely different flux direction and magnitude.
 1113

1114 Streambed temperature data indicated one distinct zone of groundwater upwelling (sensor O-
 1115 gw in Figure 26), located in OLE_{sc} . Distinct zones of groundwater upwelling have been observed by many
 1116 researchers (e.g. Hansen, 1975; Bhaskar et al., 2012); potential conceptual models explaining why
 1117 groundwater discharge is focused to sections of the streambed have been proposed (e.g. Bhaskar et al.,
 1118 2012) (Figure 29). Additionally, channel depositional processes and structures facilitate preferential
 1119 subsurface flow paths and may help explain the presence of distinct zones of groundwater discharge to
 1120 the stream (e.g. inter-connected open framework gravels: Lunt and Bridge, 2007).
 1121



1122
 1123 Figure 29. Conceptual models illustrating the interaction of hyporheic and groundwater flow paths in relation to
 1124 bedforms. In (b) notice the localized zone of groundwater discharge to the stream. (Figure copied from Bhaskar et
 1125 al. (2012).)
 1126

1127 Errors and uncertainties associated with the measurement of hydrogeological parameters
 1128 determined in this study arise from a number of sources. For example, VHG data, though relatively easy
 1129 to measure, can be misrepresented by vertical leakage (“short circuiting”) along the outside of the
 1130 piezometer casing (related issues in similar physical settings are extensively discussed by Kondolf et al.
 1131 (2008) and others). In coarse-grained bed sediments, short circuiting is difficult to quantify; I attempted
 1132 to minimize vertical leakage by packing sediment near the piezometers with my wading boots after
 1133 installations. A second concern related to slug tests and streambed hydraulic property characterization
 1134 was the influence of frictional losses in the piezometer may inhibit my ability to obtain high resolution
 1135 datasets for K_h determination (e.g. McElwee and Butler, 1996; Butler, 1998). These concerns were
 1136 alleviated by laboratory tests of the field piezometer design (Woessner and Rambo, 2012, unpublished

1137 data). Larger errors came from fitting graphical solutions to the observed slug response datasets.
1138 Because of the rapid response of piezometer water levels and the 0.5 to 1 second measurement interval
1139 available in the transducers used, it was not always clear that a detailed enough dataset was collected.
1140 Future work in similar settings should not only use an instantaneous slug removal (e.g. Butler, 1998) but
1141 also transducers that can record at 0.1 second measurement intervals. In spite of the issues listed above,
1142 curve matching of head response data generally provided K_h values within the range of expected values
1143 (Figure 15a).

1144 2A) Valley-scale geomorphology

1146 My hypothesis 2A, which related spawning occurrence to areas of alluvial valley narrowing, was
1147 not supported. This hypothesis was based on the premise that bull trout spawning is commonly
1148 associated with alluvial valley sections where hyporheic water and groundwater discharge to the stream
1149 to create favorable spawning and incubation temperature regimes (e.g. Stanford and Ward, 1993;
1150 Baxter and Hauer, 2000). It is also based on the premise that as valleys narrow, the cross sectional
1151 alluvial area transmitting down-valley flowing groundwater decreases causing a rise in the water table
1152 and thus there is an increase in groundwater discharge to the stream channel (e.g. Stanford and Ward,
1153 1993; Baxter and Hauer, 2000; Tonina and Buffington, 2009a).

1154 Only in Ole did a high density spawning reach correlate with distinct valley wall narrowing
1155 (Figure 19). However, no data on the change in valley alluvial cross-sectional area was available for any
1156 of the study catchments. In Quartz and Whale, high density spawning reaches were continuously
1157 distributed throughout extensive unconfined valleys and appeared to have no correlation with valley
1158 narrowing. It is possible that the base level of Quartz Lake acts to confine the cross sectional alluvial area
1159 for down-valley transport in the Quartz drainage and causes upwelling of hyporheic water and valley
1160 groundwater. In Trail, there was no high density spawning reach, and only 1 of the 8 redds (13% of the
1161 2011 Trail redd count) was located in an unconfined valley.

1162 The high percentage (74%, this study) of redds in unconfined valleys suggests that unconfined
1163 (alluvial) valleys provide important spawning habitat for bull trout. Many studies corroborate this finding
1164 (e.g. Stanford and Ward, 1993; Baxter and Hauer, 2000). Physical characteristics of alluvial valleys cited
1165 as important for spawning and ecosystem health include a floodplain accessible by high flows and high
1166 channel roughness factors. Overbank flows and high hydraulic roughness (due to bar, bank, and wood
1167 roughness: e.g. Buffington and Montgomery, 1999b) act to decrease bed shear stress relative to total
1168 boundary shear stress of high flow events. Additionally, large woody debris and side channels contribute
1169 to spawning habitat complexity and help protect incubating salmonid eggs from scour (Shellberg et al.,
1170 2010). Furthermore, alluvial valleys are known to host extensive hyporheic and groundwater exchange
1171 with stream water (e.g. Woessner, 2000).

1172 Baxter and Hauer (2000) observed a lack of bull trout redds in unconfined alluvial valleys at the
1173 mouth of their study streams. Similarly, I did not observe bull trout redds near the downstream extent
1174 of the Ole, Trail, or Whale catchments. From topographic map analyses, they termed these valley
1175 segments as “unbounded” alluvial valleys because they did not possess a constricting knickpoint at their
1176 downstream extent. Baxter and Hauer (2000) speculated that the lack of bull trout spawning in these
1177 unbounded alluvial valley sections may be attributed to the lack of a confining knickpoint that would
1178 decrease the alluvial valley cross-sectional area and theoretically provide thermally moderating
1179 hyporheic and groundwater discharge to the stream channel. I observed other likely factors contributing
1180 to the lack of spawning – namely incised channels and substrate too coarse for spawning. Coarse-scale
1181 DEM observations of the Trail and Whale catchment mouths show broad alluvial valleys that merge with
1182 the valley floor of the North Fork of the Flathead River. However, finer-scale DEM observations, as well
1183 as field observations, show an incised stream channel and an elevated, disconnected floodplain –
1184 indicating a likelihood of streambed coarsening (and high streambed shear stresses and high potential

1185 for scour of spawning appropriate gravels). Pebble counts confirmed that the dominant textural facies in
1186 the sampled sections of these unbounded alluvial valleys were too coarse for spawning (Baxter and
1187 McPhail, 1996; Dunham et al., 2001). Another reason potentially contributing to the lack of spawning
1188 near the downstream extent of the Whale catchment may be that the downstream third of the
1189 catchment burned in the early 2000s, and no 2011 bull trout redds were observed in the burned area.
1190 Wildfire and loss of riparian vegetation can increase stream temperatures (e.g. Isaak et al., 2010;
1191 Boughton et al., 2012) and fine sediment delivery to streams; both factors are detrimental to bull trout
1192 spawning habitat (e.g. Isaak et al., 2010).

1193 Whereas valley confinement ratio (VCR) did not correlate with redd density ($R^2=0.08$, $p=0.6$),
1194 relationships between VCR and field-measured geomorphic and hydrogeologic variables appear evident,
1195 but none were statistically significant. As theoretically expected, VCR influenced reach-average grain size
1196 distribution and channel slope. Surprisingly, channel slope exhibited no measureable control on grain
1197 size. The lack of control of channel slope on grain size distributions is likely attributable in part to
1198 hydraulic roughness factors (e.g. Buffington and Montgomery, 1999b).

1199 Hydrogeologically, VCR exhibited the strongest apparent influence on reach-average VHG.
1200 Among the study reaches, as VCR increased, reach-average VHG trended from higher negative values
1201 towards zero. This trend may indicate that the higher VCR study reaches exhibited more variable
1202 (positive and negative) VHGs throughout the study reach than the study reaches with low VCR, which
1203 showed dominantly downward VHG.

1204

1205 2B) Valley-scale hydrogeology

1206 My hypothesis 2B, which related spawning occurrence to areas of hyporheic water and
1207 groundwater discharge to the stream, was supported. This is most notable in the Ole catchment. The
1208 buffered and cooled stream temperature signals of OLE_{mc} (sensor O-4mc) and OLE_{sc} (sensor O-5sc)
1209 relative to the O-1mc (Figures 24, 25, 26) indicate substantial stream temperature moderation within
1210 the spawning reaches. I attribute this temperature moderation to valley-scale groundwater discharging
1211 to the stream channel; the groundwater temperature signal is represented by temperature sensor O-gw
1212 (Figure 26). Temperature moderation of unconfined valley portion of the Ole spawning reach is further
1213 substantiated by the decrease in variation in stream temperature with time whereas the stream
1214 temperature sensors 2 km upstream (O-1mc) and 5 km downstream (O-6mc) increase in variation with
1215 time (Figure 25). Conceptually, as stream flow decreases through the summer and fall, groundwater
1216 contribution to stream flow (“baseflow”) becomes a greater percentage of total streamflow, and the
1217 thermally moderating effect of groundwater becomes more evident in reaches experiencing
1218 groundwater discharge (e.g. Figure 25a: sensors O-4mc, O-5mc).

1219 The catchment-wide spatial scale of these water temperature measurements was essential to
1220 facilitate observations of the thermally moderated spawning reaches in OLE_{mc} and OLE_{sc} . Arrigoni et al.
1221 (2008) found hyporheic discharge temperatures in a section of the Umatilla River, Oregon (a gravel and
1222 cobble bedded system) to be primarily buffered and lagged (as opposed to cooled) relative to diurnal
1223 temperature cycles of the main channel. In the Ole catchment, only when considering stream
1224 temperatures kilometers upstream and downstream does the water temperature in the study reaches
1225 of Ole show evidence of substantial cooling. This highlights the importance of measuring and
1226 considering catchment-wide water temperatures in evaluating relative buffering, lagging, and cooling to
1227 interpret roles of hyporheic water and groundwater contribution to stream and floodplain water
1228 temperatures. Catchment-wide point measurements of specific electrical conductance may be an
1229 alternative way to delineate zones of long residence time groundwater contribution to the stream
1230 channel (e.g. Haria et al., 2013).

1231 These groundwater moderated stream temperatures of OLE_{mc} and OLE_{sc} may continue
1232 downstream to the 19 redds (48% of total in Ole) in the confined valley section downstream of the Ole

1233 study reaches. However, the moderated stream temperatures do not persist to the mouth of Ole Creek.
1234 At the mouth, the O-6mc temperature signal has a similar average, diurnal variation, and rate of change
1235 as O-1mc (Figure 24, Figure 25). Therefore, for the O-1mc and O-6mc sections of Ole Creek, stream
1236 temperatures are presumably dominated by air temperature and solar radiation.

1237 Potential reasons why Ole temperature sensor O-1mc exhibits a relatively unmoderated stream
1238 water temperature signal despite being within an alluvial valley segment *and* proximally downstream of
1239 another unconfined valley segment include: 1) it is near the upstream extent of an unconfined valley so
1240 hyporheic and groundwater interaction are limited, 2) the unconfined valley upstream of O-1mc may be
1241 falsely delineated or may not possess adequately deep or conductive alluvial sediments to allow water
1242 temperature moderation.

1243 In the Quartz drainage, Cerulean Lake is fed by melt water from Rainbow Glacier. Standard
1244 deviations in stream temperature downstream of Cerulean Lake (Q-1mc) and upstream of Quartz Lake
1245 (Q-2mc) were equal; however, Q-2mc average water temperature was warmed ~0.4°C relative to Q-
1246 1mc. Arrigoni et al. (2008) attributed warming of shallow hyporheic water (relative to main channel
1247 water) to either 1) solar heating of floodplain sediments, or 2) heating of channel water in stagnant
1248 sections by solar radiation prior to it entering the hyporheic zone. I have no floodplain water
1249 temperature data in Quartz, but I frequently observed calm eddies and backwater environments in the
1250 wood-forced, pool-riffle channel. I also commonly observed ponded floodplain depressions in the
1251 Quartz unconfined valley section. These still water bodies indicate potential for warming of hyporheic
1252 floodplain temperatures. Because hyporheic temperature differences tend to increase with flow path
1253 length, (Arrigoni et al., 2008), I interpret the lack of change in standard deviation and relatively small
1254 change in average temperature from between Q-1mc and Q-2mc to indicate hyporheic exchange in the
1255 unconfined alluvial valley upstream of Quartz Lake is dominated by short and fast hyporheic flow paths.
1256 Similarly, other researchers report that short hyporheic flow paths tend to dominate hyporheic
1257 exchange in streams (e.g. Arrigoni et al., 2008; Poole et al., 2008; Cardenas et al., 2004; Haggerty et al.,
1258 2002; Gooseff et al., 2003; Kasahara and Wondzell, 2003). Another potential reason for the lack of
1259 change in water temperature from Q-1mc to Q-2mc is that the Quartz drainage is heavily vegetated and
1260 riparian vegetation overhangs much of the stream channel. Riparian shading acts to cool stream water
1261 (Bhaskar et al., 2012); therefore, it is possible that the cooling effect of the dense riparian vegetation
1262 countered solar heating of calm waters and caused the temperature signals of Q-1mc and Q-2mc to
1263 remain similar.

1264 Mellina et al. (2007) reported that mountain streams with headwater lakes tend to cool as they
1265 flow downstream due to relatively warm lake outlet temperatures and cold groundwater inflows. The
1266 apparent moderate warming and lack of buffering between Q-1mc and Q-2mc may indicate a lack of
1267 thermally moderating groundwater contribution to the stream channel in the unconfined alluvial valley
1268 portion of the Quartz drainage. This could mean that 1) groundwater does not discharge to the stream
1269 (i.e. the stream channel is dominantly losing or exhibits parallel flow conditions (Woessner, 2000) in the
1270 unconfined valley) or 2) there is not enough conductive alluvial sediment volume or depth to develop a
1271 water temperature regime representative of “groundwater”. Although groundwater does not play an
1272 obvious role in moderating stream temperature in the Quartz drainage, variation in stream temperature
1273 (and Quartz Lake temperature) decreases from September through October (Figure 25). The Q-1mc
1274 temperature sensor indicates that Cerulean Lake outlet stream temperatures also decrease over time.
1275 This is consistent with previously published literature: alpine lakes serve as thermal moderators of
1276 stream temperature (e.g. Mellina et al., 2002; Hieber et al., 2002). Compared to downstream stream
1277 segments, stream temperatures at alpine lake outlets tend to exhibit higher maximum water
1278 temperatures and lower daily temperature fluctuations (Hieber et al., 2002). Between Q-1mc and Q-2mc
1279 is the confluence of Rainbow and Quartz creeks. The mixing of stream temperature regimes at the
1280 confluence, combined with a potential lack of groundwater input in the unconfined alluvial valley, and

1281 potential warming of hyporheic water in floodplain sediments (e.g. Arrigoni et al., 2008) appear to
1282 complicate the usual trend of downstream cooling reported by Mellina et al. (2007). Regardless, it is
1283 apparent that Cerulean Lake, supplied by glacial melt water, provides an aspect of thermal moderation
1284 to the stream water (which is usually attributed to groundwater input).

1285 The Trail and Whale stream temperature data indicates that groundwater likely moderates of
1286 stream temperatures. Observations contributing to this conclusion include: 1) the stream temperatures
1287 decrease in variability over time (Figure 25); 2) all measured average stream temperatures in both
1288 drainages plot in the range of expected groundwater temperature (Figure 24); and standard deviations
1289 in stream temperature are similar to those in OLE_{mc} and OLE_{sc} (Figure 24), which were shown to be
1290 substantially thermally influenced by groundwater input. The cooler September water temperatures of
1291 Trail and Whale compared to Ole and Quartz could also be attributed to cooler air temperatures
1292 measured in the study reaches (Figure 27).

1293 In Trail, the effect of the intermittent channel section (between sensors T-1mc and T-3mc) on
1294 water temperature moderation is unclear. Installation of stream temperature sensors above and below
1295 the intermittent section would inform this question. The shallow (~1-1.4 m below ground surface)
1296 floodplain water temperature signals in Trail and Whale exhibit almost no daily variation and are ~1°C+
1297 warmer than the stream temperature and expected groundwater temperature at 10-25 m depth (Figure
1298 24, Figure 25). Similar to Quartz, I attribute warming of shallow floodplain water to solar heating of
1299 floodplain sediments and/or solar warming of channel or floodplain ponded areas prior to entering the
1300 hyporheic zone (e.g. Arrigoni et al., 2008). Shallow floodplain water temperatures, such as those
1301 measured in my study areas, may not be representative of regional groundwater temperature or short
1302 residence-time hyporheic water. Future studies could clarify floodplain water thermal regimes and
1303 sources by installing deeper floodplain wells and temperature sensors at various depths.

1304

1305 The Big Picture

1306 My results show that geophysical, thermal, and hydrological factors appear to influence bull
1307 trout spawning occurrence at multiple spatial scales. At the subreach and reach-scales, high density
1308 spawning tends to occur where dominant textural facies exhibit mobile spawning appropriate gravels
1309 where streambed hydraulic conductivities and rates of streambed hyporheic exchange are high. Specific
1310 local-scale pre-spawning streambed flux direction and magnitude may be less relevant because redd
1311 structure induces the necessary hyporheic flows through the redd gravels (e.g. Tonina and Buffington,
1312 2011). In streams and reaches where dominant textural facies are not fine enough for redd construction,
1313 redd distribution is patchy, occurring in isolated gravel accumulations not represented by sub-reach
1314 scale characterization (e.g. behind boulders or large woody debris). Spawning bull trout in these study
1315 streams tended to select fine-grained textural facies easily mobilized and reworked by geomorphically
1316 significant flows in alluvial valleys, suggesting that bull trout are responsive to the most dynamic
1317 sections of catchments where flows, sediments, and nutrients are most actively cycled. Transport and
1318 reworking of these streambed sections also appears to result in higher vertical hydraulic conductivity
1319 (K_v) of the streambed. However, spawning preference for streambed sections of mobile sediment at
1320 bankfull flows indicates that redds may be susceptible to scour during late fall, winter, and early spring
1321 high flow events. Such high flow events can be caused by heavy rains, rain on snow events, or snowmelt.

1322 At the valley scale, high density spawning reaches tend to occur in unconfined alluvial valley
1323 segments where stream temperatures are moderated (buffered and cooled or warmed – depending on
1324 the season) by hyporheic and groundwater discharge to the stream. Unconfined alluvial valley segments
1325 tend to host more spatially extensive suitable spawning gravels than confined valley segments because
1326 of increased hydraulic roughness factors (e.g. bars, banks, wood, riparian vegetation, and an accessible
1327 floodplain at high flows: Buffington and Montgomery, 1999b). Hydraulic roughness factors act to
1328 decrease the amount of total channel shear stress applied to the streambed and allows for more

1329 extensive distributions of spawning appropriate gravels. Additionally, alluvial valley sediment
1330 depositional processes determine alluvial depth, structure, and horizontal and vertical hydraulic
1331 conductivities. Interrelations of these factors contribute to the development of various surface and
1332 subsurface temperature regimes, which are dependent on flow path residence time and depth.
1333 Discharge of hyporheic and groundwater to the stream channel can moderate (buffer, lag, warm or cool:
1334 Arrigoni et al., 2008) stream water temperatures and help support salmonid spawning habitat.

1335 Implications and applications of this study and related research are many. My study shows that
1336 dimensionless variables such as Shields stress (or Shields stress adjusted for bed stress only) and the
1337 coefficient of variation in water temperature can be used to evaluate ecologically important physical
1338 conditions and processes within and between stream systems and to assess salmonid spawning habitat
1339 and other ecological topics in similar physical systems.

1340 My study provides further evidence that alluvial valleys in snowmelt-dominated mountain
1341 streams are essential components of natural ecosystem function; as these features cannot be created,
1342 their preservation is important. Further, I illustrate how remote sensing of landscape features (e.g.
1343 confined and unconfined valley segments) can be used to relate physical processes to ecological
1344 responses, such as relating of bull trout spawning occurrence to alluvial valley presence and surface
1345 water – groundwater exchange.

1346 To delineate and protect critical interior coho salmon spawning habitat, McRae et al. (2012)
1347 recommend intensive sampling of physical and chemical hyporheic zone characteristics. My study
1348 indicates that less resource intensive, broader-scale salmonid habitat assessments (of variables such as
1349 valley confinement, streambed mobility, stream temperature variability, and groundwater discharge
1350 zones) may be efficient and effective in delineating critical habitat zones and prioritizing conservation
1351 and management plans.

1352 Changes in habitat suitability due to climate change is a topic of recent research (e.g. Rieman et
1353 al., 2007; Isaak et al., 2010; Wenger et al., 2011; Isaak et al., 2012; Jones et al., *in press*). Isaak et al.
1354 (2012) suggest that, for the period 1950-2009, flows have increased in winter months in the Flathead
1355 River Basin. My spawning gravel competence results suggest that a shift in timing of high flows could
1356 increase the likelihood of bull trout redd scour.

1357 Thermal sensitivity has long been a focus of bull trout habitat studies. My data indicate that
1358 groundwater is a more dominant control on stream temperature than snow- or ice-melt during the fall
1359 bull trout spawning season in the Flathead River Basin. One reason for the diminished role of glacial melt
1360 on stream temperature cooling in the Quartz drainage and similar glacier drainages in Glacier National
1361 Park is the thermal moderation (warming) of headwater lakes that intercept the melt water prior to
1362 flowing downstream into bull trout spawning reaches (e.g. Mellina et al., 2002; Hieber et al., 2002).
1363 Supporting this, Jones et al. (*in press*) used empirical temperature data to model stream temperatures in
1364 the Flathead River Basin and found significant warming (+3°C) of summer (August) stream temperatures
1365 downstream of lakes. Streams dominated by groundwater thermal moderation may be more buffered
1366 from habitat fragmentation due to climate warming. Therefore, to reduce existing and future stressors,
1367 an important conservation strategy is to protect and enhance the physical connectivity of existing high
1368 quality bull trout habitat (Jones et al., *in press*).

1369 Salmonid habitat suitability studies can be particularly applicable to stream restoration. My
1370 study emphasizes the importance the physical and biological connection of the stream, hyporheic, and
1371 groundwater systems. Protection and improvement of spatially extensive suitable physical and thermal
1372 habitat is important for conserving threatened bull trout populations in the northern Rocky Mountains
1373 and Pacific Northwest.

1374
1375

1376 **CONCLUSIONS**

1377 My findings indicate that physical processes at multiple-spatial scales influence bull trout redd
1378 occurrence in snowmelt dominated systems. At the subreach- and reach-scale, redd occurrence tends to
1379 be associated with mobile surface gravels that have high horizontal and vertical hydraulic conductivities.
1380 At the valley-scale, redd occurrence tends to be associated with unconfined alluvial valleys where
1381 stream temperatures are thermally suitable. Groundwater appears to play a major role in providing
1382 favorable conditions for bull trout spawning reaches. In light of the spawning gravel competence results,
1383 shifts in timing of high flows associated with climate change (e.g. Isaak et al., 2012) could adversely
1384 affect bull trout spawning by increasing the likelihood of redd scour.

1385 The difference between my findings and previous studies related to streambed mobility and
1386 salmonid spawning site selection merits further attention. In terms of using and expanding on the
1387 findings of this study, basin-wide grain size prediction models (e.g. Buffington et al., 2004) could be used
1388 to assess the broader-scale distribution of physically suitable spawning habitat. Basin-wide valley
1389 confinement delineations and stream temperature monitoring networks could be used to further assess
1390 stream thermal regimes and identify the role of groundwater in modifying the thermal regime of this
1391 system. Further clarification of the role of groundwater in patch and subreach-scale bull trout spawning
1392 site selection is also merited.

1393

1394 List of abbreviations and symbols used in text and their definitions

1395	OLE_{mc}	Ole Creek main channel study reach
1396	OLE_{sc}	Ole Creek secondary channel study reach
1397	QTZ	Quartz Creek study reach
1398	TRL	Trail Creek study reach
1399	WHL_{mc}	Whale Creek main channel study reach
1400	WHL_{sc}	Whale Creek secondary channel study reach
1401	τ_o	total boundary shear stress
1402	τ'	bed shear stress
1403	τ^*	Shields stress (incorporates τ_o)
1404	τ^{**}	adjusted Shields stress (incorporates τ')
1405	ρ_w	water density
1406	ρ_s	sediment density
1407	VHG	vertical hydraulic gradient
1408	K_h	horizontal hydraulic conductivity
1409	K_v	vertical hydraulic conductivity
1410	K_h/K_v	hydraulic conductivity anisotropy ratio
1411	q_v	specific discharge
1412	C_v	coefficient of variation in stream temperature

1413

1414

1415 **REFERENCES**

- 1416 Al-Chokhachy, R., B.B. Roper, T. Bowerman, and P. Budy. 2010. A review of bull trout habitat
1417 associations and exploratory analyses of patterns across the interior Columbia River Basin. *North*
1418 *American Journal of Fisheries Management* 30 (2): 464–480.
- 1419
1420 Alexander, M.D., and D. Caissie. 2003. Variability and comparison of hyporheic water temperatures and
1421 seepage fluxes in a small Atlantic salmon stream. *Ground Water* 41 (1): 72–82.
- 1422
1423 Arrigoni, A.S., G.C. Poole, L.A.K. Mertes, S.J. O’Daniel, W.W. Woessner, and S.A. Thomas. 2008. Buffered,
1424 lagged, or cooled? Disentangling hyporheic influences on temperature cycles in stream channels. *Water*
1425 *Resources Research* 44: W09418.
- 1426
1427 Barnes, H.H. 1967. Roughness characteristics of natural channels. USGS Water Supply Paper 1849.
- 1428
1429 Baxter, C., F.R. Hauer, and W.W. Woessner. 2003. Measuring groundwater-stream water exchange: new
1430 techniques for installing minipiezometers and estimating hydraulic conductivity. *Transactions of the*
1431 *American Fisheries Society* 132 (3): 493–502.
- 1432
1433 Baxter, C.V., and F.R. Hauer. 2000. Geomorphology, hyporheic exchange, and selection of spawning
1434 habitat by bull trout (*Salvelinus Confluentus*). *Canadian Journal of Fisheries and Aquatic Sciences* 57 (7):
1435 1470–1481.
- 1436
1437 Baxter, C.V., C.A. Frissell, and F.R. Hauer. 1999. Geomorphology, logging roads, and the distribution of
1438 bull trout spawning in a forested river basin: implications for management and conservation.
1439 *Transactions of the American Fisheries Society* 128 (5): 854–867.
- 1440
1441 Baxter, J.S., and J.D. McPhail. 1999. The influence of redd site selection, groundwater upwelling, and
1442 over-winter incubation temperature on survival of bull trout (*Salvelinus Confluentus*) from egg to alevin.
1443 *Canadian Journal of Zoology* 77 (8): 1233–1239.
- 1444
1445 Baxter, J.S., and J.D. McPhail. 1996. A review of bull trout (*Salvelinus Confluentus*) life-history and
1446 habitat use in relation to compensation and improvement opportunities. Fisheries Management Report
1447 Number 104. Ministry of Environment, Lands and Parks.
- 1448
1449 Benson, N.G. 1953. The importance of groundwater to trout populations in the Pigeon River, Michigan.
1450 *In Transactions of the North American Wildlife Conference* (18): 260–281.
- 1451
1452 Benson, N.G. 1955. Observations on anchor ice in a Michigan trout stream. *Ecology* 36 (3): 529–530.
- 1453
1454 Bhaskar, A.S., J.W. Harvey, and E.J. Henry. 2012. Resolving hyporheic and groundwater components of
1455 streambed water flux using heat as a tracer. *Water Resources Research* 48: W08524.
- 1456
1457 Bjornn, T.C., and D.W. Reiser. 1991. Habitat requirements of salmonids in streams. *American Fisheries*
1458 *Society Special Publication* (19): 83–138.
- 1459
1460 Boulton, A.J., T. Datry, T. Kasahara, M. Mutz, and J.A. Stanford. 2010. Ecology and management of the
1461 hyporheic zone: stream-groundwater interactions of running waters and their floodplains. *Journal of the*
1462 *North American Benthological Society* 29 (1): 26–40.

1463
1464 Boughton, D.A., C. Hatch, and E. Mora. 2012. Identifying distinct thermal components of a creek. *Water*
1465 *Resources Research* 48: W09506.
1466
1467 Buffington, J.M., D.R. Montgomery, and H.M. Greenberg. 2004. Basin-scale availability of salmonid
1468 spawning gravel as influenced by channel type and hydraulic roughness in mountain catchments.
1469 *Canadian Journal of Fisheries and Aquatic Sciences* 61 (11): 2085–2096.
1470
1471 Buffington, J.M., and D.R. Montgomery. 1997. A systematic analysis of eight decades of incipient motion
1472 studies, with special reference to gravel-bedded rivers. *Water Resources Research* 33 (8): 1993–2029.
1473
1474 Buffington, J.M., and D.R. Montgomery. 1999a. A procedure for classifying textural facies in gravel-bed
1475 rivers. *Water Resources Research* 35 (6): 1903–1914.
1476
1477 Buffington, J.M., and D.R. Montgomery. 1999b. Effects of hydraulic roughness on surface textures of
1478 gravel-bed rivers. *Water Resources Research* 35 (11): 3507–3521.
1479
1480 Bunte, K. and S.R. Abt. 2001. Sampling surface and sub-surface particle size distributions in wadeable
1481 gravel- and cobble-bed streams for analysis in sediment transport, hydraulics, and streambed
1482 Monitoring. USDA Forest Service, General Technical Report, RMRS-GTR-74. 450 pp.
1483
1484 Burner, C.J. 1951. Characteristics of Spawning Nests of Columbia River Salmon. US Department of the
1485 Interior.
1486
1487 Butler, J.J. Jr. 1998. The design, performance, and analysis of slug tests. Lewis Publishers.
1488
1489 Brunner, G.W. 2010. HEC-RAS River Analysis System: user’s manual. US Army Corps of Engineers,
1490 Hydrologic Engineering Center.
1491
1492 Cardenas, M.B., J.L. Wilson, and V.A. Zlotnik. 2004. Impact of heterogeneity, bed forms, and stream
1493 curvature on subchannel hyporheic exchange. *Water Resources Research* 40 (8): W08307.
1494
1495 Caissie, D. The thermal regime of rivers: a review. *Freshwater Biology* 51: 1389–1406.
1496
1497 Chen, X. 2000. Measurement of streambed hydraulic conductivity and its anisotropy. *Environmental*
1498 *Geology* 39 (12): 1317–1324.
1499
1500 Chevalier, B., C. Carson, and W.J. Miller. 1984. Report of Engineering and Biological Literature Pertaining
1501 to the Aquatic Environment: With Special Emphasis on Dissolved Oxygen and Sediment Effects on
1502 Salmonid Habitat. Colorado State University, Department of Agriculture and Chemical Engineering.
1503
1504 Church, M. 2006. Bed material transport and the morphology of alluvial river channels. *Annual Review*
1505 *of Earth and Planetary Sciences* 34: 325–354.
1506
1507 Church, M.A., D.G. McLean, and J.F. Wolcott. 1987. River bed gravels: sampling and analysis. *Sediment*
1508 *transport in Gravel-Bed Rivers*. John Wiley and Sons New York. 43-88.
1509

1510 Cordone, A.J., and D.W. Kelley. 1961. The influences of inorganic sediment on the aquatic life of
1511 streams. California Fish and Game 47.
1512

1513 Cunjak, R.A., and G. Power. 1986. Winter habitat utilization by stream resident brook trout (*Salvelinus*
1514 *fontinalis*) and brown trout (*Salmo trutta*). Canadian Journal of Fisheries and Aquatic Sciences 43 (10):
1515 1970–1981.
1516

1517 Curry, R.A., and D.L. Noakes. 1995. Groundwater and the selection of spawning sites by brook trout
1518 (*Salvelinus fontinalis*). Canadian Journal of Fisheries and Aquatic Sciences 52 (8): 1733–1740.
1519

1520 Daly, D., and G. Taylor. 1998. Montana average annual precipitation (1961-1990). Oregon Climate
1521 Service at Oregon State University.
1522

1523 DeVries, P. 1997. Riverine salmonid egg burial depths: review of published data and implications for
1524 scour studies. Canadian Journal of Fisheries and Aquatic Sciences 54 (8): 1685-1698.
1525

1526 DeVries, P. 2002. Bedload layer thickness and disturbance depth in gravel bed streams. Journal of
1527 Hydraulic Engineering. 128 (11): 983-991.
1528

1529 Dingman, S. L. 2009. Fluvial Hydraulics. Oxford University Press.
1530

1531 Dunham, J., B. Rieman, and K. Davis. 2001. Sources and magnitude of sampling error in redd counts for
1532 bull trout. North American Journal of Fisheries Management 21 (2): 343–352.
1533

1534 Dunham, J., C. Baxter, K. Fausch, W. Fredenberg, S. Kitano, I. Koizumi, K. Morita, et al. 2008. Evolution,
1535 ecology, and conservation of dolly varden, white spotted char, and bull trout. Fisheries 33 (11): 537–550.
1536

1537 Embody, G. C. 1927. An outline of stream study and the development of a stocking policy. Aquicultural
1538 Laboratory, Cornell University: 1-21.
1539

1540 Einstein, H.A., and R.B. Banks. 1950. Fluid resistance of composite roughness, American Geophysical
1541 Union Eos Transactions 31: 603–610.
1542

1543 Einstein, H.A., and N.L. Barbarossa. 1952. River channel roughness. Transaction of the American Society
1544 of Civil Engineers 117: 1121–1146.
1545

1546 Ellis, B.K., J.A. Stanford, D. Goodman, C.P. Stafford, D.L. Gustafson, D.A. Beauchamp, D.W. Chess, J.A.
1547 Craft, M.A. Deleray, and B.S. Hansen. 2011. Long-term effects of a trophic cascade in a large lake
1548 ecosystem. Proceedings of the National Academy of Sciences 108 (3): 1070–1075.
1549

1550 Fetter, C. W. 2001. Applied Hydrogeology, 4th Ed. Prentice Hall.
1551

1552 Fraley, J. 2010. Bull trout counts steady in the Flathead, up in the South Fork, down in the Swan.
1553 Montana Fish, Wildlife, and Parks News Release.
1554

1555 Fraley, J.J., and B.B. Shepard. 1989. Life history, ecology and population status of migratory bull trout
1556 (*Salvelinus confluentus*) in the Flathead Lake and River system. Northwest Science 63 (4): 133–143.
1557

1558 Gibson, R.J. 1966. Some factors influencing the distributions of brook trout and young Atlantic salmon.
1559 Journal of the Fisheries Board of Canada 23 (12): 1977–1980.
1560

1561 Goetz, F. 1989. Biology of the Bull Trout, *Salvelinus Confluentus*: a Literature Review. Oregon State
1562 University, Department of Fisheries and Wildlife.
1563

1564 Gooseff, M.N., J.M. Wondzell, R. Haggerty, and J. Anderson. 2003. Comparing transient storage
1565 modeling and residence time distribution(RTD) analysis in geomorphically varied reaches in the Lookout
1566 CreekBasin, Oregon, USA. Advanced Water Resources. 26 (9): 925– 937.
1567

1568 Haggerty, R., S.M. Wondzell, and M.A. Johnson. 2002. Power-law residence time distribution in the
1569 hyporheic zone of a 2nd-order mountain stream. Geophysical Research Letters 29 (13): GL014743.
1570

1571 Hall, J.E., Holzer, D.M. and Beechie, T.J. 2007. Predicting river floodplain and lateral channel migration
1572 for salmon habitat conservation. Journal of the American Water Resources Association 43: 786–797.
1573

1574 Hansen, E.A. 1975. Some effects of groundwater on brown trout redds. Transactions of the American
1575 Fisheries Society 104 (1): 100–110.
1576

1577 Haria, A.H., P. Shand, C. Soulsby, and S. Noorduijn. 2013. Spatial delineation of groundwater-surface
1578 water (GW-SW) interactions through intensive in-stream profiling. Hydrological Processes 27: 628-634.
1579

1580 Hatch, C.E., A.T. Fisher, J.S. Revenaugh, J. Constantz, and C. Ruehl. 2006. Quantifying surface water-
1581 groundwater interactions using time series analysis of streambed thermal records: method
1582 development. Water Resources Research 42: W10410.
1583

1584 Healey, M. C. 1991. Life history of chinook salmon (*Oncorhynchus shawytscha*). Pacific Salmon Life
1585 Histories: 313–393.
1586

1587 Hieber, M., C.T. Robinson, U. Uehlinger, and J.V. Ward. 2002. Are alpine lake outlets less harsh than
1588 other alpine streams? Archiv fur Hydrobiologie 154: 199-223.
1589

1590 Isaak, D.J., C.C. Muhlfeld, A.S. Todd, R. Al-Chokhachy, J. Roberts, J.L. Kershner, K.D. Fausch, S.W.
1591 Hostetler. The past as prelude to the future for understanding 21st-Century climate effects on Rocky
1592 Mountain trout. Fisheries Management 37: 542-556.
1593

1594 Isaak, D.J., C. H. Luce, B.E. Rieman, D.E. Nagel, E.E. Peterson, D.L. Horan, S. Parkes, and G.L. Chandler.
1595 2010. Effects of climate change and wildfire on stream temperatures and salmonid thermal habitat in a
1596 mountain river network. Ecological Applications 20 (5): 1350–1371.
1597

1598 Janssen, F., M.B. Cardenas, A.H. Sawyer, T. Dammrich, J. Krietsch, and D. de Beer. 2012. A comparative
1599 experimental and multiphysics computational fluid dynamics study of coupled surface–subsurface flow
1600 in bed forms. Water Resources Research 48: W08514.
1601

1602 Johnson, A.N., B.R. Boer, W.W. Woessner, J.A. Stanford, G.C. Poole, S.A. Thomas, and S.J. O’Daniel. 2005.
1603 Evaluation of an inexpensive small-diameter temperature logger for documenting ground water–river
1604 interactions. Ground Water Monitoring & Remediation 25 (4): 68–74.
1605

1606 Kasahara, T., and S.M. Wondzell. 2003. Geomorphic controls on hyporheic exchange flow in mountain
1607 streams. *Water Resources Research* 39.
1608

1609 Kasenow, M. 2001. *Applied ground-water hydrology and well hydraulics*. Water Resources Publication.
1610

1611 Keery, J., A. Binley, N. Crook, and J.W.N. Smith. 2007. Temporal and spatial variability of groundwater-
1612 surface water fluxes: development and application of an analytical method using temperature time
1613 series. *Journal of Hydrology* 336: 1–16.
1614

1615 Keller, E.A., and G.M. Kondolf. 1990. Groundwater and fluvial processes; selected observations. *In*::
1616 *Groundwater Geomorphology: The role of subsurface water in earth-surface processes and landforms*.
1617 Geological Society of America. 319-340.
1618

1619 Kellerhals, R., and D.I. Bray. 1971. Sampling procedures for coarse fluvial sediments, *Journal Hydraulics*
1620 *Division American Society of Civil Engineers* 97: 1165–1180.
1621

1622 Kondolf, G.M. 2000. Assessing salmonid spawning gravel quality. *Transactions of the American Fisheries*
1623 *Society* 129 (1): 262–281.
1624

1625 Kondolf, G.M., T.E. Lisle, and G.M. Wolman. 2003. Bed sediment measurement. *In*: *Tools in Fluvial*
1626 *Geomorphology*, edited by G.M. Kondolf and H. Piegay, 347-395.
1627

1628 Kondolf, G.M., and M.G. Wolman. 1993. The sizes of salmonid spawning gravels. *Water Resources*
1629 *Research* 29 (7): 2275–2285.
1630

1631 Kondolf, G.M., J.G. Williams, T.C. Horner, and D. Milan. 2008. Assessing physical quality of spawning
1632 habitat. *In*: , 65.
1633

1634 Latta, W.C. 1964. Relationship of young of-the-year trout to mature trout and groundwater.
1635 *Transactions of the American Fisheries Society* 94: 32-39.
1636

1637 Lawlor, S.M. 2004. Determination of channel-morphology characteristics, bankfull discharge, and
1638 various design-peak discharges in Western Montana. *USGS Special Investigations Report 2004-5263*: 1-
1639 26.
1640

1641 Lee, D.R., and J.A. Cherry. 1978. A field exercise on groundwater flow using seepage meters and mini-
1642 piezometers. *Journal of Geological Education* 27: 6–10.
1643

1644 Lunt, I.A., and J.S. Bridge. 2006. Formation and preservation of open-framework gravel strata in
1645 unidirectional flows. *Sedimentology* 54 (1): 71–87.
1646

1647 Malcolm, I.A., A.F. Youngson, and C. Soulsby. 2003. Survival of salmonid eggs in a degraded gravel-bed
1648 stream: effects of groundwater–surface water interactions. *River Research and Applications* 19 (4): 303–
1649 316.
1650

1651 Malcolm, I.A., C. Soulsby, A.F. Youngson, and D.M. Hannah. 2005. Catchment-scale controls on
1652 groundwater-surface water interactions in the hyporheic zone: implications for salmon embryo survival.
1653 *River Research and Applications* 21 (9): 977–989.

1654
1655 Marion, A., A.I. Packman, M. Zaramella, and A. Bottacin-Busolin. 2008. Hyporheic flows in stratified
1656 beds. *Water Resources Research* 44 (9).
1657
1658 McCullough, D.A., J.M. Bartholow, H.I. Jager, R.L. Beschta, E.F. Cheslak, M.L. Deas, J.L. Ebersole. 2009.
1659 Research in thermal biology: burning questions for coldwater stream fishes. *Reviews in Fisheries*
1660 *Science* 17 (1): 90–115.
1661
1662 McElwee, C.D. and J. J. Butler, Jr. 1996. Experimental verification of a general model for slug tets. Kansas
1663 Geological Survey Open-File Report 96-47.
1664
1665 McPhail, J.D., and C.B. Murray. 1979. The early life-history and ecology of Dolly Varden (*Salvelinus*
1666 *malma*) in the upper Arrow Lakes. Department of Zoology and Institute of Animal Resources, University
1667 of British Columbia.
1668
1669 Mellina E., R.D. Moore, S.G. Hinch, J.S. Macdonald, and G. Pearson. 2002. Stream temperature
1670 responses to clearcut logging in British Columbia: the moderating influences of groundwater and
1671 headwater lakes. *Canadian Journal of Fisheries and Aquatic Sciences* 59, 1886-1900.
1672
1673 Moir, H.J., C.N. Gibbins, J.M. Buffington, J.H. Webb, C. Soulsby, M.J. Brewer, and others. 2009. A new
1674 method to identify the fluvial regimes used by spawning salmonids. *Canadian Journal of Fisheries and*
1675 *Aquatic Sciences* 66 (9): 1404–1408.
1676
1677 Moir, H.J., C. Soulsby, and A.F. Youngson. 2002. Hydraulic and sedimentary controls on the availability
1678 and use of Atlantic salmon (*Salmo Salar*) spawning habitat in the River Dee system, northeast Scotland.
1679 *Geomorphology* 45 (3): 291–308.
1680
1681 Moir, H.J., C.N. Gibbins, C. Soulsby, and J.H. Webb. 2006. Discharge and hydraulic interactions in
1682 contrasting channel morphologies and their influence on site utilization by spawning Atlantic salmon
1683 (*Salmo salar*). *Canadian Journal of Fisheries and Aquatic Sciences* 63 (11): 2567–2585.
1684
1685 Montgomery, D.R., E.M. Beamer, G.R. Pess, and T.P. Quinn. 1999. Channel type and salmonid spawning
1686 distribution and abundance. *Canadian Journal of Fisheries and Aquatic Sciences* 56 (3): 377–387.
1687
1688 Montgomery, D.R., and J.M. Buffington. 1997. Channel-reach morphology in mountain drainage basins.
1689 *Geological Society of America Bulletin* 109 (5): 596-611.
1690
1691 Montgomery, D.R., J.M. Buffington, N.P. Peterson, D. Schuett-Hames, and T.P. Quinn. 1996. Stream-bed
1692 scour, egg burial depths, and the influence of salmonid spawning on bed surface mobility and embryo
1693 survival. *Canadian Journal of Fisheries and Aquatic Sciences* 53 (5): 1061–1070.
1694
1695 Muhlfeld, C.C., M.L. Taper, D.F. Staples, and B.B. Shepard. 2006. Observer error structure in bull trout
1696 redd counts in Montana streams: implications for inference on true redd numbers. *Transactions of the*
1697 *American Fisheries Society* 135 (3): 643–654.
1698
1699 Muhlfeld, C.C., S. Glutting, R. Hunt, D. Daniels, and B. Marotz. 2003. Winter diel habitat use and
1700 movement by subadult bull trout in the Upper Flathead River, Montana. *North American Journal of*
1701 *Fisheries Management* 23 (1): 163–171.

1702
1703 Muhlfeld, C.C., S.T. Kalinowski, T.E. McMahon, M.L. Taper, S. Painter, R.F. Leary, and F.W. Allendorf.
1704 2009. Hybridization rapidly reduces fitness of a native trout in the wild. *Biology Letters* 5 (3): 328-331.
1705
1706 Muhlfeld, C.C., L. Jones, D. Kotter, W.J. Miller, D. Geise, J. Tohtz, and B. Marotz. 2011. Assessing the
1707 impacts of river regulation on native bull trout (*Salvelinus Confluentus*) and western cutthroat trout
1708 (*Oncorhynchus Clarkii Lewisii*) habitats in the Upper Flathead River, Montana, USA. *River Research and*
1709 *Applications: RRA.1494.*
1710
1711 Muhlfeld, C.C., and B. Marotz. 2005. Seasonal movement and habitat use by subadult bull trout in the
1712 Upper Flathead River System, Montana. *North American Journal of Fisheries Management* 25 (3): 797–
1713 810.
1714
1715 Muhlfeld, C.C., J.J. Giersch, and B. Marotz. 2012. Seasonal movements of non-native lake trout in a
1716 connected lake and river system. *Fisheries Management and Ecology* 19: 224-232.
1717
1718 Nagel, D.E., J.M. Buffington, S.L. Parkes, S. Wenger, and J Goode. *In press*. A landscape scale valley
1719 confinement algorithm: delineating unconfined valley bottoms for geomorphic, aquatic, and riparian
1720 applications. USDA/USFS Rocky Mountain Research Station General Technical Report Draft.
1721
1722 NAIP. 2011. U.S. Farm Services Agency National Agricultural Imagery Program (NAIP): Natural-color
1723 aerial photos of Montana. http://nris.mt.gov/nsdi/orthophotos/naip_2011.asp
1724
1725 Nielsen, J.L., T.E. Lisle, and V. Ozaki. 1994. Thermally stratified pools and their use by steelhead in
1726 northern California streams. *Transactions of the American Fisheries Society* 123 (4): 613–626.
1727
1728 Pandit, N.S., and R.F. Miner. 1986. Interpretation of slug test data. *Ground Water* 24 (6): 743–749.
1729
1730 Parker, G., and A.W. Peterson. 1980. Bar resistance of gravel-bed streams. *Journal Hydraulics Division of*
1731 *the American Society of Civil Engineers* 106, 1559–1575.
1732
1733 Parrett, C., D.R. Johnson. 2004. Methods for Estimating Flood Frequency in Montana Based on Data
1734 Through Water Year 1998. US Department of the Interior, US Geological Survey.
1735
1736 Pettijohn, F.J. 1975. *Sedimentary Rocks*. 3rd Ed. Harper & Row, New York.
1737
1738 Poff, N. 1996. A hydrogeography of unregulated streams in the United States and an examination of
1739 scale-dependence in some hydrological descriptors. *Freshwater Biology* 36 (1): 71–79.
1740
1741 Poole, G.C., S.J. O’Daniel, K.L. Jones, W.W. Woessner, E.S. Bernhardt, A.M. Helton, J.A. Stanford, B.R.
1742 Boer, and T.J. Beechie. 2008. Hydrologic spiralling: the role of multiple interactive flow paths in stream
1743 ecosystems. *River Research and Applications* 24 (7): 1018–1031.
1744
1745 Poole, G.C. 2010. Stream hydrogeomorphology as a physical science basis for advances in stream
1746 ecology. *Journal of the North American Benthological Society* 29 (1): 12–25.
1747

1748 Rieman, B.E., D.C. Lee, and R.F. Thurow. 1997. Distribution, status, and likely future trends of bull trout
1749 within the Columbia River and Klamath River basins. *North American Journal of Fisheries Management*
1750 17 (4): 1111–1125.

1751

1752 Rieman, B.E., D. Isaak, S. Adams, D. Horan, D. Nagel, C. Luce, and D. Myers. 2007. Anticipated climate
1753 warming effects on bull trout habitats and populations across the interior Columbia River Basin.
1754 *Transactions of the American Fisheries Society* 136 (6): 1552–1565.

1755

1756 Rieman, B.E., and J.D. McIntyre. 1993. Demographic and Habitat Requirements for Conservation of Bull
1757 Trout. USDA General Technical Report.

1758

1759 Santhi, C., P.M. Allen, R.S. Muttiah, J.G. Arnold, and P. Tuppada. 2008. Regional estimation of base flow
1760 for the conterminous United States by hydrologic landscape regions. *Journal of Hydrology* 351 (1): 139–
1761 153.

1762

1763 Sauter, S.T., J. McMillan, and J. Dunham. 2001. Salmonid behavior and water temperature. US
1764 Environmental Protection Agency Report EPA-910-D0-01-001.

1765

1766 Schlumberger, 2011. AquiferTest 2011.1 software package.

1767

1768 Shapiro, S.S., and M.B. Wilk. 1965. An analysis of variance test for normality (complete samples).
1769 *Biometrika* 52 (3/4): 591–611.

1770

1771 Shellberg, J.G. 2002. Hydrologic, geomorphic, and biologic influences on redd scour in bull char
1772 (*Salvelinus confluentus*) spawning streams. M.S. thesis, University of Washington, College of Forest
1773 Resources.

1774

1775 Shellberg, J.G., S.M. Bolton, and D.R. Montgomery. 2010. Hydrogeomorphic effects on bedload scour in
1776 bull char (*Salvelinus confluentus*) spawning habitat, western Washington, USA. *Canadian Journal of*
1777 *Fisheries and Aquatic Sciences* 67 (4): 626–640.

1778

1779 Shields, A. 1936. Anwendung der Aehnlichkeitsmechanik und der Turbulenzforschung auf die
1780 Geschiebebewegung, Mitt. Preuss. Versuchsanst. Wasserbau Schiffbau, 26.

1781

1782 Stanford, J.A, and J.V. Ward. 1993. An ecosystem perspective of alluvial rivers: connectivity and the
1783 hyporheic corridor. *Journal of the North American Benthological Society* 12 (1): 48–60.

1784

1785 Swanson, T.E., and M.B. Cardenas. 2011. Ex-Stream: a MATLAB program for calculating fluid flux through
1786 sediment-water interfaces based on steady and transient temperature profiles. *Computers &*
1787 *Geosciences* 37 (10): 1664–1669.

1788

1789 Tague, C., G. Grant, M. Farrell, J. Choate, and A. Jefferson. 2008. Deep groundwater mediates
1790 streamflow response to climate warming in the Oregon Cascades. *Climatic Change* 86 (1): 189–210.

1791

1792 Tennant, L. 2010. Spawning and early life-history characteristics of bull trout in a headwater-lake
1793 ecosystem. M.S. thesis, Montana State University, Fish and Wildlife Management.

1794

1795 Tonina, D., and J. M. Buffington. 2009a. Hyporheic exchange in mountain rivers I: mechanics and
1796 environmental effects. *Geography Compass* 3 (3): 1063–1086.
1797

1798 Tonina, D., and J.M. Buffington. 2009b. A three-dimensional model for analyzing the effects of salmon
1799 redds on hyporheic exchange and egg pocket habitat. *Canadian Journal of Fisheries and Aquatic Sciences*
1800 66 (12): 2157–2173.
1801

1802 Tonina, D., and J.M. Buffington. 2011. Effects of stream discharge, alluvial depth and bar amplitude on
1803 hyporheic flow in pool-riffle channels. *Water Resources Research* 47.
1804

1805 USFWS, 2008. Montana bull trout distribution. Draft map created by the US Fish and Wildlife Service
1806 (USFWS) Montana Ecological Services Field Office.
1807

1808 U.S. Office of the Federal Register. 1998. Endangered and threatened wildlife and plants; determination
1809 of threatened status for the Klamath River and Columbia River distinct population segments of bull
1810 trout. *Federal Register* 63: 111: 31647-31674.
1811

1812 U.S. Office of the Federal Register. 2010. Endangered and threatened wildlife and plants; revised
1813 sesignation of critical habitat for bull trout in the coterminous United States; final rule. *Federal Register*
1814 75: 200: 63898-64070.
1815

1816 Van Grinsven, M., A. Mayer, and C. Huckins. 2011. Estimation of streambed groundwater fluxes
1817 associated with coaster brook trout spawning habitat. *Ground Water* 50 (3): 432–441.
1818

1819 Vuke, S.M., K.W. Porter, J.D. Conn, and D.A. Lopez. 2007. *Geologic Map of Montana*. Montana Bureau of
1820 Mines and Geology Geologic Map 62.
1821

1822 Weaver, T., and J. Fraley. 1991. Flathead Basin forest practices water quality and fisheries cooperative
1823 program: fisheries habitat and fish populations. Flathead Basin Commission, Kalispell, Montana.
1824

1825 Weaver, T.M., and R.G. White. 1985. Coal Creek fisheries monitoring study number III. Quarterly
1826 progress report to USDA FS, Montana State Cooperative Fisheries Research Unit, Bozeman, Montana.
1827

1828 Wilcock, P.R., J. Pitlick, and Y. Cui. 2009. Sediment transport primer: estimating bed-material transport
1829 in gravel-bed rivers. USDA Rocky Mountain Research Station, Fort Collins, CO.
1830

1831 Wilcox, A.C. 2012. GEO560 Fluvial Geomorphology lecture notes. The University of Montana
1832 Geosciences Department.
1833

1834 Wolman, M.G. 1954. A method of sampling coarse river-bed material. *American Geophysical Union*.
1835

1836 Wolman, M.G., and J.P. Miller. 1960. Magnitude and frequency of forces in geomorphic processes.
1837 *Journal of Geology* 68 (1): 54-74.
1838

1839 Wolock, D.M., T.C. Winter, and G. McMahon. 2004. Delineation and evaluation of hydrologic-landscape
1840 regions in the United States using geographic information system tools and multivariate statistical
1841 analyses. *Environmental Management* 34: 71–88.
1842

1843 Yalin, M.S., and E. Karahan. 1979. Inception of sediment transport. Journal Hydraulics Division of the
1844 American Society of Civil Engineers 105: 1433–1443.
1845
1846

1847 **APPENDIX 1A: Reach-scale Geomorphology**

1848

1849 **1.A.i. Study reach stream discharge estimation**

1850 Q_{spawn} is the discharge measured in the field via float tests in late August. Float tests was not
 1851 conducted in TRL or WHL_{sc} . Estimation of TRL Q_{spawn} was described in the methods section. To estimate
 1852 stream channel cross sectional area for the discharge float tests, water depth was measured every 0.5 m
 1853 across a specified cross section. Flow velocity was estimated by measuring the float time of a small stick
 1854 as it traveled from 10 m above the measured cross section to 10 m below the cross section. The average
 1855 velocity of three float tests was multiplied by 0.8 to estimate the average velocity of the in-stream water
 1856 according to standard methods (Embody, 1927). Discharge was estimated by multiplying this average
 1857 flow velocity estimate by the total cross sectional area.

1858 For Q_2 (Q_{bf}) estimation using the USGS Montana ungaged basin flood-frequency calculator
 1859 (Parrett and Johnson, 2004), drainage area was calculated from 30 m DEMs at the locations where the
 1860 field discharge measurements were conducted. Two different SNOTEL sites (Emery Creek #469,
 1861 elevation 1326 m; Graves Creek #500, elevation 1311 m) were used to estimate the average annual
 1862 precipitation (AAP) in the basins of our study streams. Both SNOTELs are within the elevation range of
 1863 our study reaches (~1250 m – 1372 m); Emery is proximal to and believed to be representative of Ole,
 1864 and Grave is proximal to and believed to be representative of Whale, Trail, and Quartz. AAP over the
 1865 last 20 years has been 102 cm at Emery and 122 cm at Graves. Therefore, AAP at Ole is estimated to be
 1866 102 cm while AAP at Whale, Trail, and Quartz is estimated to be 122 cm. Field observations of
 1867 vegetation density and type agree with the estimation that Ole receives less precipitation than the other
 1868 study streams.

1869 Percent forest cover, the final parameter used in the USGS discharge calculator was only a
 1870 required parameter for the Western Region streams (Quartz, Trail, and Whale). Field and aerial photo
 1871 observations suggest that Whale, Trail, and Quartz are all heavily forested. Decreased forest cover
 1872 density in Whale and Trail compared to Quartz due to road construction and other anthropogenic
 1873 factors are assumed to be countered by the steeper valley walls and more prominently outcropping
 1874 bedrock in Quartz which also decrease forest cover density. Therefore, I estimated Whale, Trail, and
 1875 Quartz to have 80% forest cover within their drainage basin upstream of the field measured discharge
 1876 cross section. It is noted that a fire about 10 years ago in the lower portion of the Whale drainage has
 1877 substantially decreased the forest cover density in that section; however, that burned section is several
 1878 kilometers downstream of the study area and therefore does not factor into the forest cover density
 1879 estimation for these discharge calculations.

1880 Q_{peak} in each study stream Twas obtained by proportionally scaling the 2011 peak discharges of
 1881 the North and Middle Forks of the Flathead River to the study streams by their respective contributing
 1882 areas. (e.g. Discharge of North Fork at USGS gage/Contributing area above the North Fork USGS gage =
 1883 Discharge of Trail Creek at bottom of study reach/Contributing area above the bottom of the Trail Creek
 1884 study reach).

1885

1886 Table 1A1. Study reach stream discharge estimates.

	Q_{spawn} (m^3/s)	Q_{bf} (m^3/s)	Q_{peak} 2011 (m^3/s)
OLE _{mc} and OLE _{sc} combined	3.4	14.3	24.7
QTZ	2.4	15	19.3
TRL	3.9	15.9	20.5
WHL _{mc}	3.5	4.1	4.6

1887

1888
 1889
 1890
 1891
 1892

1.A.ii. Gaged basin flood recurrence interval analyses

Table 1A2. Middle Fork Flathead River peak annual flow flood frequency analysis. (USGS gage number 12358500: M F Flathead River near West Glacier MT). The 2011 peak flow information is bold.

Rank 1940- 2011	Date	Q (cfs)	Recurrence interval (RI)	Probability (%)
1	6/9/1964	140000	73	1
2	6/20/1975	63600	37	3
3	5/19/1991	35000	24	4
4	5/20/1954	34500	18	5
5	11/12/1989	33700	15	7
6	5/17/1997	33000	12	8
7	5/23/1948	32600	10	10
8	6/18/1974	31900	9	11
9	5/19/2008	30700	8	12
10	3/2/1972	29600	7	14
11	5/22/1956	28300	7	15
12	5/23/1967	27900	6	16
13	5/27/1961	27100	6	18
14	6/6/1959	25800	5	19
15	6/8/2011	25200	5	21
16	6/13/1953	24800	5	22
17	5/5/1957	24200	4	23
18	5/28/1971	23900	4	25
19	5/9/1947	23600	4	26
20	6/6/1950	23600	4	27
21	6/5/1970	23400	3	29
22	6/9/1996	23300	3	30
23	5/11/1976	22600	3	32
24	6/16/2006	22500	3	33
25	5/31/2002	22400	3	34
26	5/27/1979	21600	3	36
27	6/4/1960	21500	3	37
28	6/19/1965	20900	3	38
29	5/26/1982	20800	3	40
30	6/18/1943	20600	2	41
31	5/26/1980	20500	2	42
32	5/26/1999	20400	2	44
33	6/8/1985	20200	2	45
34	5/12/1951	20100	2	47
35	5/15/1993	19900	2	48
36	5/26/2003	19800	2	49

37	5/22/1981	19600	2	51
38	5/14/1949	19500	2	52
39	5/13/1958	19400	2	53
40	5/30/1986	19400	2	55
41	5/31/2009	19100	2	56
42	5/11/1989	19000	2	58
43	5/1/1987	18700	2	59
44	11/8/2006	18700	2	60
45	5/29/1946	18500	2	62
46	5/31/1966	18400	2	63
47	5/31/1984	18200	2	64
48	4/28/1952	18100	2	66
49	6/3/1968	18000	1	67
50	5/18/1973	17900	1	68
51	6/6/1978	17600	1	70
52	6/14/1955	17500	1	71
53	5/27/1983	17400	1	73
54	6/1/1945	16400	1	74
55	5/24/1942	15700	1	75
56	5/23/2000	15300	1	77
57	5/13/1994	15200	1	78
58	6/7/1995	14900	1	79
59	5/19/2010	14300	1	81
60	5/15/1969	14200	1	82
61	5/20/1962	13900	1	84
62	5/13/1988	13100	1	85
63	5/1/1992	13000	1	86
64	5/26/2001	13000	1	88
65	5/12/1940	12800	1	89
66	5/27/1998	12800	1	90
67	6/4/2005	12800	1	92
68	5/31/1963	12700	1	93
69	5/20/1944	11300	1	95
70	5/5/2004	11100	1	96
71	5/11/1977	10400	1	97
72	5/14/1941	7620	1	99

1893

1894

1895

Table 1A3. North Fork Flathead River peak annual flow flood frequency analysis. (USGS gage number 12355500: N F Flathead River nr Columbia Falls MT). The 2011 peak flow information is bold.

Rank 1911- 2011	Date	Q (cfs)	Recurrence interval (RI)	Probability (%)
1	6/9/1964	69100	91	1
2	6/7/1995	59200	46	2

3	6/18/1974	34300	30	3
4	5/21/1954	31500	23	4
5	6/2/1972	31400	18	5
6	6/21/1975	30700	15	7
7	6/20/1916	30100	13	8
8	5/28/1961	29900	11	9
9	5/22/1956	29700	10	10
10	5/17/1997	29300	9	11
11	5/24/1948	26400	8	12
12	6/9/1996	26400	8	13
13	5/23/1967	26000	7	14
14	5/20/1991	25800	7	15
15	6/17/1917	25400	6	16
16	6/6/1959	25200	6	18
17	6/17/1933	24400	5	19
18	5/11/1976	24200	5	20
19	5/28/1938	24000	5	21
20	6/2/1913	23800	5	22
21	6/14/1953	23800	4	23
22	5/19/2008	23600	4	24
23	5/10/1947	23500	4	25
24	6/19/1965	23300	4	26
25	5/7/1957	23000	4	27
26	5/29/1986	22900	4	29
27	5/31/2002	22600	3	30
28	5/28/1971	22200	3	31
29	5/29/1946	22000	3	32
30	5/20/2006	21600	3	33
31	5/23/1932	21200	3	34
32	6/8/2011	21100	3	35
33	6/23/1950	21000	3	36
34	5/24/1935	20800	3	37
35	5/12/1951	20800	3	38
36	6/4/1960	20700	3	40
37	5/26/1999	20500	2	41
38	5/13/1958	20400	2	42
39	5/24/1929	20300	2	43
40	5/27/1983	20000	2	44
41	5/14/1949	19900	2	45
42	5/26/1982	19900	2	46
43	6/1/1966	19500	2	47
44	4/26/1934	19400	2	48
45	6/1/1990	19300	2	49

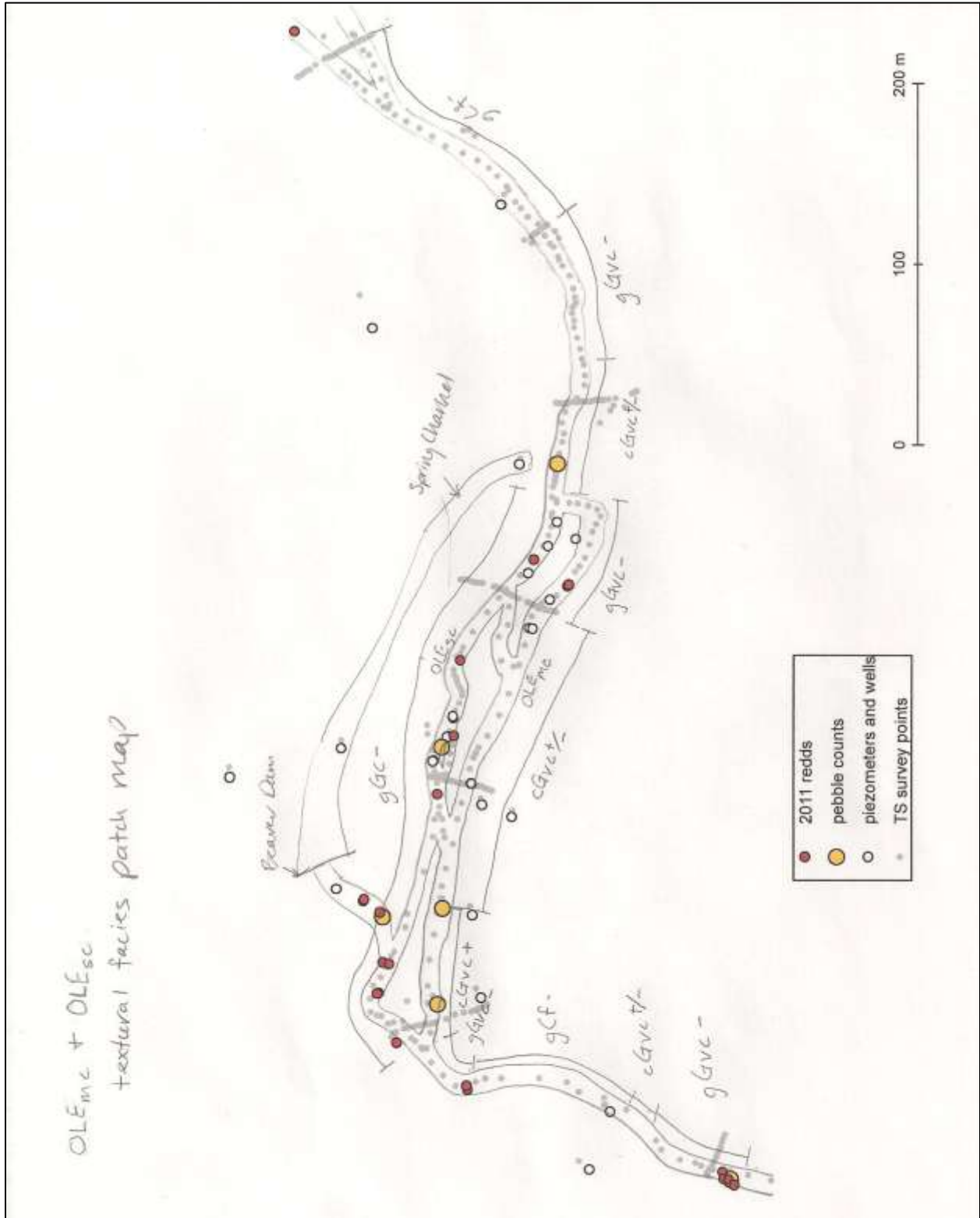
46	11/8/2006	19200	2	51
47	5/16/1936	19000	2	52
48	6/14/1955	18700	2	53
49	5/15/1993	18700	2	54
50	5/18/1973	18600	2	55
51	5/27/1979	18600	2	56
52	5/25/1985	18600	2	57
53	5/2/1987	18600	2	58
54	5/27/1970	18400	2	59
55	5/26/1980	18400	2	60
56	4/28/1952	18100	2	62
57	5/27/1942	18000	2	63
58	6/6/1978	18000	2	64
59	5/23/1981	18000	2	65
60	5/14/1969	17600	2	66
61	6/4/1968	17500	1	67
62	5/31/2009	16900	1	68
63	5/30/2003	16800	1	69
64	5/10/1989	16500	1	70
65	5/23/2000	16500	1	71
66	5/28/1998	16400	1	73
67	6/2/1945	15400	1	74
68	5/31/1984	15400	1	75
69	5/28/1943	15300	1	76
70	6/14/1911	15100	1	77
71	5/17/1931	15000	1	78
72	5/13/1994	14300	1	79
73	5/29/1962	14200	1	80
74	6/8/2005	14200	1	81
75	4/30/1939	14000	1	82
76	5/28/1937	13900	1	84
77	5/12/1940	13900	1	85
78	5/31/1963	13800	1	86
79	6/4/1914	13300	1	87
80	6/22/2010	13200	1	88
81	5/13/1988	12300	1	89
82	5/31/1930	11800	1	90
83	5/17/1912	11700	1	91
84	5/26/2001	11300	1	92
85	5/8/1992	10900	1	93
86	5/5/2004	10700	1	95
87	6/27/1915	8540	1	96
88	5/11/1977	8520	1	97

1896
1897

89	5/3/1941	8010	1	98
90	5/17/1944	7850	1	99

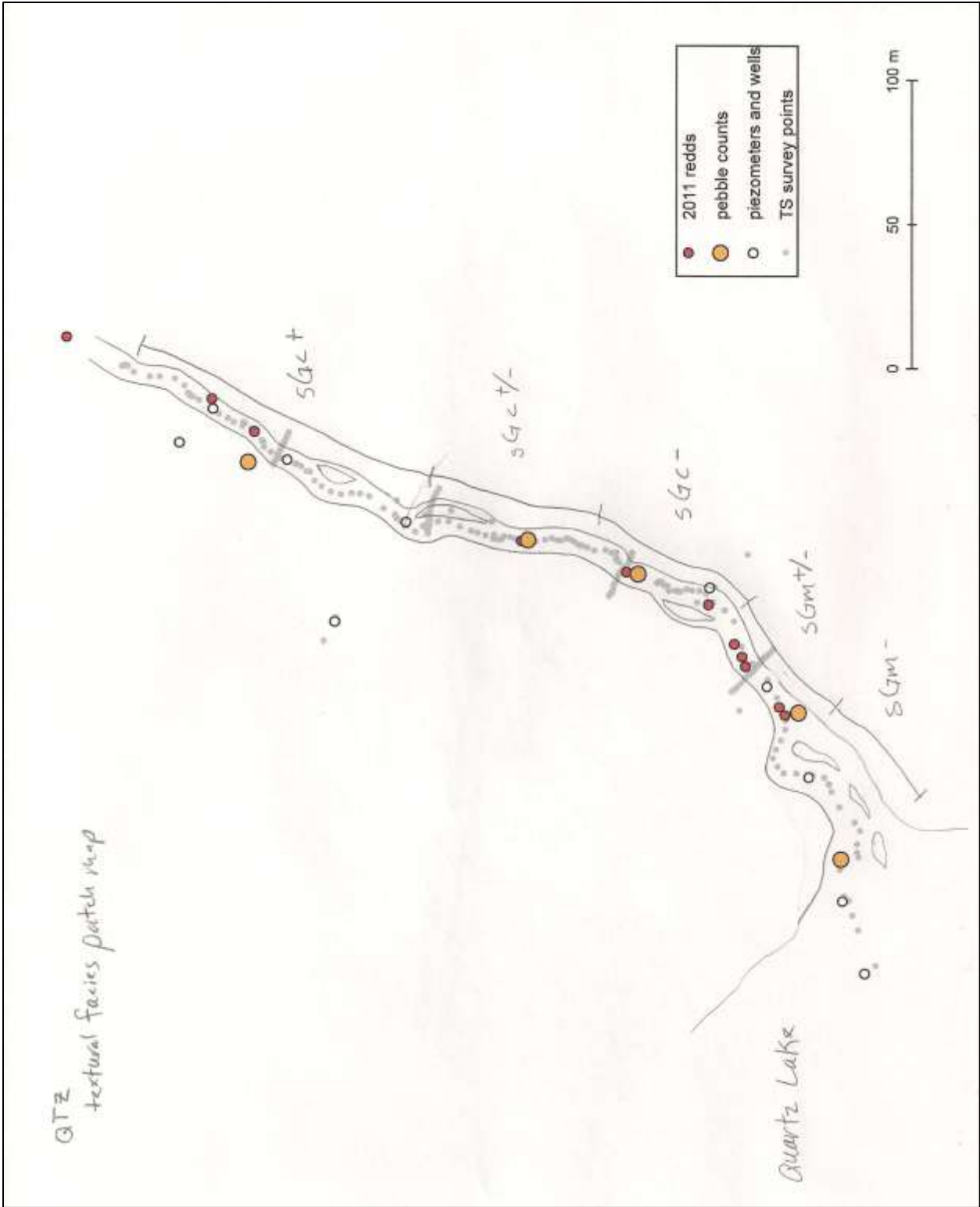
1898
1899

1.A.iii. Study reach textural facies analyses



1900
1901

Figure 1A1. OLE_{mc} and OLE_{sc} textural facies patch maps.



1902
1903

Figure 1A2. QTZ textural facies patch map.

1904
1905

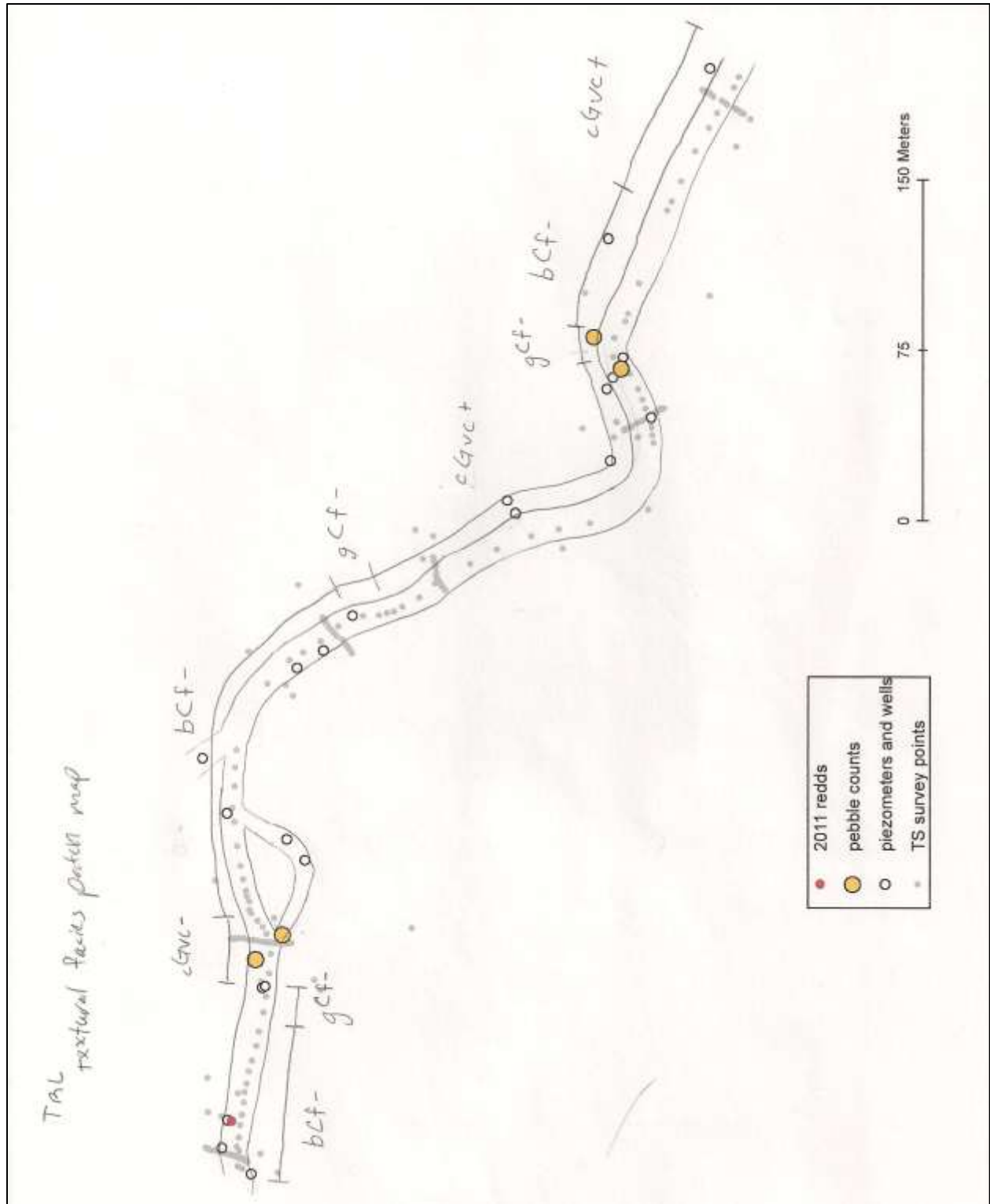
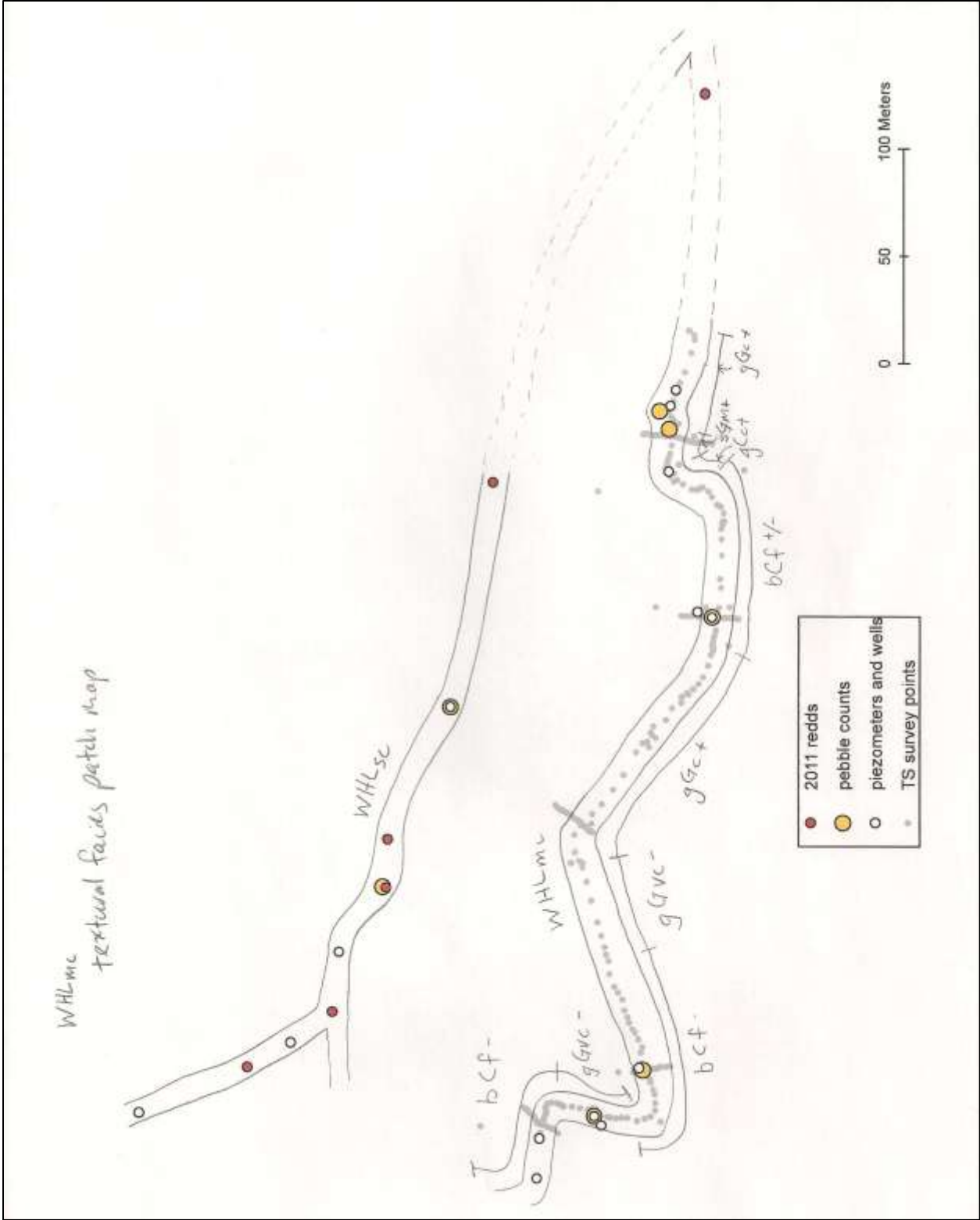


Figure 1A3. TRL textural facies patch map.



1906
1907
1908
1909

Figure 1A4. WHL_{mc} textural facies patch map.

1910 Table 1A4. Summary of OLE_{mc} and OLE_{sc} patch map textural facies and the pebble count (PC) source of the D₅₀
 1911 values.

Code ^a	D ₅₀ (m)	PC name
gCf-	0.064	(inferred) ^b
cGvc+	0.058	pc89
cGvc+/-	0.045	pc51, pc86 ^c
gGvc-	0.035	pc101
gGc-	0.018	pc85

1912 ^a Textural facies descriptions are based on the system described by Buffington and Montgomery (1999a). The
 1913 supplemental +, +/-, and – symbols indicate whether the grain size distribution lies within the coarser, middle, or
 1914 finer end of the spectrum of the dominant grain size fraction descriptors (e.g. gCf- means gravely cobble and that
 1915 the cobbles are near the fine end of the fine cobble spectrum (0.064 m – 0.128 m).

1916 ^b No pebble counts were conducted in the gCf- patches, so I estimated the D₅₀ value. I chose 0.064 because the
 1917 patches appeared to be at the fine end of the cobble spectrum, and 0.064 m is the boundary between cobble and
 1918 boulder.

1919 ^c The textural facies of both the pc51 (D₅₀ = 0.046 m) and pc86 (D₅₀ = 0.043 m) pebble counts was cGvc+/-.
 1920 Therefore, these D₅₀ values were averaged to obtain the cGvc+/- D₅₀ value.

1921
 1922 Table 1A5. OLE_{mc} and OLE_{sc} textural facies and D₅₀s per HEC-RAS subreach channel section.

HEC-RAS		Textural facies		D ₅₀	
River Station	τ _{obf} (N/m ²)	OLE _{mc}	OLE _{sc}	OLE _{mc} (m)	OLE _{sc} (m)
7	62.25	gCf-		0.064	
6.875*	58.78	gCf-		0.064	
6.75*	62.55	gCf-		0.064	
6.625*	57.43	gCf-		0.064	
6.5*	68.07	gCf-		0.064	
6.375*	61.06	gCf-		0.064	
6.25*	75.78	gCf-		0.064	
6.125*	45.91	gCf-		0.064	
6	25.73	gCf-		0.064	
5.8*	23.96	gGvc-		0.035	
5.6*	25.18	gGvc-		0.035	
5.4*	29.24	gGvc-		0.035	
5.2*	38.59	gGvc-		0.035	
5	101.87	cGvc+/-		0.045	
4.833*	86.80	cGvc+/-		0.045	
4.666*	65.45	cGvc+/-		0.045	
4.5*	50.35	gGvc-		0.035	
4.333*	42.50	gGvc-	gGc-	0.035	0.018
4.166*	41.61	gGvc-	gGc-	0.035	0.018
4	47.64	gGvc-	gGc-	0.035	0.018
3.833*	44.19	gGvc-	gGc-	0.035	0.018
3.666*	43.53	cGvc+/-	gGc-	0.045	0.018

3.5*	39.55	cGvc+/-	gGc-	0.045	0.018
3.333*	36.36	cGvc+/-	gGc-	0.045	0.018
3.166*	39.23	cGvc+/-	gGc-	0.045	0.018
3	68.07	cGvc+/-	gGc-	0.045	0.018
2.857*	76.98	cGvc+/-	gGc-	0.045	0.018
2.714*	74.30	cGvc+/-	gGc-	0.045	0.018
2.571*	70.50	cGvc+/-	gGc-	0.045	0.018
2.428*	63.35	cGvc+/-	gGc-	0.045	0.018
2.285*	63.46	cGvc+/-	gGc-	0.045	0.018
2.142*	49.35	cGvc+	gGc-	0.058	0.018
2	71.42	cGvc+	gGc-	0.058	0.018
1.888*	77.22	cGvc+	gGc-	0.058	0.018
1.777*	83.60	gGvc-		0.035	
1.666*	89.26	gCf-		0.064	
1.555*	93.37	gCf-		0.064	
1.444*	99.42	gCf-		0.064	
1.333*	103.48	gCf-		0.064	
1.222*	106.20	cGvc+/-		0.045	
1.111*	110.41	gGvc-		0.035	
1	118.85	gGvc-		0.035	

1923

1924

Table 1A6. OLE_{mc} and OLE_{sc} textural facies distribution.

HEC-RAS subreach sections per textural facies		Ole patch map textural facies				
OLE _{mc}	OLE _{sc}	Code	D ₁₆ (m)	D ₅₀ (m)	D ₈₄ (m)	PC name
13	0	gCf-	0.027	0.064	0.118	inferred
3	0	cGvc+	0.015	0.058	0.112	pcpz89
14	0	cGvc+/-	0.021	0.045	0.080	avg(pcpz51,pcpz86)
12	0	gGvc-	0.013	0.035	0.085	pcpz101
0	17	gGc-	0.004	0.018	0.032	pcpz85
Total X.S.s	42					

1925

1926

1927

1928

1929

^a These sections were coarser than cGvc+. The D₅₀ of 0.064 m was selected b/c it is the boundary between gravel and cobble. D₁₆ and D₈₄ were estimated by taking the largest measured D₁₆ and D₈₄ and adding the difference in measured D₅₀ between gCf- and cGvc+ (0.064 m - 0.058 m).

Table 1A7. Summary of Quartz patch map textural facies and the pebble count source of the D50 values.

Code	D ₅₀ (m)	PC name
sGc+	0.03	pc42
sGc+/-	0.025	pc25
sGc-	0.016	pc19
sGm+/-	0.011	pc07

1930

1931

1932 Table 1A8. QTZ textural facies and D₅₀s per HEC-RAS subreach channel section.

HEC-RAS		Textural facies	D ₅₀ (m)
River Station	τ _{obf} (N/m ²)		
4	33.35	sGc+	0.030
3.666*	29.75	sGc+	0.030
3.333*	33.53	sGc+	0.030
3	22.76	sGc+/-	0.025
2.75*	16.44	sGc+/-	0.025
2.5*	12.83	sGc+/-	0.025
2.25*	12.30	sGc-	0.016
2	24.43	sGc-	0.016
1.666*	26.86	sGc-	0.016
1.333*	21.89	sGc-	0.016
1	17.26	sGm+/-	0.011

1933

1934 Table 1A9. QTZ textural facies distribution.

HECRAS X.S.s per patch	Quartz patch map textural facies				
	Code	D ₁₆ (m)	D ₅₀ (m)	D ₈₄ (m)	PC name
3	sGc+	0.010	0.030	0.050	pcpz42
3	sGc+/-	0.010	0.025	0.040	pcpz25
4	sGc-	0.005	0.016	0.034	pcpz19
1	sGm+/-	0.005	0.011	0.031	pcpz07
Total X.S.s	11				

1935

1936

1937 Table 1A10. Summary of Trail patch map textural facies and the pebble count source of the D50 values.

Code	D ₅₀ (m)	PC name
bCf-	0.09	(inferred) ^a
gCf-	0.075	pc18
cGvc+	0.064	pc2
cGvc-	0.04	pc51

1938 ^a No pebble counts were conducted in the bCf- patches, so I estimated the D50 to be about 0.09 based on field observations and comparisons with the other pebble count D50 values.

1939

1940

1941 Table 1A11. TRL textural facies and D₅₀s per HEC-RAS subreach channel section.

HEC-RAS		Textural facies	D ₅₀ (m)
River Station	τ _{obf} (N/m ²)		
6	86.95	bCf-	0.090
5.8*	74.43	bCf-	0.090
5.6*	63.17	bCf-	0.090
5.4*	52.90	gCf-	0.075

5.2*	41.38	cGvc-	0.040
5	36.21	cGvc-	0.040
4.857*	41.84	bCf-	0.090
4.714*	50.40	bCf-	0.090
4.571*	57.98	bCf-	0.090
4.428*	69.21	bCf-	0.090
4.285*	78.63	bCf-	0.090
4.142*	90.91	bCf-	0.090
4	94.07	bCf-	0.090
3.666*	90.25	gCf-	0.075
3.333*	84.84	cGvc+	0.064
3	56.85	cGvc+	0.064
2.833*	59.13	cGvc+	0.064
2.666*	59.02	cGvc+	0.064
2.5*	61.55	cGvc+	0.064
2.333*	65.21	cGvc+	0.064
2.166*	68.84	cGvc+	0.064
2	81.24	cGvc+	0.064
1.875*	81.85	gCf-	0.075
1.75*	82.45	bCf-	0.090
1.625*	82.77	bCf-	0.090
1.5*	82.34	bCf-	0.090
1.375*	80.58	bCf-	0.090
1.25*	75.54	cGvc+	0.064
1.125*	65.81	cGvc+	0.064
1	52.47	cGvc+	0.064

1942

1943

Table 1A12. TRL textural facies distribution.

	HECRAS X.S.s per patch	Trail patch map textural facies				
		Code	D ₁₆ (m)	D ₅₀ (m)	D ₈₄ (m)	PC name
	14	bCf-	0.055	0.090	0.125	inferred ^a
	3	gCf-	0.040	0.075	0.110	pcpz18
	11	cGvc+	0.025	0.064	0.110	pcpz2
	2	cGvc-	0.006	0.040	0.090	pcpz51
Total X.S.s	30					

1944

1945

1946

1947

1948

1949

1950

^a The grain sizes of this textural facies were estimated based on the other pebble count data. Pebble counts were not conducted in this textural facies because the streambed appeared far too coarse for spawning and in several places the stream was too deep or fast to wade and conduct the pebble counts. The D₅₀ was first estimated; then the D₁₆ and D₈₄ were estimated by taking the coarsest measured D₁₆ or D₈₄ and adding the difference in D₅₀ between bCf- and gCf- (0.09 m - 0.075 m).

Table 1A13. Summary of Whale patch map textural facies and the pebble count source of the D50 values.

Code	D ₅₀ (m)	PC name
bCf+/-	0.076	pcpz20

bCf-	0.065	pcxs3
gGvc-	0.035	pcpz36
gGc+	0.027	pcpz09
sGm+	0.016	pcpz19+9m

1951

1952

Table 1A14. WHL_{mc} textural facies and D_{50} s per HEC-RAS subreach channel section.

HEC-RAS		Textural facies	D_{50} (m)
River Station	τ_{obf} (N/m^2)		
5	40.48	bCf-	0.065
4.666*	36.15	gGvc-	0.035
4.333*	28.22	bCf-	0.065
4	17.42	bCf-	0.065
3.833*	15.55	bCf-	0.065
3.666*	14.05	gGvc-	0.035
3.5*	12.85	gGvc-	0.035
3.333*	11.87	gGvc-	0.035
3.166*	11.07	gGc+	0.027
3	10.41	gGc+	0.027
2.833*	12.09	gGc+	0.027
2.666*	14.18	gGc+	0.027
2.5*	17.01	gGc+	0.027
2.333*	19.7	gGc+	0.027
2.166*	25.98	gGc+	0.027
2	62.65	bCf+/-	0.076
1.8*	50.75	bCf+/-	0.076
1.6*	45.77	bCf+/-	0.076
1.4*	31.48	bCf+/-	0.076
1.2*	14.18	gGc+	0.027
1	6.31	sGm+	0.016

1953

1954

Table 1A15. WHL_{mc} and WHL_{sc} textural facies distribution.

	HECRAS X.S.s per patch	Whale patch map textural facies				
		Code	D_{16} (m)	D_{50} (m)	D_{84} (m)	PC name
WHL_{mc}	4	bCf+/-	0.016	0.076	0.119	pcpz20
	4	bCf-	0.020	0.065	0.125	pcxs3
	4	gGvc-	0.008	0.035	0.065	pcpz36
	8	gGc+	0.013	0.027	0.050	pcpz09
	1	sGm+	0.006	0.016	0.029	pcpz09+9m
Total X.S.s	21					
WHL_{sc}	10.5	sGm+ (2)	0.010	0.016	0.028	pc at redd 2/3
	10.5	sGm+ (3)	0.004	0.015	0.030	pzsc16stdns

Total equivalent X.S.s	21
------------------------	----

1955 ^a The grain sizes of this textural facies were estimated based on the other pebble count data. Pebble counts were
 1956 not conducted in this textural facies because the streambed appeared far too coarse for spawning and in several
 1957 places the stream was too deep or fast to wade and conduct the pebble counts. The D_{50} was first estimated; then
 1958 the D_{16} and D_{84} were estimated by taking the coarsest measured D_{16} or D_{84} and adding the difference in D_{50}
 1959 between bCf- and gCf- (0.09 m - 0.075 m).
 1960

1961 Each HEC-RAS measured and interpolated cross section was assigned a textural facies; and each
 1962 textural facies is described by a pebble count. The corresponding D_{16} , D_{50} , and D_{84} of these pebble
 1963 counts were then assigned to each HEC-RAS cross section and average D_{16} , D_{50} , and D_{84} per study reach
 1964 were calculated.
 1965

1966 Table 1A16. Spatially weighted grain size distributions in each study stream based on textural facies classifications
 1967 and pebble count data.

	D_{16} (m)	D_{50} (m)	D_{84} (m)
OLE _{mc}	0.020	0.049	0.095
OLE _{sc}	0.004	0.018	0.032
QTZ	0.008	0.022	0.040
TRL	0.039	0.076	0.116
WHL _{mc}	0.014	0.045	0.079
WHL _{sc}	0.007	0.016	0.029

1968 Table 1A17. Study reach wetted channel width estimates at Q_{spawn} . Widths were estimated to the nearest meter
 1969 from visual observations of the Q_{spawn} profile in HEC-RAS.
 1970

River station	OLE _{mc}	OLE _{sc}	QTZ	TRL	WHL _{mc}	WHL _{sc}
7	17					
6	10			14		
5	10			22	13	
4	9	8	9	15	11	
3	15	6	10	11	14	
2	9	8	7	18	13	
1	10		6	15	16	
	OLE _{mc}	OLE _{sc}	QTZ	TRL	WHL _{mc}	WHL _{sc}
Avg wetted width	11.4	7.3	8.0	15.8	13.4	
Avg wetted width	11	7	8	16	13	6 ^a

1971 ^a Visual field estimate.
 1972

1973 **1.A.iv. HEC-RAS**

1974 The maximum channel distance between HEC-RAS cross-sections (measured and interpolated)
 1975 was set to 20 m. Channel roughness values were iterated between 0.024-0.075 until modeled water
 1976 level was < 10% of measured water level for the spawning discharge. Manning’s n values 0.024-0.075
 1977 were used because that is the range of channel conditions reported for Western US by Barnes,
 1978 1967:<http://wwwrcamnl.wr.usgs.gov/sws/fieldmethods/Indirects/nvalues/index.htm>).

1979 Overbank roughness values were estimated from Chow (1959) recommended values based on
 1980 field observations (Table 3-1 in the HEC-RAS help file link). Relative ranking of the study reaches based
 1981 on wood (tree and brush) roughness from most rough to least rough is Quartz, Whale, Ole, then Trail.
 1982 Medium to dense brush normally ranges from 0.07 in winter to 0.1 in summer; heavy timber ranges
 1983 from 0.1 with little undergrowth to 0.12 with flow through low branches (Chow, 1959). Based on this
 1984 range, and the relative ranking of the streams, overbank roughness for each stream was assigned as
 1985 follows: Quartz = 0.11; Whale = 0.10; Ole = 0.09; Trail = 0.08. For simplicity and to minimize "hand-
 1986 waviness", these overbank roughness values were kept constant per cross section in each stream.

1987 For plotting and spatial comparison purposes, distance between the HEC-RAS measured and
 1988 interpolated cross sections were scaled to match the distances measured by the total station long
 1989 profile using the following procedure (see the “HECRAS simulation results.xlsx” file for the actual
 1990 calculations).

- 1991 1. the long profile distance downstream of each measured cross section was calculated and
 1992 recorded; if the cross section did not plot on a long profile point, the distance upstream or
 1993 downstream from the most proximal long profile point was added or subtracted to obtain the
 1994 appropriate distance downstream of the measured cross section.
- 1995 2. the distance from one measured cross section to the subsequent downstream cross section was
 1996 then divided by the number of interpolated cross sections in between yielding the scaled
 1997 incremental distance from the upstream measured cross section to each of the downstream
 1998 interpolated cross sections
- 1999 3. this process was repeated between each of the measured cross sections to obtain distances
 2000 downstream in the total station long profile of each measured and interpolated cross section.

2001 To scale the HEC-RAS output data to the topographic survey long profile data and relate the
 2002 HEC-RAS data to true redd locations, I used the following process. In ArcMap 10.0, each cross section
 2003 was assigned a total station long profile distance downstream based on its location within the long
 2004 profile data points. The difference between the downstream distance of adjacent cross sections was
 2005 divided by the number of interpolated cross sections (+1 for the downstream cross section) in order to
 2006 obtain constant incremental distances downstream between each interpolated cross section. These
 2007 distances were added consecutively to the downstream distance of the upstream measured cross
 2008 section. The process was repeated between each set of measured cross sections.

2009
 2010

Table 1A18. Summary of HEC-RAS input details for bankfull discharge in each stream.

Study reach	HEC-RAS River Station ^a	Channel length (m)	Cumulative channel length (m)	Channel elevations			Manning's n ^e	
				Min. ^b (m)	LOB ^c (m)	ROB ^d (m)	Main channel	Overbank
OLE _{mc} and OLE _{sc}	7	18.37	0.00	1271.30	1272.33	1272.41	0.040	0.090
	6.875*	18.37	18.37	1270.98	1271.99	1272.08	0.039	0.090
	6.75*	18.37	36.74	1270.65	1271.65	1271.75	0.039	0.090
	6.625*	18.37	55.11	1270.33	1271.31	1271.41	0.038	0.090
	6.5*	18.37	73.48	1270.00	1270.97	1271.08	0.038	0.090
	6.375*	18.37	91.85	1269.68	1270.62	1270.75	0.037	0.090

	6.25*	18.37	110.22	1269.35	1270.28	1270.42	0.036	0.090
	6.125*	18.37	128.59	1269.03	1269.94	1270.08	0.036	0.090
	6	19.57	146.96	1268.70	1269.60	1269.75	0.035	0.090
	5.8*	19.57	166.53	1268.61	1269.54	1269.73	0.042	0.090
	5.6*	19.57	186.10	1268.52	1269.48	1269.71	0.049	0.090
	5.4*	19.57	205.67	1268.42	1269.41	1269.69	0.056	0.090
	5.2*	19.57	225.24	1268.33	1269.35	1269.67	0.063	0.090
	5	19.34	244.81	1268.24	1269.29	1269.65	0.070	0.090
	4.833*	19.34	264.15	1267.97	1269.10	1269.45	0.067	0.090
	4.666*	19.34	283.49	1267.70	1268.91	1269.24	0.063	0.090
	4.5*	19.34	302.83	1267.44	1268.72	1269.04	0.060	0.090
	4.333*	19.34	322.17	1267.17	1268.53	1268.84	0.057	0.090
	4.166*	19.34	341.51	1266.90	1268.34	1268.63	0.053	0.090
	4	17.97	360.85	1266.63	1268.15	1268.43	0.050	0.090
	3.833*	17.97	378.82	1266.53	1267.94	1268.18	0.051	0.090
	3.666*	17.97	396.79	1266.43	1267.73	1267.94	0.052	0.090
	3.5*	17.97	414.76	1266.33	1267.52	1267.69	0.052	0.090
	3.333*	17.97	432.73	1266.22	1267.30	1267.44	0.053	0.090
	3.166*	17.97	450.70	1266.12	1267.09	1267.20	0.054	0.090
	3	19.72	468.67	1266.02	1266.88	1266.95	0.055	0.090
	2.857*	19.72	488.39	1265.75	1266.60	1266.81	0.054	0.090
	2.714*	19.72	508.11	1265.49	1266.32	1266.67	0.052	0.090
	2.571*	19.72	527.83	1265.22	1266.04	1266.53	0.051	0.090
	2.428*	19.72	547.55	1264.95	1265.76	1266.38	0.049	0.090
	2.285*	19.72	567.27	1264.68	1265.48	1266.24	0.048	0.090
	2.142*	19.72	586.99	1264.42	1265.20	1266.10	0.046	0.090
	2	19.24	606.71	1264.15	1264.92	1265.96	0.045	0.090
	1.888*	19.24	625.95	1263.73	1264.52	1265.50	0.048	0.090
	1.777*	19.24	645.19	1263.30	1264.11	1265.04	0.052	0.090
	1.666*	19.24	664.43	1262.88	1263.71	1264.59	0.055	0.090
	1.555*	19.24	683.67	1262.46	1263.31	1264.13	0.058	0.090
	1.444*	19.24	702.91	1262.03	1262.90	1263.67	0.062	0.090
	1.333*	19.24	722.15	1261.61	1262.50	1263.21	0.065	0.090
	1.222*	19.24	741.39	1261.19	1262.10	1262.76	0.068	0.090
	1.111*	19.24	760.63	1260.76	1261.69	1262.30	0.072	0.090
	1		779.87	1260.34	1261.29	1261.84	0.075	0.090
QTZ	4	19.33	0	1356.04	1356.62	1357.16	0.035	0.11
	3.666*	19.33	19.33	1355.78	1356.4	1356.75	0.035	0.11
	3.333*	19.33	38.66	1355.52	1356.18	1356.34	0.035	0.11
	3	17.76	57.99	1355.26	1355.96	1355.93	0.035	0.11
	2.75*	17.76	75.75	1355.16	1355.85	1355.84	0.035	0.11
	2.5*	17.76	93.51	1355.07	1355.74	1355.75	0.035	0.11
	2.25*	17.76	111.27	1354.97	1355.63	1355.65	0.035	0.11
	2	19.21	129.03	1354.87	1355.52	1355.56	0.035	0.11
	1.666*	19.21	148.24	1354.73	1355.33	1355.35	0.031	0.11
	1.333*	19.21	167.45	1354.58	1355.14	1355.13	0.028	0.11
	1		186.66	1354.44	1354.95	1354.92	0.024	0.11
TRL	6	18.99	0	1252.34	1253.32	1253.3	0.075	0.08
	5.8*	18.99	18.99	1252.24	1253.16	1253.17	0.066	0.08
	5.6*	18.99	37.98	1252.14	1253.01	1253.03	0.057	0.08
	5.4*	18.99	56.97	1252.05	1252.85	1252.9	0.048	0.08
	5.2*	18.99	75.96	1251.95	1252.7	1252.76	0.039	0.08
	5	19.56	94.95	1251.85	1252.54	1252.63	0.03	0.08

	4.857*	19.56	114.51	1251.56	1252.31	1252.35	0.036	0.08
	4.714*	19.56	134.07	1251.26	1252.09	1252.07	0.043	0.08
	4.571*	19.56	153.63	1250.97	1251.86	1251.79	0.049	0.08
	4.428*	19.56	173.19	1250.67	1251.64	1251.5	0.056	0.08
	4.285*	19.56	192.75	1250.38	1251.41	1251.22	0.062	0.08
	4.142*	19.56	212.31	1250.08	1251.19	1250.94	0.069	0.08
	4	16.46	231.87	1249.79	1250.96	1250.66	0.075	0.08
	3.666*	16.46	248.33	1249.47	1250.61	1250.48	0.062	0.08
	3.333*	16.46	264.79	1249.15	1250.27	1250.31	0.048	0.08
	3	19.44	281.25	1248.83	1249.92	1250.13	0.035	0.08
	2.833*	19.44	300.69	1248.71	1249.76	1249.95	0.042	0.08
	2.666*	19.44	320.13	1248.58	1249.6	1249.78	0.048	0.08
	2.5*	19.44	339.57	1248.46	1249.44	1249.6	0.055	0.08
	2.333*	19.44	359.01	1248.34	1249.28	1249.42	0.062	0.08
	2.166*	19.44	378.45	1248.21	1249.12	1249.25	0.068	0.08
	2	17.91	397.89	1248.09	1248.96	1249.07	0.075	0.08
	1.875*	17.91	415.8	1247.88	1248.75	1248.88	0.075	0.08
	1.75*	17.91	433.71	1247.66	1248.53	1248.68	0.075	0.08
	1.625*	17.91	451.62	1247.45	1248.32	1248.49	0.075	0.08
	1.5*	17.91	469.53	1247.23	1248.1	1248.3	0.075	0.08
	1.375*	17.91	487.44	1247.02	1247.89	1248.1	0.075	0.08
	1.25*	17.91	505.35	1246.8	1247.67	1247.91	0.075	0.08
	1.125*	17.91	523.26	1246.59	1247.46	1247.71	0.075	0.08
	1		541.17	1246.37	1247.24	1247.52	0.075	0.08
WHL _{mc}	5	18.38	0	1277.74	1278.62	1278.85	0.035	0.1
	4.666*	18.38	18.38	1277.65	1278.54	1278.86	0.031	0.1
	4.333*	18.38	36.76	1277.56	1278.47	1278.87	0.028	0.1
	4	19.65	55.14	1277.47	1278.39	1278.88	0.024	0.1
	3.833*	19.65	74.79	1277.42	1278.38	1278.79	0.024	0.1
	3.666*	19.65	94.44	1277.37	1278.36	1278.69	0.024	0.1
	3.5*	19.65	114.09	1277.33	1278.35	1278.6	0.024	0.1
	3.333*	19.65	133.74	1277.28	1278.33	1278.51	0.024	0.1
	3.166*	19.65	153.39	1277.23	1278.32	1278.41	0.024	0.1
	3	19.25	173.04	1277.18	1278.3	1278.32	0.024	0.1
	2.833*	19.25	192.29	1277.16	1278.18	1278.24	0.026	0.1
	2.666*	19.25	211.54	1277.13	1278.06	1278.15	0.028	0.1
	2.5*	19.25	230.79	1277.11	1277.94	1278.07	0.03	0.1
	2.333*	19.25	250.04	1277.09	1277.81	1277.98	0.031	0.1
	2.166*	19.25	269.29	1277.06	1277.69	1277.9	0.033	0.1
	2	17.42	288.54	1277.04	1277.57	1277.81	0.035	0.1
	1.8*	17.42	305.96	1276.85	1277.48	1277.72	0.033	0.1
	1.6*	17.42	323.38	1276.67	1277.39	1277.63	0.031	0.1
	1.4*	17.42	340.8	1276.48	1277.3	1277.54	0.028	0.1
	1.2*	17.42	358.22	1276.3	1277.21	1277.45	0.026	0.1
	1		375.64	1276.11	1277.12	1277.36	0.024	0.1

2011 ^a An asterisk (*) indicates an interpolated cross-section; no * indicates a measured cross-section.

2012 ^b Minimum channel elevation.

2013 ^c Left overbank station elevation.

2014 ^d Right overbank station elevation.

2015 ^e See text above for a description of the channel and overbank roughness designations.

2016

2017

2018 Table 1A19. Summary of HEC-RAS output for bankfull discharge in each stream.

Study Reach	River station	Ch. shear stress (N/m ²)	Energy grade slope	Flow velocity (m/s)	Max. flow depth (m)	Top width (m)	Flow area (m ²)	Froude # Ch.
OLE _{mc}	7	62.25	1.55%	1.72	0.54	20.01	8.33	0.85
	6.875*	58.78	1.41%	1.72	0.59	19.19	8.31	0.84
OLE _{sc}	6.75*	62.55	1.61%	1.75	0.64	20.23	8.15	0.88
	6.625*	57.43	1.49%	1.72	0.68	20.81	8.30	0.87
	6.5*	68.07	1.76%	1.88	0.68	19.00	7.62	0.95
	6.375*	61.06	1.39%	1.87	0.71	16.81	7.67	0.88
	6.25*	75.78	1.69%	2.14	0.70	14.29	6.67	1.00
	6.125*	45.91	0.76%	1.75	0.87	12.67	8.15	0.70
	6	25.73	0.30%	1.43	1.15	14.45	10.21	0.48
	5.8*	23.96	0.27%	1.16	1.21	20.69	13.02	0.38
	5.6*	25.18	0.29%	1.01	1.26	27.49	15.34	0.34
	5.4*	29.24	0.36%	0.94	1.30	33.57	16.86	0.33
	5.2*	38.59	0.55%	0.94	1.31	34.66	16.95	0.35
	5	101.87	2.20%	1.28	1.16	28.87	11.94	0.59
	4.833*	86.80	1.81%	1.25	1.05	24.81	11.74	0.56
	4.666*	65.45	1.30%	1.16	1.03	24.89	12.41	0.51
	4.5*	50.35	1.00%	1.07	1.08	25.62	13.38	0.47
	4.333*	42.50	0.87%	1.03	1.17	27.34	13.91	0.46
	4.166*	41.61	0.93%	1.08	1.26	28.09	13.25	0.50
	4	47.64	0.91%	1.26	1.33	20.27	11.39	0.53
	3.833*	44.19	1.08%	1.14	1.26	29.39	12.58	0.55
	3.666*	43.53	1.09%	1.10	1.17	31.34	12.97	0.55
	3.5*	39.55	0.96%	1.06	1.09	33.17	13.63	0.52
	3.333*	36.36	0.75%	1.02	1.05	30.23	14.42	0.46
	3.166*	39.23	0.71%	1.07	1.02	32.17	14.90	0.45
	3	68.07	1.35%	1.36	0.92	28.81	12.73	0.60
	2.857*	76.98	1.54%	1.47	0.88	23.67	10.57	0.65
	2.714*	74.30	1.55%	1.49	0.83	21.27	9.82	0.67
	2.571*	70.50	1.54%	1.46	0.80	20.65	9.76	0.68
	2.428*	63.35	1.44%	1.44	0.77	21.95	9.96	0.68
	2.285*	63.46	1.54%	1.45	0.75	23.22	9.86	0.71
	2.142*	49.35	1.19%	1.34	0.75	44.37	11.51	0.65
	2	71.42	2.15%	1.58	0.68	48.50	10.04	0.86
	1.888*	77.22	2.13%	1.57	0.69	37.16	9.46	0.82
	1.777*	83.60	2.12%	1.53	0.72	31.40	9.54	0.76
	1.666*	89.26	2.09%	1.51	0.74	27.44	9.55	0.73
	1.555*	93.37	2.02%	1.48	0.77	25.03	9.70	0.69
	1.444*	99.42	1.98%	1.45	0.82	24.00	9.94	0.64

	1.333*	103.48	1.92%	1.43	0.86	23.58	10.16	0.61
	1.222*	106.20	1.82%	1.40	0.93	23.24	10.49	0.58
	1.111*	110.41	1.74%	1.37	1.02	22.88	10.93	0.54
	1	118.85	1.77%	1.38	1.10	20.31	10.96	0.52
QTZ	4	33.35	1.22%	1.35	0.57	14.28	3.14	0.79
	3.666*	29.75	1.11%	1.27	0.62	12.72	3.25	0.76
	3.333*	33.53	1.39%	1.32	0.63	12.12	3.10	0.84
	3	22.76	0.86%	1.11	0.70	13.27	3.71	0.67
	2.75*	16.44	0.56%	0.96	0.69	14.00	4.28	0.55
	2.5*	12.83	0.40%	0.86	0.70	16.19	4.81	0.48
	2.25*	12.30	0.40%	0.84	0.73	20.70	5.09	0.47
	2	24.43	0.93%	1.15	0.69	16.93	3.69	0.69
	1.666*	26.86	1.14%	1.33	0.61	12.55	3.08	0.86
	1.333*	21.89	0.72%	1.39	0.58	9.37	2.95	0.79
	1	17.26	0.41%	1.52	0.60	6.37	2.72	0.72
TRL	6	86.95	1.13%	1.21	1.05	16.46	13.19	0.43
	5.8*	74.43	1.08%	1.24	0.93	17.79	12.78	0.47
	5.6*	63.17	1.03%	1.30	0.82	19.11	12.20	0.52
	5.4*	52.90	0.98%	1.39	0.71	20.48	11.47	0.59
	5.2*	41.38	0.87%	1.48	0.62	21.90	10.76	0.67
	5	36.21	0.94%	1.73	0.51	23.24	9.18	0.88
	4.857*	41.84	0.97%	1.58	0.63	22.62	10.05	0.76
	4.714*	50.40	1.06%	1.48	0.74	21.86	10.75	0.67
	4.571*	57.98	1.12%	1.41	0.82	21.04	11.27	0.62
	4.428*	69.21	1.24%	1.37	0.90	20.20	11.64	0.57
	4.285*	78.63	1.31%	1.33	0.94	19.34	11.95	0.54
	4.142*	90.91	1.41%	1.30	0.98	18.47	12.24	0.51
	4	94.07	1.34%	1.24	1.01	17.65	12.89	0.46
	3.666*	90.25	1.36%	1.45	1.07	15.75	10.97	0.55
	3.333*	84.84	1.40%	1.79	1.10	13.79	8.89	0.71
	3	56.85	0.93%	2.01	1.19	12.13	7.91	0.79
	2.833*	59.13	0.90%	1.73	1.17	13.27	9.20	0.66
	2.666*	59.02	0.85%	1.52	1.15	14.44	10.43	0.57
	2.5*	61.55	0.86%	1.37	1.12	15.63	11.64	0.50
	2.333*	65.21	0.89%	1.25	1.08	16.80	12.70	0.46
	2.166*	68.84	0.94%	1.17	1.04	17.95	13.56	0.43
	2	81.24	1.15%	1.15	0.96	19.00	13.85	0.43
	1.875*	81.85	1.15%	1.15	0.97	18.76	13.77	0.43
	1.75*	82.45	1.15%	1.16	0.98	18.51	13.70	0.43
	1.625*	82.77	1.14%	1.17	0.99	18.28	13.65	0.43
	1.5*	82.34	1.12%	1.16	1.01	18.06	13.66	0.43
	1.375*	80.58	1.07%	1.16	1.02	17.87	13.77	0.42

	1.25*	75.54	0.97%	1.13	1.06	17.74	14.14	0.40
	1.125*	65.81	0.79%	1.06	1.12	17.80	15.01	0.37
	1	52.47	0.57%	0.97	1.22	19.29	16.62	0.31
WHL _{mc}	5	40.48	0.72%	1.67	0.96	15.63	9.13	0.68
	4.666*	36.15	0.64%	1.79	0.91	14.36	8.43	0.73
	4.333*	28.22	0.46%	1.77	0.90	12.95	8.48	0.69
	4	17.42	0.26%	1.65	0.94	12.03	9.08	0.61
	3.833*	15.55	0.23%	1.56	0.96	12.98	9.62	0.58
	3.666*	14.05	0.21%	1.48	0.97	13.96	10.13	0.55
	3.5*	12.85	0.19%	1.41	0.98	14.93	10.62	0.53
	3.333*	11.87	0.18%	1.35	1.00	15.90	11.07	0.52
	3.166*	11.07	0.17%	1.30	1.02	16.85	11.50	0.50
	3	10.41	0.17%	1.26	1.04	17.79	11.90	0.49
	2.833*	12.09	0.19%	1.26	1.02	17.45	11.89	0.49
	2.666*	14.18	0.21%	1.28	1.01	17.87	11.81	0.48
	2.5*	17.01	0.25%	1.31	0.98	17.43	11.58	0.49
	2.333*	19.70	0.29%	1.36	0.95	16.74	11.14	0.51
	2.166*	25.98	0.38%	1.47	0.90	15.88	10.39	0.56
	2	62.65	1.23%	2.05	0.68	14.26	7.36	0.90
	1.8*	50.75	1.09%	1.93	0.69	16.26	7.79	0.88
	1.6*	45.77	1.08%	1.92	0.68	17.67	7.83	0.92
	1.4*	31.48	0.77%	1.75	0.73	19.78	8.57	0.85
	1.2*	14.18	0.29%	1.30	0.88	22.18	11.53	0.58
1	6.31	0.11%	0.97	1.07	25.44	15.52	0.39	

2019

2020

2021

Table 1A20. Bankfull and bankfull adjusted Shields stress compilation. Red numbers in the HEC-RAS river station column indicate that that subreach channel section hosted one or more 2011 bull trout redds.

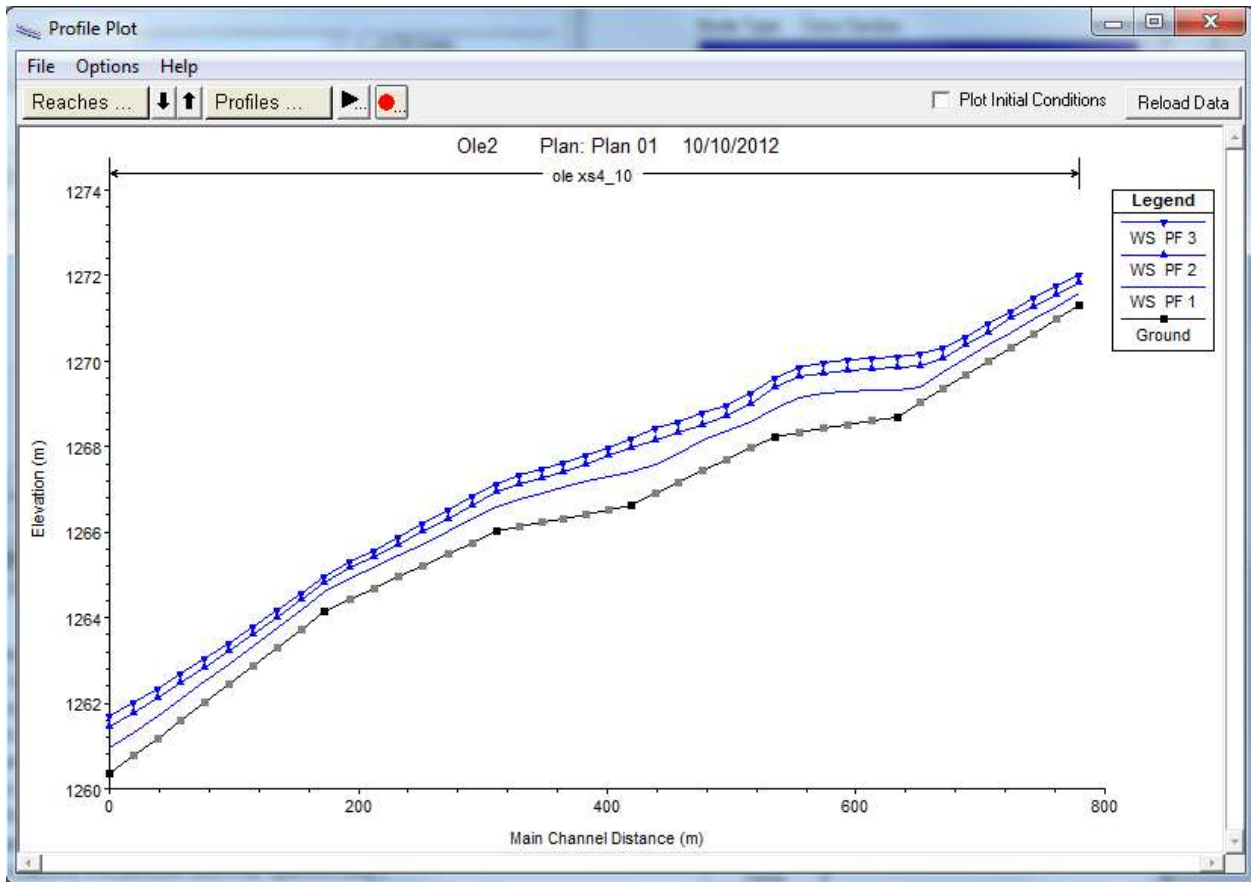
Study reach	HEC-RAS river station	Textural facies D ₅₀ (m)	HEC-RAS Q _{bf} output			τ'_{bf} (N/m ²)	τ^*_{bf}	τ^{**}_{bf}
			Slope	U (m/s)	τ_{obf} (N/m ²)			
OLE _{mc}	7	0.064	1.55%	1.72	62.25	40.5	0.060	0.039
	6.875*	0.064	1.41%	1.72	58.78	39.6	0.057	0.038
	6.75*	0.064	1.61%	1.75	62.55	42.0	0.060	0.041
	6.625*	0.064	1.49%	1.72	57.43	40.1	0.055	0.039
	6.5*	0.064	1.76%	1.88	68.07	47.8	0.066	0.046
	6.375*	0.064	1.39%	1.87	61.06	44.7	0.059	0.043
	6.25*	0.064	1.69%	2.14	75.78	57.5	0.073	0.056
	6.125*	0.064	0.76%	1.75	45.91	34.8	0.044	0.034
	6	0.064	0.30%	1.43	25.73	20.5	0.025	0.020
	5.8*	0.035	0.27%	1.16	23.96	12.5	0.042	0.022
	5.6*	0.035	0.29%	1.01	25.18	10.3	0.044	0.018

	5.4*	0.035	0.36%	0.94	29.24	9.8	0.052	0.017
	5.2*	0.035	0.55%	0.94	38.59	10.8	0.068	0.019
	5	0.045	2.20%	1.28	101.87	26.0	0.140	0.036
	4.833*	0.045	1.81%	1.25	86.80	23.9	0.119	0.033
	4.666*	0.045	1.30%	1.16	65.45	19.7	0.090	0.027
	4.5*	0.035	1.00%	1.07	50.35	15.3	0.089	0.027
	4.333*	0.035	0.87%	1.03	42.50	14.0	0.075	0.025
	4.166*	0.035	0.93%	1.08	41.61	15.2	0.074	0.027
	4	0.035	0.91%	1.26	47.64	19.1	0.084	0.034
	3.833*	0.035	1.08%	1.14	44.19	17.2	0.078	0.030
	3.666*	0.045	1.09%	1.10	43.53	17.4	0.060	0.024
	3.5*	0.045	0.96%	1.06	39.55	15.9	0.054	0.022
	3.333*	0.045	0.75%	1.02	36.36	14.1	0.050	0.019
	3.166*	0.045	0.71%	1.07	39.23	15.0	0.054	0.021
	3	0.045	1.35%	1.36	68.07	25.2	0.094	0.035
	2.857*	0.045	1.54%	1.47	76.98	29.3	0.106	0.040
	2.714*	0.045	1.55%	1.49	74.30	29.9	0.102	0.041
	2.571*	0.045	1.54%	1.46	70.50	29.0	0.097	0.040
	2.428*	0.045	1.44%	1.44	63.35	27.9	0.087	0.038
	2.285*	0.045	1.54%	1.45	63.46	28.7	0.087	0.039
	2.142*	0.058	1.19%	1.34	49.35	25.4	0.053	0.027
	2	0.058	2.15%	1.58	71.42	37.8	0.076	0.040
	1.888*	0.058	2.13%	1.57	77.22	37.3	0.082	0.040
	1.777*	0.035	2.12%	1.53	83.60	31.6	0.148	0.056
	1.666*	0.064	2.09%	1.51	89.26	35.9	0.086	0.035
	1.555*	0.064	2.02%	1.48	93.37	34.6	0.090	0.033
	1.444*	0.064	1.98%	1.45	99.42	33.3	0.096	0.032
	1.333*	0.064	1.92%	1.43	103.48	32.4	0.100	0.031
	1.222*	0.045	1.82%	1.40	106.20	28.4	0.146	0.039
	1.111*	0.035	1.74%	1.37	110.41	25.5	0.195	0.045
	1	0.035	1.77%	1.38	118.85	25.9	0.210	0.046
OLE _{sc}	4.166*	0.018	0.93%	1.08	41.61	12.9	0.143	0.044
	4	0.018	0.91%	1.26	47.64	16.2	0.164	0.056
	3.833*	0.018	1.08%	1.14	44.19	14.6	0.152	0.050
	3.666*	0.018	1.09%	1.10	43.53	13.8	0.150	0.048
	3.5*	0.018	0.96%	1.06	39.55	12.7	0.136	0.044
	3.333*	0.018	0.75%	1.02	36.36	11.2	0.125	0.039
	3.166*	0.018	0.71%	1.07	39.23	11.9	0.135	0.041
	3	0.018	1.35%	1.36	68.07	20.0	0.234	0.069

	2.857*	0.018	1.54%	1.47	76.98	23.3	0.264	0.080
	2.714*	0.018	1.55%	1.49	74.30	23.8	0.255	0.082
	2.571*	0.018	1.54%	1.46	70.50	23.0	0.242	0.079
	2.428*	0.018	1.44%	1.44	63.35	22.2	0.218	0.076
	2.285*	0.018	1.54%	1.45	63.46	22.8	0.218	0.078
	2.142*	0.018	1.19%	1.34	49.35	19.0	0.170	0.065
	2	0.018	2.15%	1.58	71.42	28.2	0.245	0.097
	1.888*	0.018	2.13%	1.57	77.22	27.9	0.265	0.096
QTZ	4	0.030	1.22%	1.35	33.35	22.0	0.069	0.045
	3.666*	0.030	1.11%	1.27	29.75	19.6	0.061	0.040
	3.333*	0.030	1.39%	1.32	33.53	21.9	0.069	0.045
	3	0.025	0.86%	1.11	22.76	14.3	0.056	0.035
	2.75*	0.025	0.56%	0.96	16.44	10.3	0.041	0.026
	2.5*	0.025	0.40%	0.86	12.83	8.1	0.032	0.020
	2.25*	0.016	0.40%	0.84	12.30	7.0	0.048	0.027
	2	0.016	0.93%	1.15	24.43	13.8	0.094	0.053
	1.666*	0.016	1.14%	1.33	26.86	18.0	0.104	0.070
	1.333*	0.016	0.72%	1.39	21.89	17.2	0.085	0.066
	1	0.011	0.41%	1.52	17.26	15.5	0.097	0.087
TRL	6	0.090	1.13%	1.21	86.95	24.0	0.060	0.017
	5.8*	0.090	1.08%	1.24	74.43	24.7	0.051	0.017
	5.6*	0.090	1.03%	1.30	63.17	26.2	0.043	0.018
	5.4*	0.075	0.98%	1.39	52.90	27.3	0.044	0.022
	5.2*	0.040	0.87%	1.48	41.38	24.9	0.064	0.038
	5	0.040	0.94%	1.73	36.21	32.1	0.056	0.050
	4.857*	0.090	0.97%	1.58	41.84	34.5	0.029	0.024
	4.714*	0.090	1.06%	1.48	50.40	32.0	0.035	0.022
	4.571*	0.090	1.12%	1.41	57.98	30.2	0.040	0.021
	4.428*	0.090	1.24%	1.37	69.21	29.7	0.048	0.020
	4.285*	0.090	1.31%	1.33	78.63	28.8	0.054	0.020
	4.142*	0.090	1.41%	1.30	90.91	28.3	0.062	0.019
	4	0.090	1.34%	1.24	94.07	26.0	0.065	0.018
	3.666*	0.075	1.36%	1.45	90.25	31.6	0.074	0.026
	3.333*	0.064	1.40%	1.79	84.84	42.0	0.082	0.041
	3	0.064	0.93%	2.01	56.85	45.0	0.055	0.044
	2.833*	0.064	0.90%	1.73	59.13	35.7	0.057	0.034
	2.666*	0.064	0.85%	1.52	59.02	29.0	0.057	0.028
	2.5*	0.064	0.86%	1.37	61.55	24.8	0.059	0.024
	2.333*	0.064	0.89%	1.25	65.21	21.9	0.063	0.021

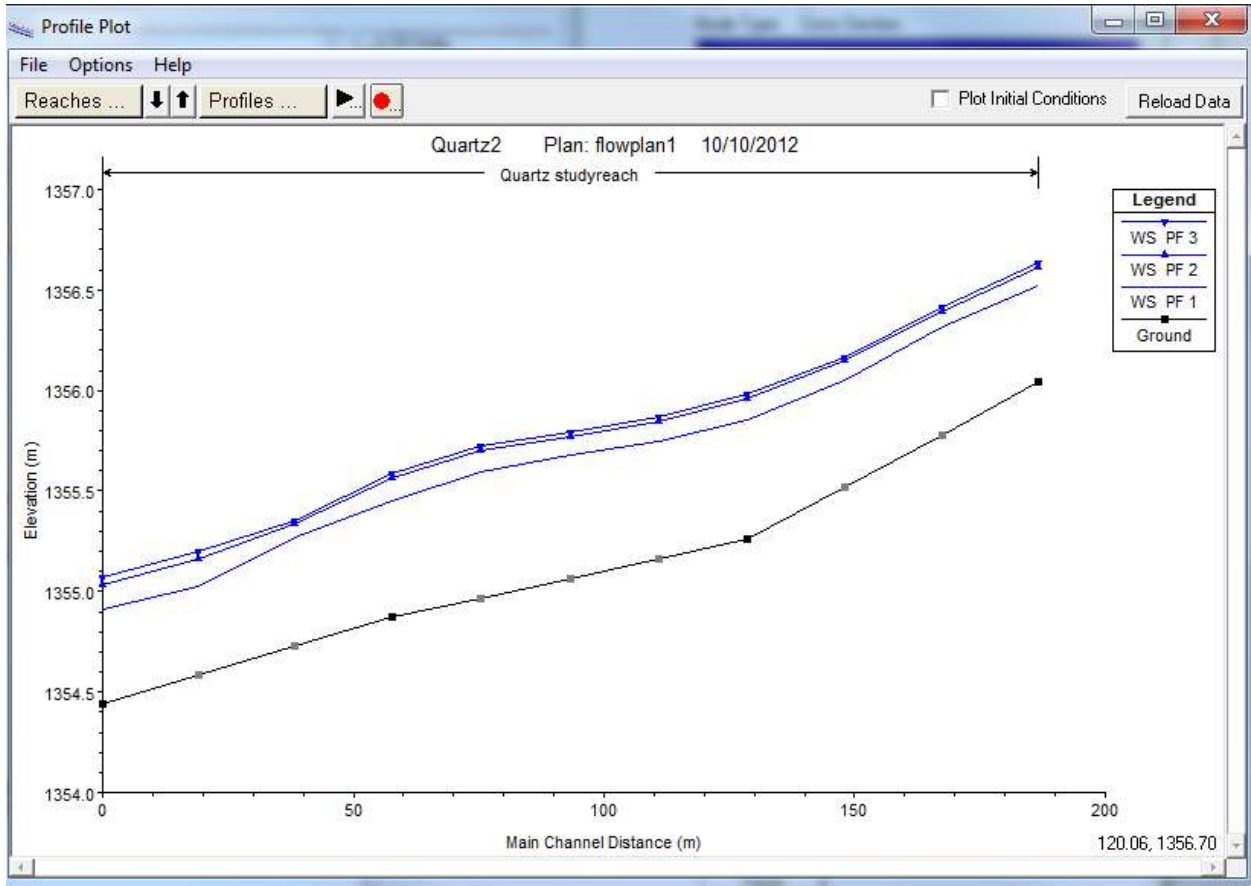
	2.166*	0.064	0.94%	1.17	68.84	20.1	0.067	0.019
	2	0.064	1.15%	1.15	81.24	20.6	0.079	0.020
	1.875*	0.075	1.15%	1.15	81.85	21.4	0.067	0.018
	1.75*	0.090	1.15%	1.16	82.45	22.7	0.057	0.016
	1.625*	0.090	1.14%	1.17	82.77	22.9	0.057	0.016
	1.5*	0.090	1.12%	1.16	82.34	22.5	0.057	0.015
	1.375*	0.090	1.07%	1.16	80.58	22.3	0.055	0.015
	1.25*	0.064	0.97%	1.13	75.54	19.2	0.073	0.019
	1.125*	0.064	0.79%	1.06	65.81	16.6	0.064	0.016
	1	0.064	0.57%	0.97	52.47	13.4	0.051	0.013
WHL _{mc}	5	0.065	0.72%	1.67	40.48	32.1	0.039	0.031
	4.666*	0.035	0.64%	1.79	36.15	29.6	0.064	0.052
	4.333*	0.065	0.46%	1.77	28.22	31.4	0.027	0.030
	4	0.065	0.26%	1.65	17.42	24.4	0.017	0.023
	3.833*	0.065	0.23%	1.56	15.55	21.8	0.015	0.021
	3.666*	0.035	0.21%	1.48	14.05	16.9	0.025	0.030
	3.5*	0.035	0.19%	1.41	12.85	15.4	0.023	0.027
	3.333*	0.035	0.18%	1.35	11.87	14.2	0.021	0.025
	3.166*	0.027	0.17%	1.30	11.07	12.4	0.025	0.028
	3	0.027	0.17%	1.26	10.41	11.7	0.024	0.027
	2.833*	0.027	0.19%	1.26	12.09	12.0	0.028	0.028
	2.666*	0.027	0.21%	1.28	14.18	12.7	0.032	0.029
	2.5*	0.027	0.25%	1.31	17.01	13.7	0.039	0.031
	2.333*	0.027	0.29%	1.36	19.70	15.0	0.045	0.034
	2.166*	0.027	0.38%	1.47	25.98	18.2	0.060	0.042
	2	0.076	1.23%	2.05	62.65	51.9	0.051	0.042
	1.8*	0.076	1.09%	1.93	50.75	46.0	0.041	0.037
	1.6*	0.076	1.08%	1.92	45.77	45.6	0.037	0.037
	1.4*	0.076	0.77%	1.75	31.48	36.4	0.026	0.030
	1.2*	0.027	0.29%	1.30	14.18	14.1	0.032	0.032
	1	0.016	0.11%	0.97	6.31	6.3	0.024	0.024

2022



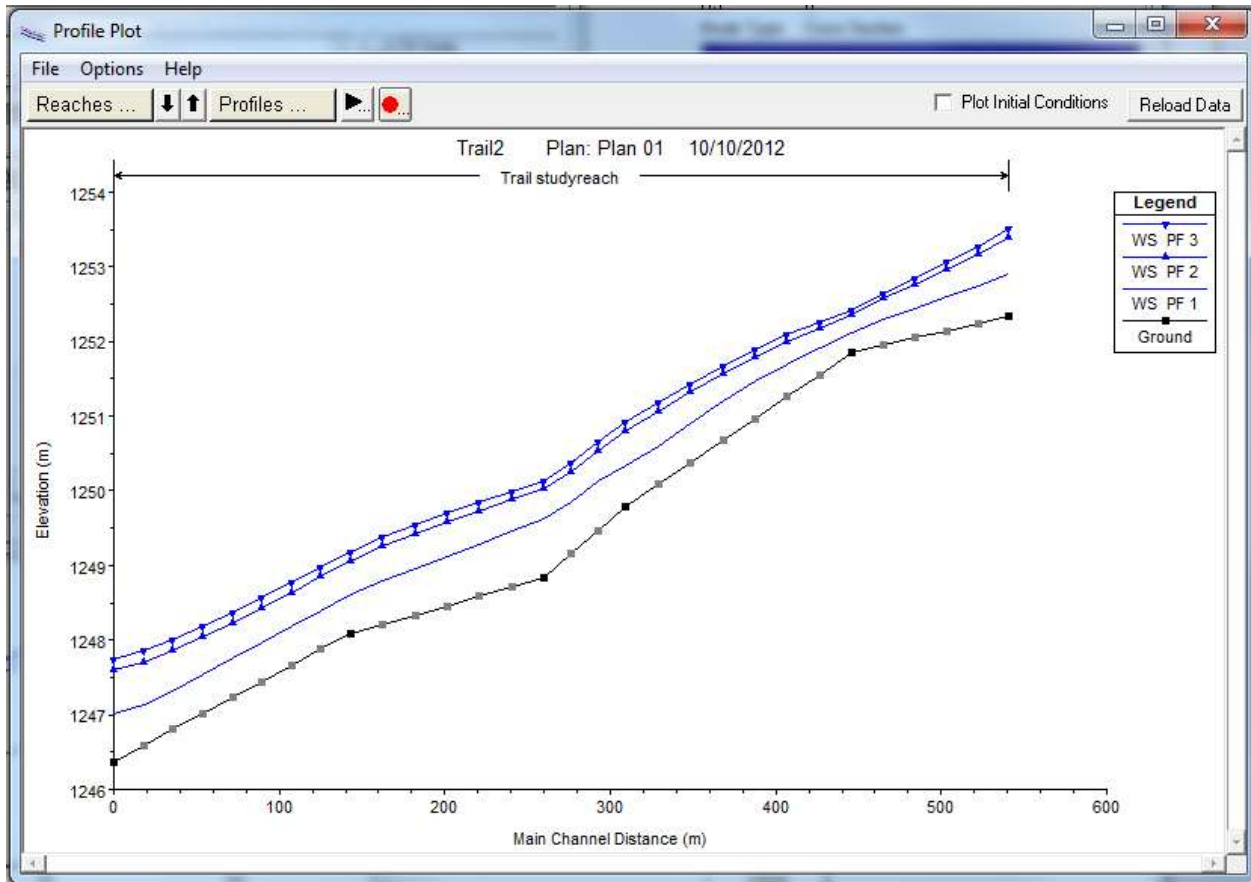
2023
2024

Figure 1A5. OLE_{mc} and OLE_{sc} HEC-RAS modeled water surface profiles.



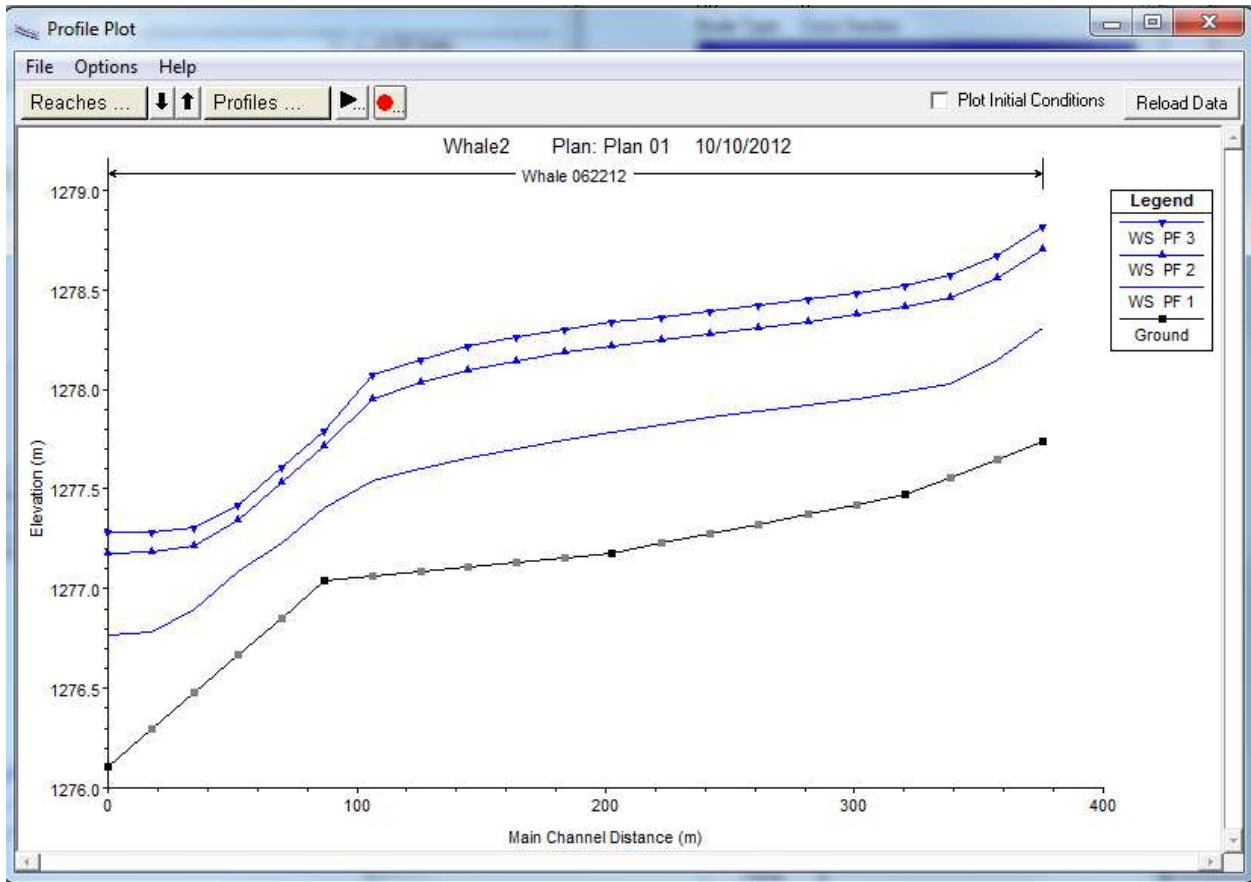
2025
2026

Figure 1A6. QTZ HEC-RAS modeled water surface profiles.



2027
2028

Figure 1A7. TRL HEC-RAS modeled water surface profiles.



2029
2030
2031

Figure 1A8. WHL_{mc} HEC-RAS modeled water surface profiles.

2032 **APPENDIX 1B: Reach-scale hydrogeology**

2033

2034 **1.B.i. Slug tests**

2035 Falling head slug tests were conducted by introducing a slug of 100 ml of water and measuring
2036 the water level change in 1 second or 0.5 second increments with a Solinst Levellogger Gold (Model
2037 3001). Every effort was made to introduce the slug instantaneously as recommended by Butler (1998).
2038 The pre-analysis processing guidelines of Butler (1998) were followed. Because of non-instantaneous
2039 slug introduction, the translation method was utilized (Pandit and Miner, 1986). For almost all data sets,
2040 H_0 was determined by standard methods of examining the data, then background static water level was
2041 determined by averaging the water levels of a 6 s window that ended 4 s prior to the determined peak.
2042 The 4 s gap between the data used to calculate static water level and initialization of the test was
2043 implemented in order to avoid water level values affected by the initial introduction of the slug of water.
2044 Water level deviations for static were then normalized (initial displacement = 1) which Butler (1998)
2045 instructs is essential when dealing with transducer data.

2046 For non-instantaneous slug introduction, estimation of initial head displacement (H_0) and
2047 initiation time (t_0) of the test can be difficult to determine. Of the common approaches utilized to
2048 estimate H_0 and t_0 , Butler (1998) reports that the translation method (Pandit and Miner, 1986) is the
2049 best approach. However, Butler (1998) notes that, “the translation method is only appropriate when a
2050 plot of the logarithm of the response data vs. time is approximately linear. In cases where the response
2051 plot has a pronounced concave-upward curvature, the translation method can introduce considerable
2052 error into the hydraulic conductivity estimate.” In terms of slug test setup and design, Butler (1998)
2053 states the following:

- 2054 1. slug out is better than slug in
2055 2. at least three slug tests should be performed per trial; and the first and last slugs should be the same
2056 amount while the middle amount(s) should be a different volume; comparison of the first and last slug
2057 tests’ data allows for better assessment of well development and potential skin effects.

2058

2059 **AquiferTest data analyses**

2060 AquiferTest software (Schlumberger 2011) was used to calculate hydraulic conductivity from our
2061 slug test data. All slug test piezometers were constructed and installed in similar fashions to similar
2062 depths. Therefore, well and aquifer dimension parameters in AquiferTest were made the same for all
2063 analyses. This was done to minimize the number of variables in the slug test data analyses. Aquifer
2064 thickness (b) was set at 10 m depth for all analyses; however, calculations of K did not appear to be
2065 dependent on b because all other variables were held constant, changes in b between 1 m and 100 m
2066 had minimal to no effect on the hydraulic conductivity calculation. Piezometers were indicated as
2067 partially penetrating an unconfined aquifer of thickness 10 m. Screen and casing radius = 1.5 cm; length
2068 of screen = 20 cm; distance from the top of the aquifer to the bottom of the screen = 60 cm (~ average
2069 for all slug test piezometers). Data windows from peak to equilibrium ranged from 4 s to 20 s depending
2070 on the dataset and amount of apparent noise. The Butler High- K analyses method was used to calculate
2071 K . In most cases the auto-fit curve provided an acceptable best-fit curve (obtained by selecting the play
2072 button “fit”). If further manual adjustment of the auto-fitted curve resulted in a new K value that was
2073 more than $\sim 2 \times 10^{-4}$ m/s different from the auto-fitted curve, then the manually adjusted curve and
2074 resulting K value was used instead of the auto-fitted curve and K value. Only two slug test curves needed
2075 manual adjustment (Ole pz86_12 and pz44_11). See the summary tables below for the AquiferTest
2076 derived K_h values.

2077

2078

2079 Table 1B1. OLE_{mc} AquiferTest K_h values from slug test data.

	auto-fit		manual adjust		Data window	
	(m/d)	(m/s)	(m/d)	(m/s)	data points	total time (s)
pz101_11	237	2.74E-03			5	5
pz101_12	90	1.04E-03			4	4
pz101_51	238	2.76E-03			11	5
pz101_52	125	1.45E-03			21	10
pz101_11 b=100m ^a	237	2.74E-03			5	4
pz101_11 b=1m ^a	262	3.03E-03			5	4
pz86_11	120	1.39E-03			16	15
pz86_12	107	1.24E-03	85	9.84E-04	26	25
pz86_51	125	1.45E-03			11	5
pz86_52	162	1.88E-03			21	10
pz81_11	129	1.49E-03			6	5
pz81_12	107	1.24E-03			8	7
pz51_11	104	1.20E-03			4	3
pz51_12	77	8.93E-04			6	5
pz44_11	588	6.81E-03	693	8.02E-03	6	5
pz44_12	274	3.17E-03			3	2
pz58_51ns	112	1.30E-03			8	3.5
pz58_52ns	115	1.33E-03			9	4

2080 ^a These tests utilized the pz101_11 slug test data, but the aquifer thickness parameter was changed from 10 m (the
 2081 default b for all my slug test analyses) to 100 m and 1 m in order to test the sensitivity of the Kh determination on
 2082 aquifer thickness. Since the difference between the derived Kh values is small; Kh determination in AquiferTest is
 2083 assumed to be mostly insensitive to aquifer thickness, and b=10 m is used for all analyses.

2084
 2085 Table 1B2. QTZ Creek. AquiferTest K_h values from slug test data.

	auto-fit		Data window	
	(m/d)	(m/s)	data points	total time (s)
pz42_12	147	1.70E-03	8	7
pz42_11	119	1.38E-03	9	8
pz39_12	226	2.62E-03	7	6
pz39_11	106	1.23E-03	8	7
pz25_12	224	2.59E-03	11	10
pz25_11	114	1.32E-03	12	11
pz09_12	62	7.22E-04	10	9
pz09_11	51	5.90E-04	9	8
pz07_12	135	1.56E-03	9	8
pz07_11	150	1.74E-03	5	4

2086
 2087

2088 Table 1B3. TRL AquiferTest K_h values from slug test data.

	auto-fit		Data window	
	(m/d)	(m/s)	data points	total time (s)
pz51_11	60	6.99E-04	12	11
pz51_12	61	7.01E-04	10	9
pz51_51 ^a	35	4.06E-04	60	30
pz51_52 ^a	67	7.75E-04	60	30
pz24_11	78	9.08E-04	9	8
pz24_12	65	7.57E-04	9	8
pz24_51	50	5.75E-04	30	15
pz24_52	48	5.51E-04	20	10
pz2_11	138	1.60E-03	10	9
pz2_12	95	1.10E-03	12	11
pz2_51	38	4.43E-04	60	30
pz2_52	43	5.03E-04	60	30
pz19_11	134	1.55E-03	8	7
pz19_12	108	1.25E-03	5	4
pz19_51 ^a	26	3.04E-04	40	20
pz19_52 ^a	25	2.95E-04	40	20
pz1_11	26	3.04E-04	9	8
pz1_12	37	4.33E-04	19	18
pz1_51	34	3.95E-04	40	20
pz1_52	34	3.91E-04	40	20
pz58sl1sg_51 ^b	18	2.04E-04	120	60
pz58sl1sg_52 ^b	18	2.05E-04	120	60

2089 ^a Noisy data and poor curve fit. AquiferTest derived K_h value not used.

2090 ^b The only redd in the Trail Creek study section was located less than 1 m from pz58. pz58 was not intended to be a slug test well; however I conducted one anyway due to the proximity of the redd. Due to the different dimensions of the well, the slug test data is not considered suitable for comparison to slug test data from the other slug tests.

2091

2092

2093

2094

2095 Table 1B4. WHL_{mc} AquiferTest K_h values from slug test data.

	auto-fit		Data window	
	(m/d)	(m/s)	data points	total time (s)
pz41_51	35	4.08E-04	33	16.5
pz41_52	34	3.91E-04	33	16.5
pz36_51	89	1.03E-03	11	5.5
pz36_52	94	1.09E-03	11	5
pz19_51	103	1.19E-03	11	5
pz19_52	82	9.45E-04	21	10
pz09_51	577	6.68E-03	21	10
pz09_52	750	8.68E-03	20	9.5

2096

2097 **1.B.ii. Streambed flux analyses**

2098 iButton calibration

2099 Vertical arrays of thermistor dataloggers (Maxim iButton, model DS1921Z) measured stream
2100 and streambed temperatures. Manufacturer accuracy limits are +/- 1 °C; however, prior to deployment,
2101 all iButtons were calibrated in a laboratory grade temperature controlled water bath and exposed to the
2102 full range of expected temperatures. After comparing the water bath temperature to each iButton's
2103 recorded temperature, correction factors were applied to each individual iButton. Corrected iButton
2104 temperatures were accurate to within +/- 0.2°C when compared with the bath temperatures.

2105

2106 Ex-Stream

2107 Vertical iButton array dataloggers recorded water temperatures at 30 minute intervals. The
2108 dataloggers are capable of storing 2048 temperature recordings with time stamps; therefore, measuring
2109 and recording temperature at 30 minutes intervals the memory capacity fills after 42.67 days. The
2110 temperature datasets were used to calculate vertical streambed flux using the MATLAB program Ex-
2111 Stream, developed by Swanson and Cardenas (2010). Sensor spacing is an input parameter for Ex-
2112 Stream and array designs and sensor spacings are explained below. For all designs, the temperature
2113 recorded by the stream dataloggers was assumed to be representative of the streambed sediment at
2114 the stream – streambed interface. The top of the upper baffle was placed flush with the streambed. The
2115 distance from the top of this upper baffle to the center point of the middle iButton pair in design 1 and 2
2116 was ~8 cm. A second baffle is positioned between the middle and lower iButton pairs in designs 1 and 2.
2117 The distance from the top of the upper baffle to the center point of the lower iButton pair in designs 1
2118 and 2 was ~25 cm. Since sensor spacing for design 3 was variable, each the spacing was measured
2119 individually for each array and these datasets were run individually in Ex-Stream to allow for more
2120 accurate flux calculations by using true sensor spacing distances. Sensor spacing for design 3 arrays was
2121 measured as the distance from the top of the streambed to the center point of the hanging iButton pair.
2122 The hanging iButton pair was tapped to a ~15 cm bolt; ~10 cm up from the iButton pair, a baffle
2123 consisting of two 2.5 cm diameter washers was held in place by three nuts.

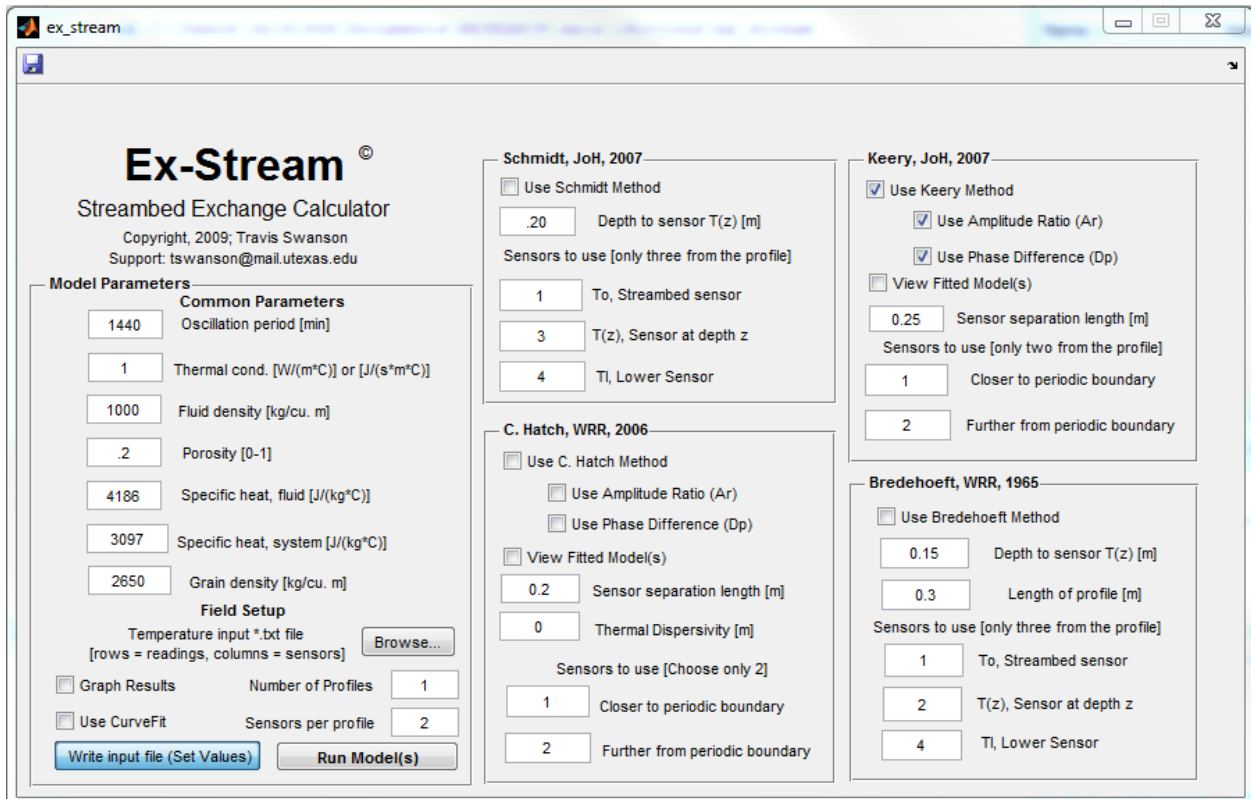
2124 Ex-Stream requires 1 min interval input data; so I linearly interpolated my 30 min interval
2125 iButton temperature datasets to 1 min using Excel. The Hatch (2006) and Keery (2007) methods
2126 (hereafter, these will be referred to as the 'Hatch method' and 'Keery method') were the appropriate
2127 analytical models to use on my data; in Ex-Stream both models assess amplitude ratio differences (Ar
2128 method) and phase differences (Dp method) between vertically separated temperature datasets to
2129 calculate daily averaged vertical streambed flux (q_v , in m/d). The Ar method reliably estimates flux
2130 magnitude and direction within a range of -5 to 3 m/d (Hatch, 2006). The Dp method calculates only flux
2131 magnitude and reliably estimates flux in a range of -7 to 7 m/d (Hatch, 2006). The Keery method is more
2132 straightforward than the Hatch method in that it does not consider thermomechanical dispersion.

2133 Swanson and Cardenas (2010) model synthetic fluid fluxes varying between +/- 0.27 m/d and
2134 found that the Hatch model (with thermal dispersivity turned off) and Keery model output the same flux
2135 value. Ar method error was $\sim 10^{-4}$ m/d, while the Dp method error was $\sim 10^{-1}$ m/d. The Dp method is
2136 more sensitive and therefore produces more error (Swanson and Cardenas, 2010).

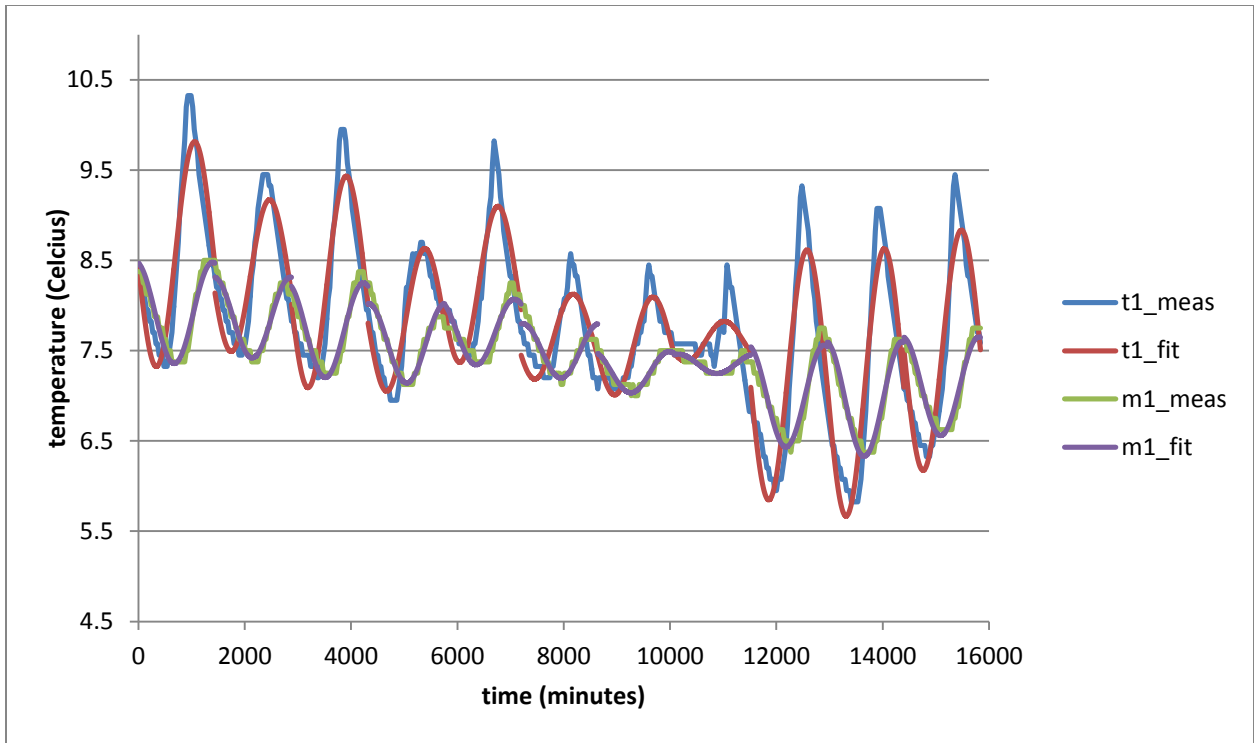
2137 In calculating flux with my data, the Hatch model constantly produced errors (e.g. Amplitude
2138 ratio too high) and was unable to analyze my data. The Keery method, however, rarely if ever produced
2139 errors and was able to output flux values for all my input temperature data. Due to the simplicity and
2140 similar performance of the Keery method compared to the Hatch method (Swanson and Cardenas,
2141 2010), I used the Keery method for all my flux calculations. Additionally, the Ar method calculated fluxes
2142 were the only fluxes considered. Dp method calculated fluxes were not considered due to incoherent
2143 output values, high sensitivity and error associated with the method, and lack of flux direction in the
2144 output.

2145 Below is a screen-shot of the input parameters and selected options I used in model runs. Default model
 2146 parameters for thermal conductivity, fluid density, specific heat and grain density were used for all
 2147 model runs. Mixed sand and gravel ranges in porosity from 20-35% while well-sorted sand and gravel
 2148 ranges from 25-50%. The streambed sediments in the four study sections are best characterized as
 2149 mixed sand and gravel; therefore, the conservative estimate of 20% porosity was used for all Ex-Stream
 2150 model runs. In Ex-Stream, porosity influences the outputted flux estimation because porosity is included
 2151 in the calculation of bulk density and other thermal properties (Swanson and Cardenas, 2010b: Ex-
 2152 Stream Help File). In assessing how Ex-Stream responds to changes in porosity, I found that computed
 2153 flux values for the Keery method had a positive correction and the Hatch method a negative correlation
 2154 with changes in porosity (e.g. increase in n caused increase in q for Keery but a decrease in q for Hatch).

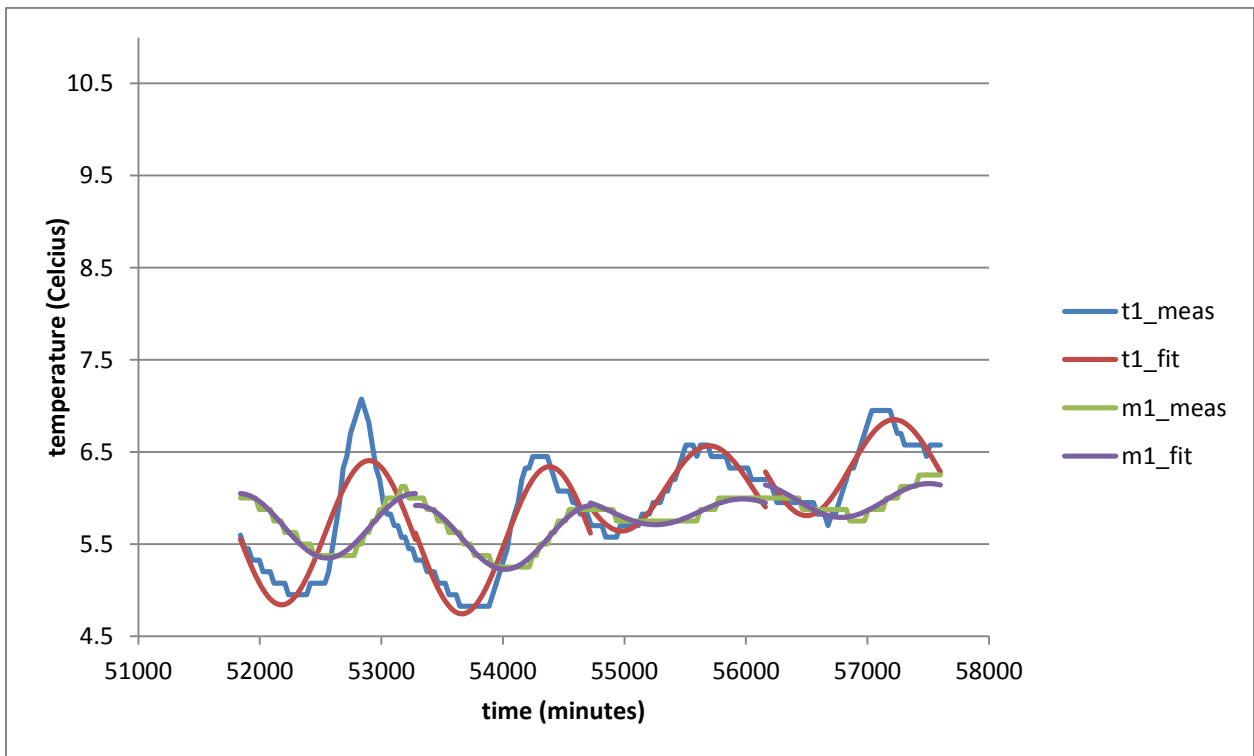
2155 Fitted curve data only outputs to the fit_data folder if "Use CurveFit" is left unselected.
 2156 Therefore, in order to conduct QA&QC on the fitted data, CurveFit was not used. The same 38 day
 2157 temperature dataset was run through Ex-Stream with and without CurveFit; there was effectively no
 2158 difference in the computed flux values.
 2159



2160 Figure 1B1. Screen-shot of Ex-Stream input parameters and selected options used to obtain vertical streambed
 2161 flux.
 2162



2163 Figure 1B2. Plot of interpolated iButton data and ExStream curve fitted lines for Ole pz44sr3sgst from 9/12/11-
 2164 9/22/11 (the t1 is the stream temperature sensor; m1 is the upper streambed sensor).
 2165
 2166



2167 Figure 1B3. Plot of interpolated iButton data and ExStream curve fitted lines for Ole pz44sr3sgst from 10/18/11-
 2168 10/21/11 (the t1 is the stream temperature sensor; m1 is the upper streambed sensor).
 2169
 2170

2171 Nonhydrostatic and hydrostatic drivers of streambed flux
 2172 Vertical streambed flux (q_v) magnitude and direction are controlled by streambed pressure
 2173 gradients caused by nonhydrostatic and hydrostatic conditions (e.g. Janssen, et al., 2012). A primary
 2174 driver of nonhydrostatic contribution to hyporheic flow arises from turbulent flow over bedforms, which
 2175 causes redirection in fluid momentum (e.g. Janssen, et al 2012). This process is known as “pumping”.
 2176 Nonhydrostatic (“pumping”) conditions cause increased streambed flux (and decreased hyporheic
 2177 residence time) with increased stream discharge (Janssen, et al. 2012). In contrast, hydrostatic
 2178 conditions cause decreased streambed flux with increased stream discharge due to flattening of the
 2179 water surface profile in relation to bedform curvature (Tonina and Buffington, 2009a). Therefore, this
 2180 balancing of streambed pressure gradient changes with small changes in stream stage due to
 2181 precipitation events during the study period can help explain the lack of change in vertical q_v at my sites.
 2182

2183 **1.B.iii. Hydraulic conductivity (K) and redd occurrence**

2184 To plot the distance downstream of slug test piezometers (and obtained horizontal hydraulic
 2185 conductivity values) in relation to redd occurrence, the piezometers and redds were matched with the
 2186 most proximal long profile topographic survey point. The piezometer or redd was then assigned this
 2187 distance downstream within the topographically surveyed long profile. Distance downstream within the
 2188 long profile is calculated by applying the distance formula to the northing and easting coordinates of
 2189 adjacent long profile points and then adding the cumulative distances between points starting with the
 2190 first long profile point as zero.
 2191

2192 Table 1B5. Slug test piezometer longitudinal study section position was estimated by matching the piezometer
 2193 location with the nearest total station surveyed long profile point using Arc10.0.

	Slug test piezometer	Long Profile	
		Surveyed point name	Distance downstream (m)
Ole	pz44	89	129
	pz51	164	301
	pz58	245	395
	pz81	362	534
	pz86	370	597
	pz101	458	871
Quartz	pz42	237	59
	pz39	242	69
	pz25	71	166
	pz09	125	277
	pz07	129	292
Trail	pz51	157	100
	pz24	48,23	417
	pz2	31	472
	pz19	33	483
	pz1	29	619
Whale	pz41	39	0
	pz36	62	41
	pz19	179	338

	pz09	267	456

2194
2195
2196

Table 1B6. Bull trout redd longitudinal study section position was estimated by matching the redd location (or redd cluster location) with the nearest total station surveyed long profile point using Arc10.0.

	Redd name	Total # of redds	Long Profile	
			surveyed point name	distance downstream
Ole	3	1		-20
	4	1	245	395
	16, 17	2	440	706
	18, 19, 20, 21	4	458	871
Quartz	10	1	225	36
	9	1	234	56
	8	1	71	166
	7	1	96	206
	6	1	118	243
	5, 4, 3	3	123	262
	2, 1	2	128	290
Trail	7	1	144	18

2197
2198
2199
2200
2201
2202

2203 **APPENDIX 2A: Valley-scale geomorphology**

2204

2205 **2.A.i. Valley-confinement**

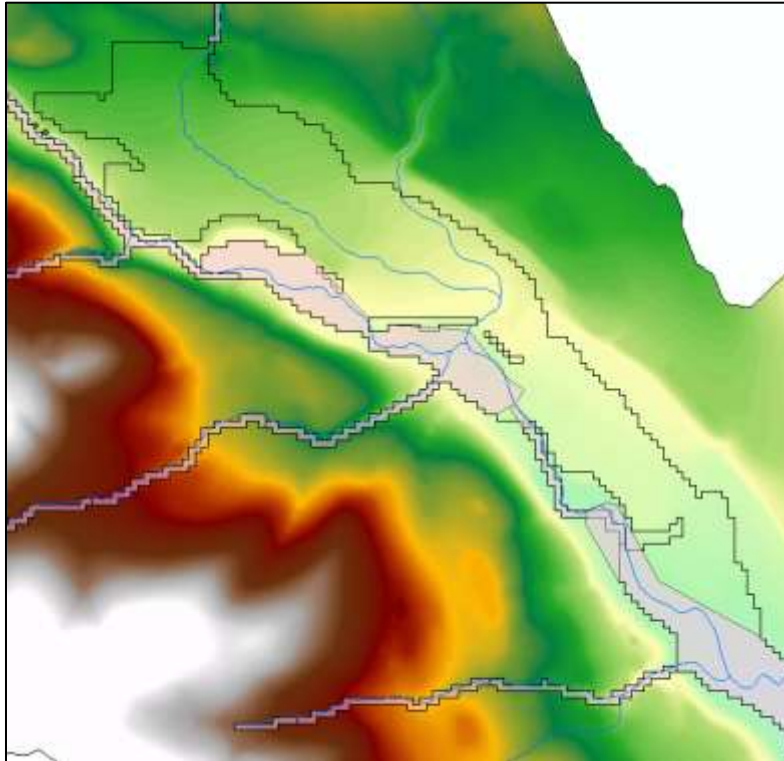
2206 Delineations of unconfined and confined valleys were conducted for all catchments of the
2207 Flathead River basin by Wenger et al. (2011). Shapefiles of these delineations were shared with me
2208 courtesy of David Nagel and Sharon Parkes with the US Forest Service Rocky Mountain Research Station
2209 in Boise, Idaho.

2210

2211 Editing Trail Creek VBclass=0, FID 152:

2212 Most of the upstream portion of this polygon is the delineation of a terrace above Trail Creek. I
2213 have edited the polygon to include only the Trail Creek valley bottom portions.

2214



2215 Figure 2A1. The original Trail Creek valley bottom polygon (FID 152) which falsely includes a terrace above the Trail
2216 Creek valley floor is indicated by the hollow outline. The pink polygons show the new, edited, more accurate valley
2217 bottom delineation.
2218

2219

2220 Extended notes and observations about valley confinement and distribution of 2011 redds

2221 In the Ole catchment, there are 2 unconfined valley segments – both are ~4 km long and are located
2222 near the midpoint of the catchment. Bull trout spawning and rearing is not known to extend into the
2223 upstream unconfined valley (USFWS, 2008). Bull trout redds observed in 2011 were clustered near the
2224 downstream extent of the lower unconfined valley (n=21) as well as 50-1500 m downstream of this
2225 unconfined valley in the confined valley segment (n=19, Figure 19a, Table 7). The furthest downstream
2226 ~3 km+ of Ole Creek is coarser and steeper and has narrower valley walls than the rest of the drainage
2227 of the highlighted spawning and rearing area. Redds are rarely observed in this section (John Fraley,
2228 2011, personal communication).

2229 In the Quartz catchment, there is a 1.5 km long unconfined valley that extends from the
2230 confluence of Rainbow and Quartz Creeks to Quartz Lake (Figure 19b). The majority of 2011 bull trout

2231 redds were distributed fairly evenly throughout this unconfined valley (n=35); several redds were
2232 located 100-280 m downstream of Cerulean Lake in the confined valley section (n=8; Figure 19, Table 7).
2233 The bull trout spawning in Rainbow Creek may be a separate resident population of Cerulean Lake
2234 (Tennant, 2010); however, genetics studies indicate that the Quartz and Cerulean Lake populations are
2235 connected (Clint Muhlfeld, 2011, personal communication).

2236 In the Trail catchment, there is a 1 km long unconfined valley segment in the known spawning
2237 and rearing reach (Figure 19c) (USFWS, 2008). Migratory spawning bull trout are unable to access much
2238 of the Trail Creek drainage because of an intermittent stream section that acts as a migration barrier
2239 during late summer and fall baseflow conditions (the bottom of the intermittent stream section is
2240 indicated by the yellow star in Figure 19c). The majority of 2011 redds in Trail were dispersed in a
2241 confined valley ranging from 60 m to 2500 m downstream from the migration barrier (n=7); the furthest
2242 downstream redd was located in the aforementioned unconfined valley segment (Figure 19c; Table 7).

2243 In the Whale catchment, there are two unconfined valley segments – the larger of which is
2244 about 12 km long and hosted all the 2011 bull trout redds observed in the Whale drainage (n=43, Figure
2245 19d, Table 7). Whale Creek Falls, located just upstream of the upstream extent of the large unconfined
2246 valley, presents a barrier to further upstream fish migration in Whale Creek (the barrier is indicated by
2247 the yellow star in Figure 19d). Bull trout can however migrate up the adjacent tributaries near the
2248 upstream extent of the large alluvial valley. These adjacent tributaries are not included in the annual
2249 “index stream” redd count surveys. However, the southern tributary, Shorty Creek, which hosts a ~2 km
2250 long unconfined valley, is known to annually host spawning bull trout (Tom Weaver, 2012, personal
2251 communication) (Figure 19d).

2252

2253 **APPENDIX 2B: Valley-scale hydrogeology**

2254

2255 **2.B.i. Spatial water temperature comparisons**

2256 Stream temperature data from above, within, and below each study area was compiled to
2257 compare variability and rates of change in stream temperature during the months immediately prior to,
2258 during, and after the 2011 spawning season (mostly August, September, and October temperatures). Dr.
2259 Clint Muhlfeld and Leslie Jones of the USGS provided stream temperatures for above and below the Ole
2260 Creek study section (Ole Upper = FHR_234; Ole Lower = FHR_092) and above and within the Quartz
2261 Creek study section (Rainbow, below the mouth of Cerulean Lake = FHR_099; Quartz, above the mouth
2262 of Quartz Creek as it drains into Upper Quartz Lake = FHR_096). Pat Van Emerien of the Flathead
2263 National Forest (FNF) provided stream temperature data from above and within the Trail Creek study
2264 reach and above and below the Whale Creek study reach. All these temperature data were collected by
2265 Hobo U22-001 units. The USGS and FNF data were collected at hourly intervals; so I filtered my data to
2266 include only hourly data points for my statistical comparisons of water temperate averages, variances,
2267 standard deviations, and rates of change. (see "All_stream_temp_spatially_compiled.xlsx" in data>water
2268 temperature>spatial comparisons.)

2269

2270 **Regional groundwater temperature estimation**

2271 Groundwater temperature is influenced by seasonal variations in surface heat from the sun and
2272 by the geothermal gradient (1.8-3.6°C/100 m (Heath, 1983); mean of 2.9°C/100 m (Todd, 1980)) – which
2273 is controlled by conductive and convective movement of heat in Earth’s interior (Kasenow, 2001).
2274 Mean annual groundwater temperature at 10-25 m depth is about 1-2°C higher than mean annual air
2275 temperature (Kasenow, 2001). In this depth range, seasonal fluctuations in groundwater temperature
2276 can occur but the temperature is relatively constant (Kasenow, 2001). Below this depth range, the
2277 increase in groundwater temperature due to the geothermal gradient is relatively constant (Kasenow,
2278 2001). Tables 2B1 and 2B2 below show that groundwater temperate at 10-25 m depth in the study
2279 areas should therefore be ~4-6°C.

2280

2281 Table 2B1. Approximate elevations above mean sea level of each study reach – estimated from a 30 m DEMs
2282 obtained from the USGS seamless server.

study reach	Elevation	
	(m)	(ft)
Ole	1260	4134
Quartz	1370	4495
Trail	1260	4134
Whale	1300	4265

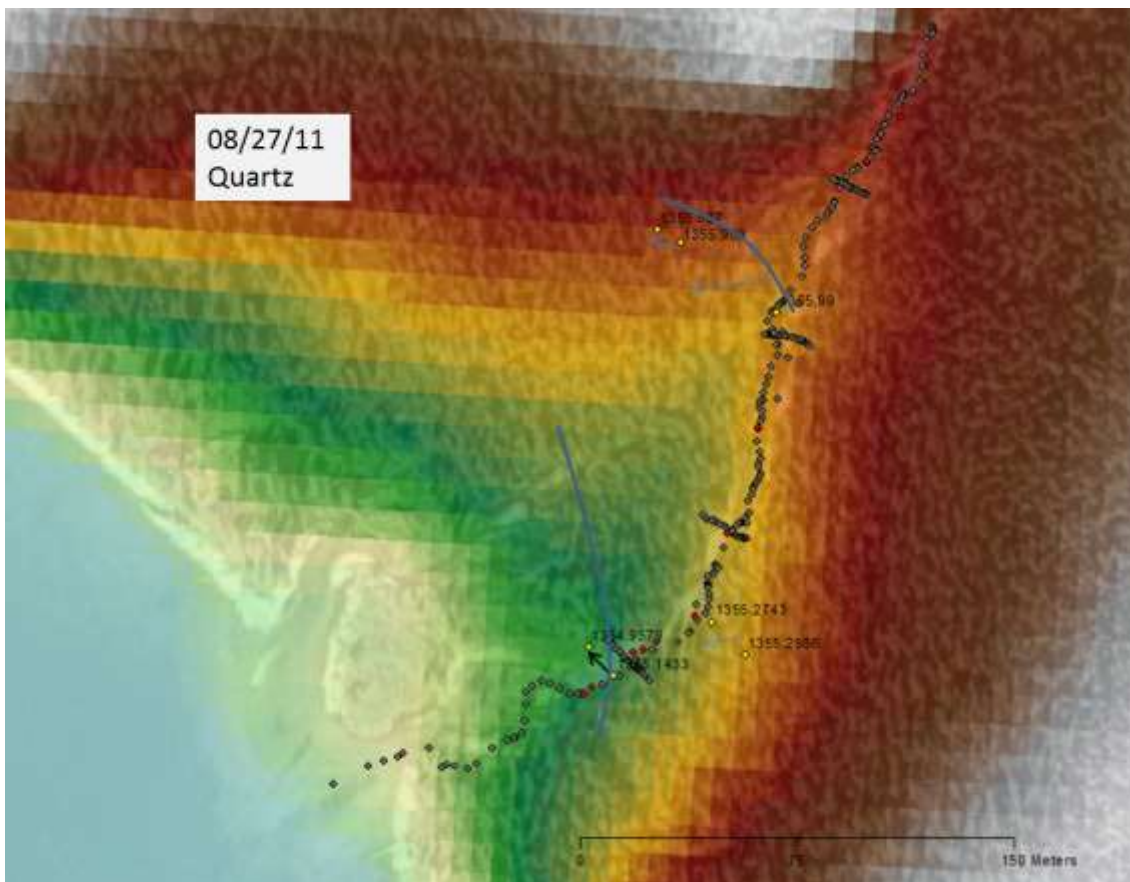
2283

2284

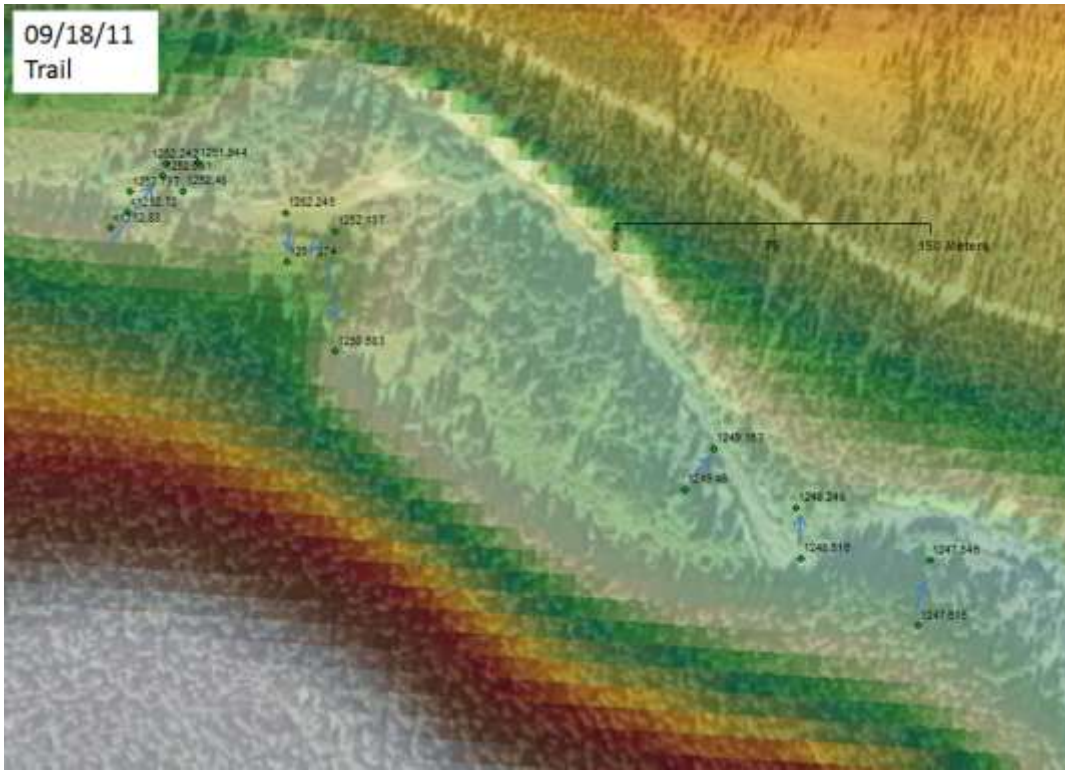
2285 Table 2B2. Average annual air temperature from the SNOTEL stations closest to the study reaches.

SNOTEL					Average Annual Air Temp (°C)					
Station	#	Elev. (ft)	Lat	Long	2007	2008	2009	2010	2011	5 yr Avg
Emery Creek	469	4350	48 deg; 26 min N	113 deg; 56 min W	4.8	4.1	4.1	3.9	3.5	4.1
Grave Creek	500	4300	48 deg; 55 min N	114 deg; 46 min W	4.8	3.8	3.9	3.8	3.6	4.0
Many Glacier	613	4900	48 deg; 48 min N	113 deg; 40 min W	5.9	4.8	4.9	4.4	4.3	4.9
									Average	4.3

2286
2287
2288

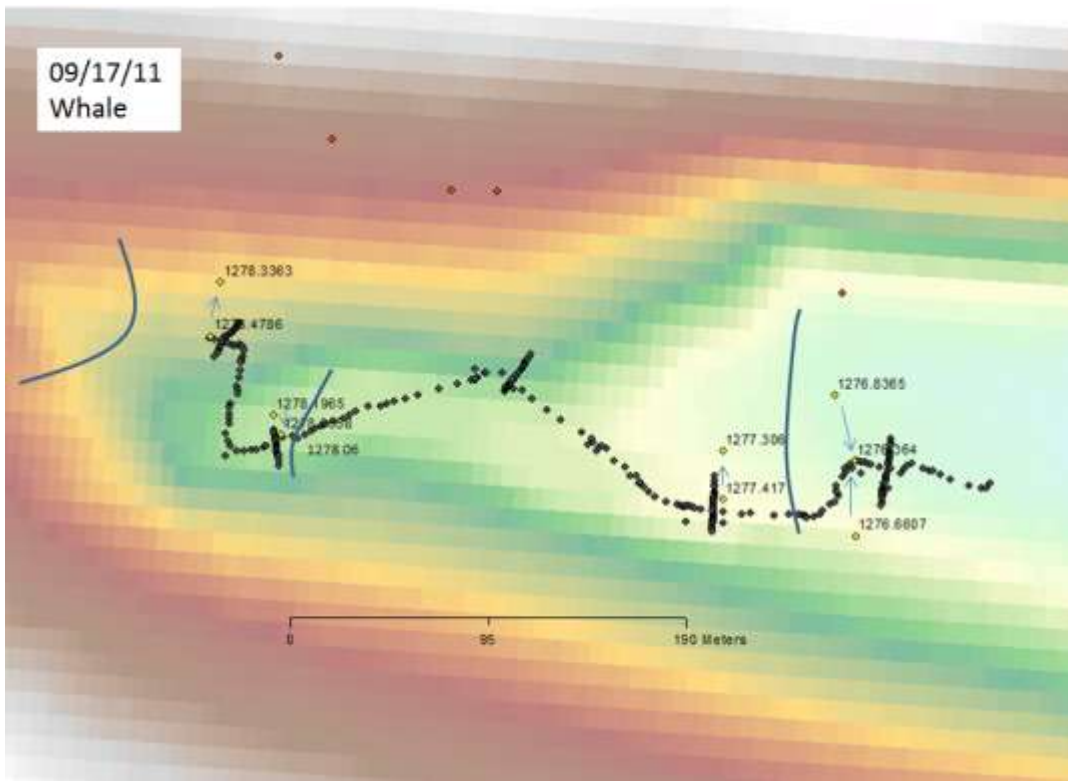


2289
2290 Figure 2B1. Inferred QTZ water table contour lines (blue).



2291
2292
2293

Figure 2B2. TRL stream and floodplain water elevations.



2294
2295
2296
2297

Figure 2B3. WHL_{mc} stream and floodplain water elevations.